The influence of silver birch vegetation on the metal availability in mining affected substrate and mycorrhiza-supported tree metal tolerance

An attempt of a holistic view on the system substrate-fungi-tree

Dissertation

zur Erlangung des akademischen Grades *doctor rerum naturalium*
(Dr. rer. nat.)

vorgelegt dem Rat der Chemisch-Geowissenschaftlichen Fakultät
der Friedrich-Schiller-Universität Jena

von M.Sc. (Biogeowissenschaften) Arno Märten
geboren am 10.12.1988 in Halle (Saale)

Gutachter:

1. Prof. Dr. Georg Büchel (Friedrich-Schiller-Universität Jena)
2. Prof. Dr. Erika Kothe (Friedrich-Schiller-Universität Jena)

Tag der öffentlichen Verteidigung: 04.07.2017

Devoted to all people debarred from their human right of education, sole due to their ethnic or national origin.

Gewidmet allen Menschen, denen alleine aufgrund ihrer ethnischen oder nationalen Herkunft ihr Menschenrecht auf Bildung verwehrt bleibt.

ABSTRACT

The work aimed the experimental study of the metal bioavailability in soil and soil solution under the influence of birch vegetation in a mesoscale pot experiment. The substrate used therein originated from a mining affected site that was mainly contaminated with Al and Cu and vast free of vegetation, despite stands of silver birch (*Betula pendula*). Natural birch saplings from this site, adapted to harsh abiotical conditions, were transplanted to the pots and grown therein for two growing seasons, opposed to an unplanted control. The pots were specifically equipped for the highly time and depth resolved monitoring of physico-chemistry and metal concentrations in soil solution. The experiment was designed as closed system, which allowed the complete quantification of inputs and outputs. The substrate solution monitoring revealed a pH-buffering effect of the birch roots. This increase of the rhizosphere pH was attributed to the release of dissociated organic acids into the root apoplast and their subsequent protonation, in order to attenuate harmful effects of increased acidification like Al-rhizotoxicity. The root induced pH-buffering resulted in a decrease of the Al and Cu concentrations in the substrate solution. Additionally the accumulation in the tree root biomass was assumed as a further potential sink for their availability in solution. The total mass balances of the metals in the substrate were not shifted, which indicated a lacking extraction by the birch vegetation. Mycorrhizal fungi associated to the tree roots were shown to accumulate high amounts of Al in their hyphae and had therefore a filter-like function for that metal, as revealed by micro-PIXE analysis. In contrast Cu was incorporated in the roots and not accumulated in the fungal biomass. Due to the substrate contamination the diversity of mycorrhizal fungi was restricted to merely three dominant species.

KURZZUSAMMENFASSUNG

Im Rahmen eines Gefäßversuchs mit einer Laufzeit von zwei Vegetationsperioden wurde die Beeinflussung der Bioverfügbarkeit von Metallen in Boden und Bodenlösung durch eine metalladaptierte Birkenvegetation untersucht. Hauptkontaminaten des von einem bis auf Hänge-Birke weitgehend vegetationsfreien, bergbaubeeinflussten Gebiet stammenden Substrats waren Al und Cu. Die Gefäße wurden als geschlossenes System konzipiert um alle Ein- und Austräge vollständig quantifizieren zu können und waren speziell für das tiefen- und zeitaufgelöste Monitoring der Metallgehalte in der Bodenlösung ausgerüstet. Die experimentell erzeugten Ergebnisse zeigten, dass die Birkenwurzeln eine effektive Pufferung des pH-Werts der Bodenlösung bewirkten, etwa durch Protonierung von in den Apoplast abgegebenen dissoziierten organischen Säuren zur Vermeidung der durch Versauerung hervorgerufenen Al-Wurzeltoxizität. Die Verfügbarkeit von Al und Cu im Bodenwasser wurde durch die Pufferwirkung der Wurzeln sowie möglicherweise zusätzlich durch Akkumulation in den Wurzeln stark reduziert. Die Metall-Gesamtbilanzen im Substrat veränderten sich jedoch während des Untersuchungszeitraums nicht. Symbiotische Mykorrhizapilze, welche die Aufnahme von Nährstoffen sowie Metall-Kontaminanten der Birkenwurzeln in hohem Maße beeinflussen können, wurden mittels Micro-PIXE analysiert. Es wurde gezeigt, dass die Ektomykorrhizapilze hohe Al-Gehalte in ihren Hyphen aufwiesen und damit eine filterähnliche Funktion für Al einnehmen. Cu wurde hingegen nicht in die Hyphen aufgenommen sondern im Gewebe des Zentralzylinders der Birkenwurzeln eingelagert. Die Diversität der Ektomykorrhizapilze war aufgrund des kontaminierten Substrats gering und nur auf drei dominante Arten beschränkt.

TABLE OF CONTENTS

LIST OF FIGURES

LIST OF TABLES

LIST OF ABBREVIATIONS

b.s.s.	Below substrate surface
bp	Base pairs
BSE	Back-scattered electrons
c.	circa
CEC_{eff}	Effective cation exchange capacity
Co.	Company
conc.	Concentration
conc.	Concentration
DA	Discriminant analysis
DI-water	Deionized water
dm	Dry matter
DOC	Dissolved organic carbon
dw	Dry weight
EC	Specific electrical conductivity
ECM	Ectomycorrhiza
FC	Field capacity
FC_{eff}	Effective field capacity
i.a.	Inter alia (amongst others)
ibid.	Ibidem (meaning: same reference as previous)
ICP-MS	Inductively coupled plasma mass spectrometry
ICP-OES	Inductively coupled plasma optical emission spectrometry
LN_2	Liquid nitrogen
LOD	Limit of detection
micro-PIXE	Micro proton induced X-ray emission
n.a.	Not available (value is missing)
ODD	Oven-dry density
ROI	Region of interest
RSD	Relative standard deviation
SD	Standard deviation
SEM	Scanning electron microscope
SOM	Soil organic matter
STIM	Scanning transmission ion microscopy

TC	Total carbon
TF	Transfer factor
TLF	Translocation factor
XRD	X-ray diffraction
XRF	X-ray fluorescence
yrs.	Years

1 INTRODUCTION

Worldwide several legacy sites from uranium (U) mining can be found that started in the late 1940s in a modern industrial way. Still today many of those sites are not remediated and cause environmental problems. They comprise radiation as well as contaminated leachate from tailings and waste rock, the latter sometimes is related to acid rock drainage (Merkel & Hasche-Berger, 2008) that is also called acid mine drainage in the literature (e.g. Akcil & Koldas, 2006). A case example therefore in Europe was the U production in East Germany, which left behind one of the world's most severe U mining legacy. Between 1945 and 1989 more than 231,000 t of triuranium octoxides (U_3O_8) were produced. The mining and milling activities affected in total an area of 100 km². Legacies were operation areas, underground mines, an open pit mine, waste rock dumps, and tailings.

For the reclamation of those legacies measures like the excavation and relocation of contaminated material, the contouring of mining heaps, facilities, and tailing ponds to increase stability and erosion resistance, the treatment of seepage water, and the coverage of contaminated areas including the promotion of vegetation were carried out (Merkel & Hasche-Berger, 2006). Besides common costly treatment techniques for U contaminated soils like soil excavation and its transfer to repositories, encapsulation, soil washing, leaching with chelating agents, electrokinetics, and ion exchange there has been increasing interest in biological clean-up techniques where microorganisms and plants are used for U removal (reviewed in Malaviya & Singh, 2012). The latter could be described by the term phytoremediation, which is, as defined by Cunningham & Berti (1993), "[…] the use of green plants to remove, contain, or render […] environmental contaminants". They stress that this definition includes all plant-influenced processes (biological, chemical, and physical) which are involved in the decontamination of polluted substrates. Phytoremediation comprises the areas phytoextraction, phytodegradation, rhizofiltration, phytovolatilization, and phytostabilzation. Phytoextraction is defined as the concentration of pollutants (metals or organics) in harvestable compartments of accumulator plants, whereas phytostabilzation means the plant-induced reduction of the contaminant's bioavailability. Often the mentioned techniques are used in connection with remediation attempts of pollution by metals like As, Cd, Cr, Cu, Hg, Pb, Sr, U, and Zn (reviewed in Salt *et al.*, 1998).

In the case that other techniques are not economic or if there is no need to rehabilitate the area within a specific time frame, the phytoremediation of (heavy) metal contaminated land using trees was suggested. The main advantage originates thereby from the stabilization of soil or waste; in some cases also the phytoextraction by woody plants might be adequate for a clean-up of the soil. The basic requirement for the application of trees in phytoremediation is their establishment at the study site (reviewed in Pulford & Watson, 2003).

Successful colonization of polluted sites by trees depends mainly on the root accessible nutrient and water supply, as well as on the level of contaminants (e.g. metals) that are potentially phytotoxic. Plant nutrients are elements that are indispensable to plants. The absence of those cause deficiency symptoms, therefore plants would not be able to complete their lifecycle. Furthermore elements are assigned to nutrients if they are contained within molecules of essential plant compartments or metabolites. Nutrients in higher plants can be divided by the content in the dry biomass

into macronutrients like N, P, K, Ca, Mg, and S and micronutrients like Fe, Mn, Zn, Cu, B, Ni, and Mo (Schilling, 2000). At the same time in higher amounts micronutrients might cause toxic effects in plants (phytotoxicity). For example an excess of ionic Cu in plants provokes the production of oxyradicals by the Fenton reaction which induce oxidative stress. Effects are chlorotic small leaves, stunted growth, and reduced root development. Especially the latter could result in lowered water and nutrient uptake and therefore in growth retardation (Momčilović, 2004). Also other metals like Al, Ni, and Zn may cause phytotoxic effects like (lateral) growth inhibition of roots and yield reduction if threshold plant concentrations are exceeded (Alloway, 2013; Rout *et al.*, 2001). Especially plants and ecosystems surrounding closed metalliferous mines are often exposed to very high concentrations of potentially toxic heavy metals. Typical for such abandoned mining sites in absence of remediation is the generation of acidic waters containing high amounts of toxic metals and metalloids (Venkateswarlu *et al.*, 2016). The acidic waters could lead to a decrease of the soil fertility and a loss of plant macronutrients like N, P, K, and organic matter. At the same time the plant micronutrients like Fe, Mn, Cu, and Zn are more soluble in acidic solution and could appear in toxic levels (Sheoran *et al.*, 2010). Both, nutrient deficiency and an excess of metals, could hinder plant growth.

This was the starting point for the present work, since the study site, an area influenced by former U mining, was affected by metal contamination with Al and Cu, low pH, as well as by nutrient deficiency. Due to these harsh abiotical conditions vegetation was almost completely absent at the study site, despite a succession with silver birch trees (*Betula pendula*). Since Pulford & Watson (2003) stated that woody plants might be used for in phytoremediation for stabilization and in some cases even for extraction of contaminants from polluted soils, there is a need to investigate different tree species for their potential application in phytoremediation purposes. For *B. pendula* it was shown that this species can accumulate high amounts of Zn in its foliage and is therefore suitable in phytoremediation to clean soil contaminated with Zn. It was furthermore mentioned to be a Zn hyperaccumulator (Dmuchowski *et al.*, 2014). Anyway, the capability to tolerate and accumulate metals in trees depends strongly on the species, the environmental and soil conditions, and the particular metal.

The idea of the present work was to simulate the effects of a natural occurring succession by birch trees, adapted to acidic Al and Cu contaminated substrate, on the availability of these metals in solution and their mobilization from or fixation to different soil fractions. To determine the influence of the birch vegetation completely, a closed system was required that enabled the tracing of all metal inputs and outputs as well as a depth and time resolved monitoring of substrate solution physicochemistry. Therefore specifically equipped mesoscale sized pots were designed, that satisfied the mentioned requirements. Those pots were used to transfer the harsh abiotical conditions of the substrate at the study site from the field scale to the mesoscale, in order to study the unbiased effects of the birch vegetation under controlled conditions without distracting biotical and abiotical influences.

This work aimed to elucidate the following questions in the course of a specifically designed mesoscale pot experiment:

1) Is the physico-chemistry (pH, redox) of the substrate solution changed substantially in the rhizosphere of the silver birch vegetation?
2) Are the available concentrations of potentially phytotoxic metals like Al and Cu in the substrate solution affected by the birch roots?
3) Can the trees contribute to a reduction of the total metal concentrations in the substrate and are there shifts in the differentially bound metal fractions?
4) Is there a potential to apply the tree species *B. pendula* in phytoremediation, either for phytostabilzation or phytoextraction of the metals Al and Cu?

The successful application of phytoremediation with trees to (former) mining areas, which requires the establishment and growth of the plants onsite, strongly depends on their ability to tolerate or minimize phytotoxic effects of metals and metalloids as well as to access plant nutrients. Possible metal detoxification strategies of plants are the fixation of the metals on cell walls and root excretions, the use of phytochelatins and metallothioneins for metals chelation, the efflux outside the cells, compartmentalization with the vacuole, and the restriction of metal uptake by associated mycorrhizal fungi (Kushwaha *et al.*, 2016).

The association with symbiotic fungi (mycorrhiza) can contribute to both metal tolerance and better nutrient and water supply. Such a mycorrhizal association is formed by over 80 % of all terrestrial plants. Thereby fungi colonize the roots of their host plant, absorb nutrients and water from the soil, and receive photosynthesis products from the plants in return (Landeweert *et al.*, 2001). A special form of mycorrhiza is the ectomycorrhiza (ECM), an association that is predominantly formed with woody perennials. Characteristically for ECM are three structural features: the mantle or sheath which consists of fungal hyphae ensheathing the root, the Hartig net which consists of hyphae growing between epidermal and cortical cells, and emanating external hyphae (extraradical mycelium) that function as the connection between both the soil and fungal fruiting bodies (sporocarps). Thereby the fungus does not penetrate the plant intracellularly, which is the main distinguishing feature to other types of mycorrhizae (Smith & Read, 2008). Ectomycorrhizae therefore represent the symbiotic organs that are predominantly formed with tree roots and act as transmitters between soil and roots (Agerer, 2006). These organs are called short roots which often form different morphotypes, depending on the symbiont's species. Mycorrhizal fungi are able to solubilize and mobilize phosphorus and metals from minerals, immobilize metals within the biomass, or precipitate them extracellularly as metal oxalates (Gadd *et al.*, 2012). The ability of ECM fungi to improve their host trees' tolerance against toxic metal concentration is quite diverse and show specificity to the fungal species as well as to the particular metal (Hall, 2002). It was reported for Al that ectomycorrhizal structures like the hyphal mantle and the Hartig net can contribute to the Al-accumulation of woody species by immobilization in the hyphal cell walls or locking in the fungal vacuoles (reviewed in Brunner & Sperisen, 2013). Therefore there is a need to investigate the spatial distribution of potentially toxic metals at the interface between specific plant species and their fungal symbionts (mycobionts).

This was the motivation in this work to study mycorrhizal roots of birch trees grown in the pot experiment and in the field regarding the spatial distribution and concentration of potentially phytotoxic metals and plant nutrients. Morphological and genetically investigations of roots colonized by ectomycorrhizae as well as microanalysis by micro-PIXE were applied to illuminate the following questions:

5) How is the composition of the fungal community growing symbiotic with silver birch in the U mining affected substrate of the pots and study site?
6) Do the mycobionts support the metal tolerance of their birch hosts as postulated in the literature by accumulating potentially toxic metals like Al and Cu in the fungal tissues?
7) Are there variances in elemental distribution patterns of different fungal species?

Since the year 2000 only a few studies dealt with microananalyis of mycorrhizae. Bücking & Heyser (2000 a, b) studied the distribution of plant nutrients in Scots pine (*Pinus sylvestris*) ectomycorrhizae by energy dispersive X-ray microanalysis of the different short root tissues using point measurements. They could show that in the case of a mycorrhizal infection the ability to increase the uptake of P under deficiency conditions as well as to reduce the amount of Ca and K in the roots varied specific to the different mycobionts *Suillus bovinus*, *Paxillus involutus*, and *Pisolithus tinctorius*. Until now there was only one microanalytical study that could show quantitative elemental maps of ectomycorrhizal roots. Turnau *et al.* (2001) used micro proton induced X-ray emission (micro-PIXE) analysis to generate distribution maps of *P. sylvestris* roots colonized by *Suillus luteus* mycobionts. They could show a strong accumulation of metals like Fe, Zn, and Pb within the fungal mantle and in the extraradical mycelium and postulated that those structures act as 'biofilter' for potentially phytotoxic elements. Nevertheless the study was accomplished on a single sample that did not allow a validation or statistical analysis of the results. Arbuscular mycorrhiza, which is another important form of mycorrhiza, was studied by micro-PIXE as well. Olsson *et al.* (2011) used it to analyze vesicles of the mycobiont *Glomus intraradices* growing symbiotic in leek (*Allium porrum*). The study proved the vesicles function as storage for P, which was accumulated therein to amounts 2-3 times higher than in the plant. They concluded that the mycobiont *G. intraradices* could satisfy the nutrient demand of its host plant, e.g. in the case of P deficiency, and might further benefit from its host. Bothe *et al.* (2013) used micro-PIXE to study the effect of arbuscular mycorrhiza on the heavy metal concentrations in zinc violets (*Viola lutea*). They concluded from the generated quantitative metal distribution maps of the violet roots that at high Zn levels in the soil the uptake into the plant is restricted, which is why the plants were classified as metal excluders. All plants were colonized with arbuscular mycorrhiza which was mentioned to be the reason for the Zn exclusion.

In general micro-PIXE is a powerful technique to study the symbiotic interaction between plants and fungi and their responses to environmental stress factors like anthropogenic pollution. Elements considered as macro- and micronutrients and potentially toxic pollutants can be measured quantitative, simultaneously, and spatially resolved. Therefore this technique could be helpful to contribute in the understanding of detoxification pathways in plants and fungi (Vogel-Mikuš *et al.*, 2009).

2 MATERIALS AND METHODS

2.1 Study area

The study area 'Kanigsberg' is located in a former U mining region in eastern Germany in the state Thuringia (center of the study area - Easting: 4,510,892; Northing: 5,632,382; coordinate system: Gauss-Krüger zone 4). An aerial image of the study area is shown in **Figure 2–1**. Geologically the area is part of the 'Ronneburg-horst' structure in the northernmost part of the Thuringian slate mountains. The bedrock consists mainly of Ordovician and Devonian siliceous sediments like quartzite and slate which is partially U bearing (Hiekel *et al.*, 2004). By exploiting these deposits in the mining areas of the states Saxony and Thuringia between 1947 and 1990 a total of 230,000 t of U were produced. The legacies of the intensive mining for decades were radioactively contaminated heaps, tailing ponds, and production premises. This led to an input of contaminants in soil, water, and atmosphere (Federal Ministry of Economics and Technology *et al.*, 2011). The mining activities ended in 1990. Since then the remediation company Wismut GmbH undertook extensive measures to rehabilitate the former mining sites. Those included the closure of mines, the rehabilitation of waste rock piles and plant premises, and the continuing treatment of contaminated water as a long-term task (Jenk *et al.*, 2014).

The study area is the base of a former mining heap ('Absetzerhalde') which covered a total area of 224.7 ha. The heap was filled up on the pristine surface without any preliminary preparation. It consisted of waste rock material that originated from an open pit ('Lichtenberg') and reached its final volume of 63.3 Mio. m³ in 1970. The average U content was 42 g t^{-1}. The deposited waste rock consisted mainly of siliceous, argillaceous, and alum shale and to smaller percentages of nodulous limestone with small percentages of aluminosilicates (5 %) and pyrite (3.3 %). After abandoning the deposition of waste rock, it was partially used as disposal site for fluid and solid operational wastes until 1994 (Wismut GmbH, 1994; Wismut GmbH, 2010). The remediation of the area comprised the removal and backfilling of the heap material into the 'Lichtenberg' open pit and a partially covering with 30-40 cm loess loam topsoil. The part of the former heap where the study area is located remained uncovered yet. Furthermore, a vegetation cover was aimed by reforestation. Tree species like durmast oak (*Quercus petraea*), common hornbeam (*Carpinus betulus*), small-leaved lime (*Tilia cordata*), European beech (*Fagus sylvatica*), Scots pine (*Pinus sylvestris*), and Norway spruce (*Picea abies*) were planted to establish a mixed forest with an excess of deciduous trees (BIOS, 2010; Gherghel, 2009). Before reforestation on average 40-50 cm of the Quaternary relicts of the pristine ground surface underlying the former heap were removed, in cases of critical radiological situation even more. To improve the growing conditions of the subsoil for the trees, the Quaternary relicts were treated with marl lime to increase the pH to 5.5 (personal communication with Mirko Köhler in April 2010). Nevertheless, due to the harsh abiotical site conditions in some areas the reforestation failed, whereas on those locations natural succession with silver birch (*B. pendula*) and sallow (*Salix caprea*) occurred (BIOS, 2010). As a consequence of the mining still today the substrate is affected by erosion, strong acidity, high fluctuations in soil moisture (often drought in summer), deficiency in

plant nutrients, and increased concentrations of possibly phyto- and ecotoxic metals (see results in section **3.1**).

The study area was screened for pH-values (**Figure 2–2**), specific electrical conductivity (EC) (**Figure 2–3**), and bioavailable concentrations of Al (**Figure 2–4**), Cu (**Figure 2–5**), and U (**Figure 2–6**) as well as Fe, Ni, and Zn (see **Figure A 1**, **Figure A 2**, **Figure A 3** in the appendix) in the substrate in the course of a preliminary investigation (Master's thesis by Naumann, 2014). Therefore 1 m core samples were removed from several locations at the study area. Within the cores layers were distinguished by macroscopic properties as color and texture. The layers in the cores were sampled separately and analyzed for the pH in the solution after suspension in DI-water according to DIN ISO 10390-05. The EC was measured in the substrate suspended with DI-water according to DIN ISO 11265-06. The cumulated concentrations of the first two fractions of the sequential extraction method according to Zeien & Brümmer (1989) are considered as the bioavailable fraction, which is potentially accessible to organisms. The concentrations were determined in solution by ICP-MS. Means for pH and concentrations were calculated for each core from the single layer values and corrected by the layer thicknesses.

Figure 2–1 Aerial image of the study area 'Kanigsberg' taken in August 2015 by a drone (straightened orthophoto). On the image the hilltop is visible as treeless area on the right (east), the slope-toe is visible as reddish uncovered area on the left (west). The slope inclines downhill from east to west, as shown by contour lines (1 m height-intervals, height data © GeoBasisDE / TLVermGeo 2014). The red circle tags the localization from which the substrate for pot-experiment was removed (Easting: 4,510,910; Northing: 5,632,349). The coordinates are given as Gauss-Krüger zone 4 coordinate system. The aerial image was used by courtesy of Dr. Daniel Mirgorodsky (Friedrich Schiller University Jena).

The pH in the substrate varied strongly from 3.3 (strongly acidic) at the slope toe (western part) to 7 (neutral) in the northern part that was covered by loess loam topsoil during the remediation. In general, the pH decrease is correlated with the inclining gradient of the slope from east to west (hilltop to slope-toe). It is assumed that the acidic pH at the slope toe is caused by higher weathering rates due to higher soil moisture. The higher soil moisture results from surface water, interflow and leachate water that are leaking from the slope toe. The substrate EC was high in the areas that were covered with topsoil during the remediation as well as at the slope toe, especially in the northwestern part. The increased ECs there could be explained by the influence of leachate water leaking from the substrate and increasing the substrate EC due to the higher saturation with dissolved main ions. The bioavailable Al had the highest concentrations in the substrate at the whole slope toe (western part) that originated presumably from the low pH in this area. At pH values around 4 after dissolution most of the Al remains in solution and is not precipitated as Al-hydroxide. The maxima of the bioavailable Cu, Ni, and U at the north-western slope-toe may result from the leaking leachate: These elements reached the highest bioavailable concentrations at the same locations of the EC maxima. Fe and Zn are not affected by the slope or by leaking leachate; the concentration pattern is more diverse and presumably more influenced by local inhomogeneity from the parent rock material the substrate evolved from.

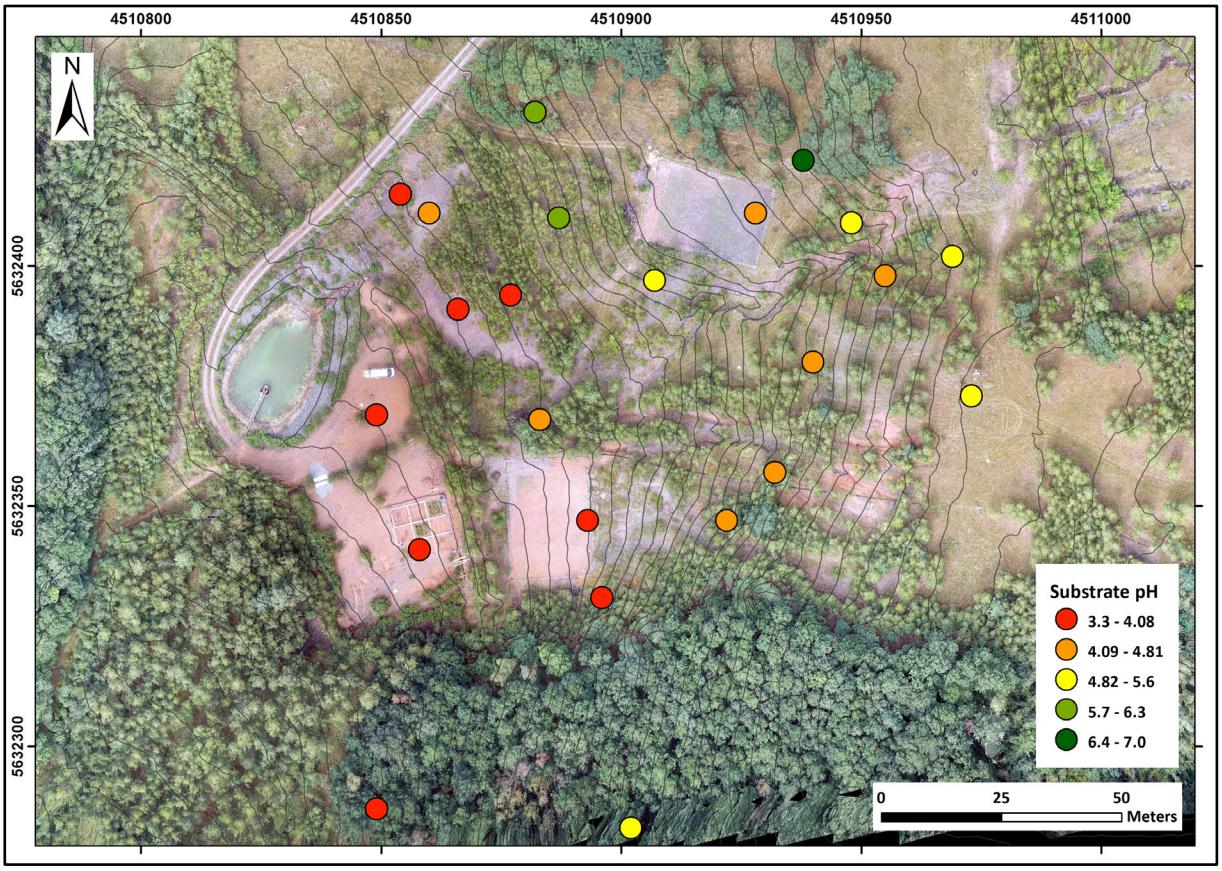

Figure 2–2 Results of the substrate pH screening at the study area by core sampling (1 m core samples, pH measured layer-wise in water-suspension). The values displayed are means calculated for each core using the depth-corrected layer values. The pH data used as database for the figure were adapted from Naumann (2013); the measuring points were projected on the aerial image.

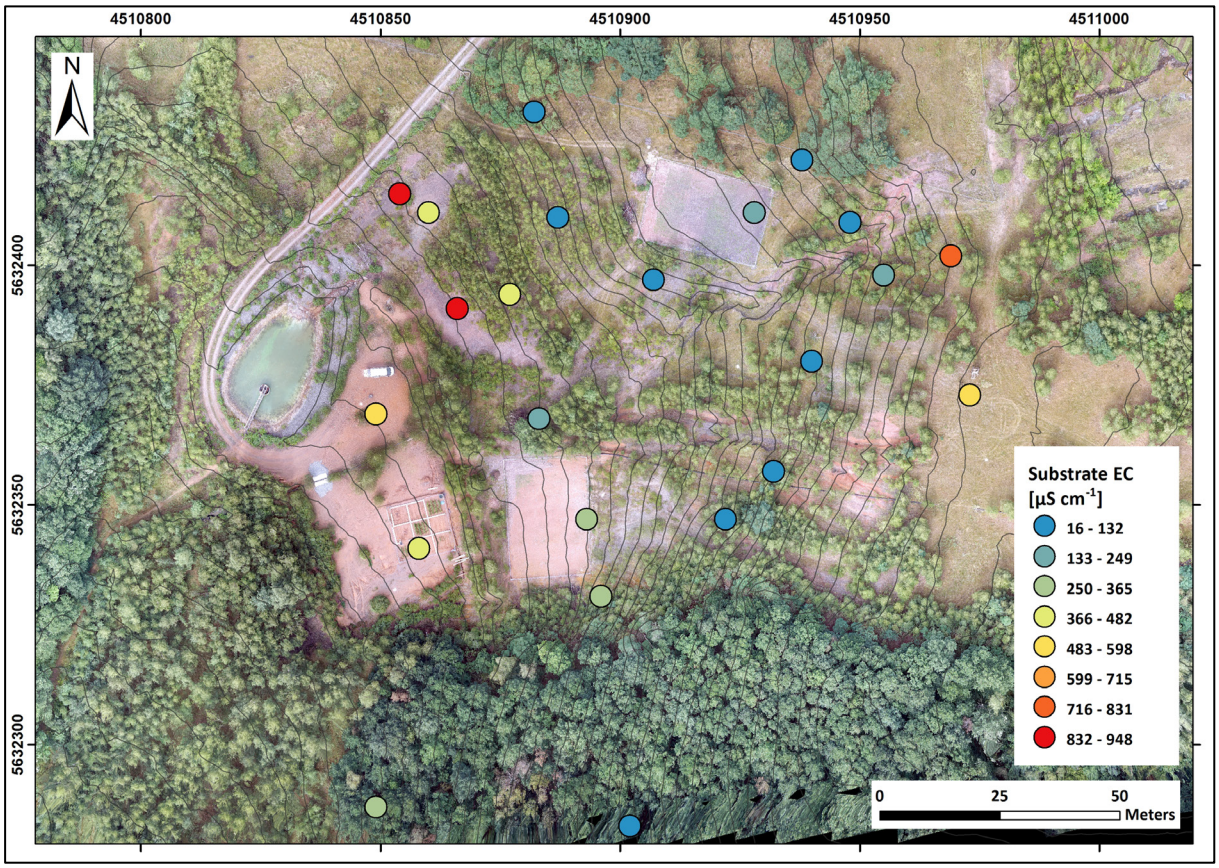

Figure 2–3 Results of the substrate EC screening at the study area by core sampling (EC measured layer-wise in water-suspension). The values displayed are means calculated for each core using the depth-corrected layer values.

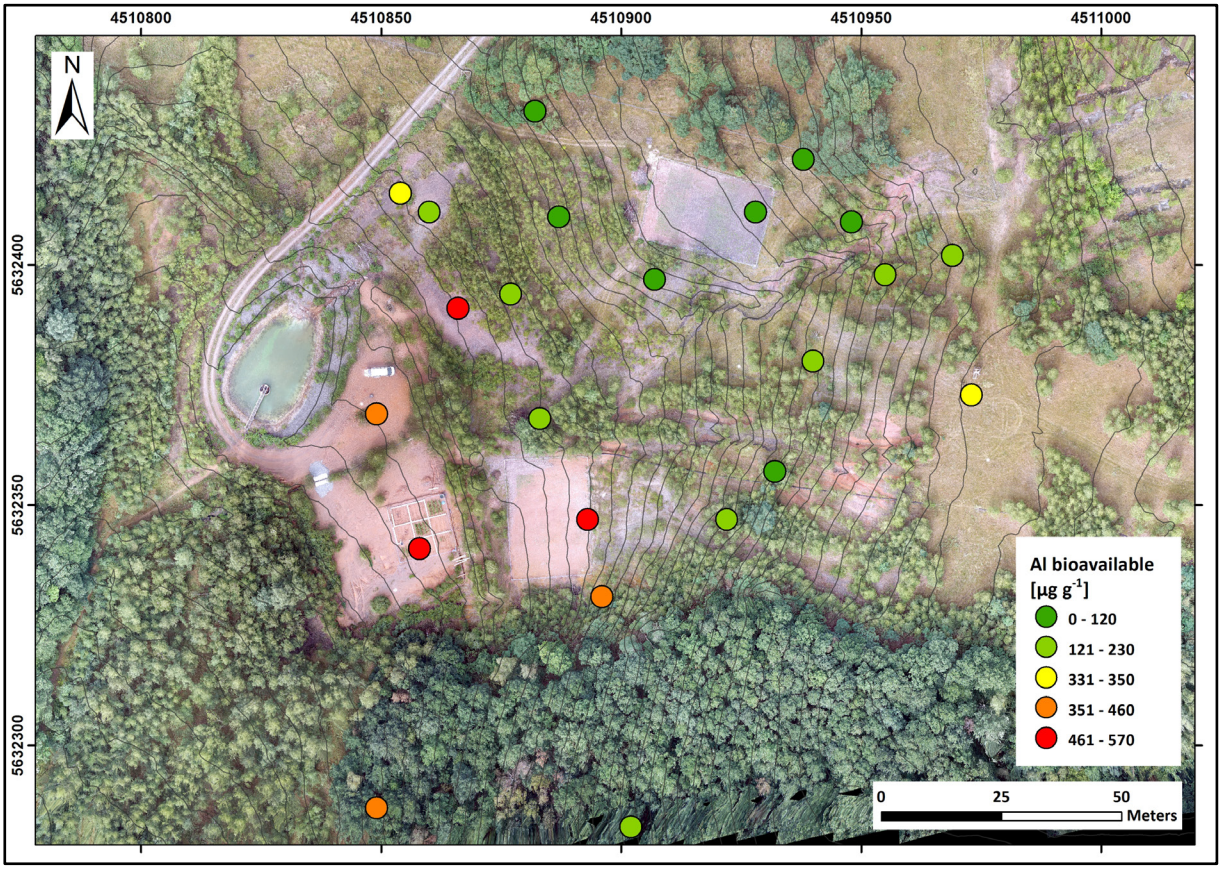

Figure 2–4 Results of the screening for the bioavailable Al concentration of the substrate at the study area by core sampling. The cumulated concentrations of the first two fractions of the sequential extraction method are considered as the bioavailable fraction.

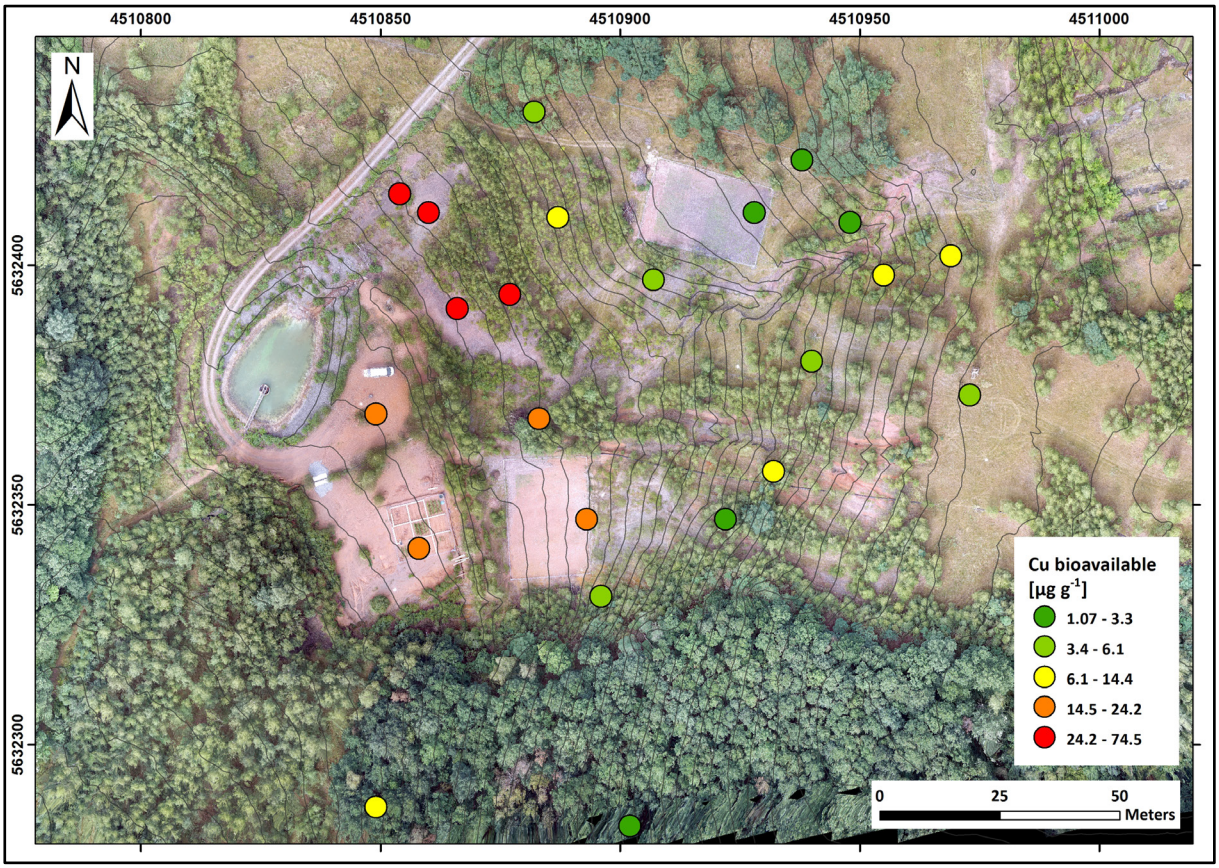

Figure 2–5 Results of the screening for the bioavailable Cu concentration of the substrate at the study area.

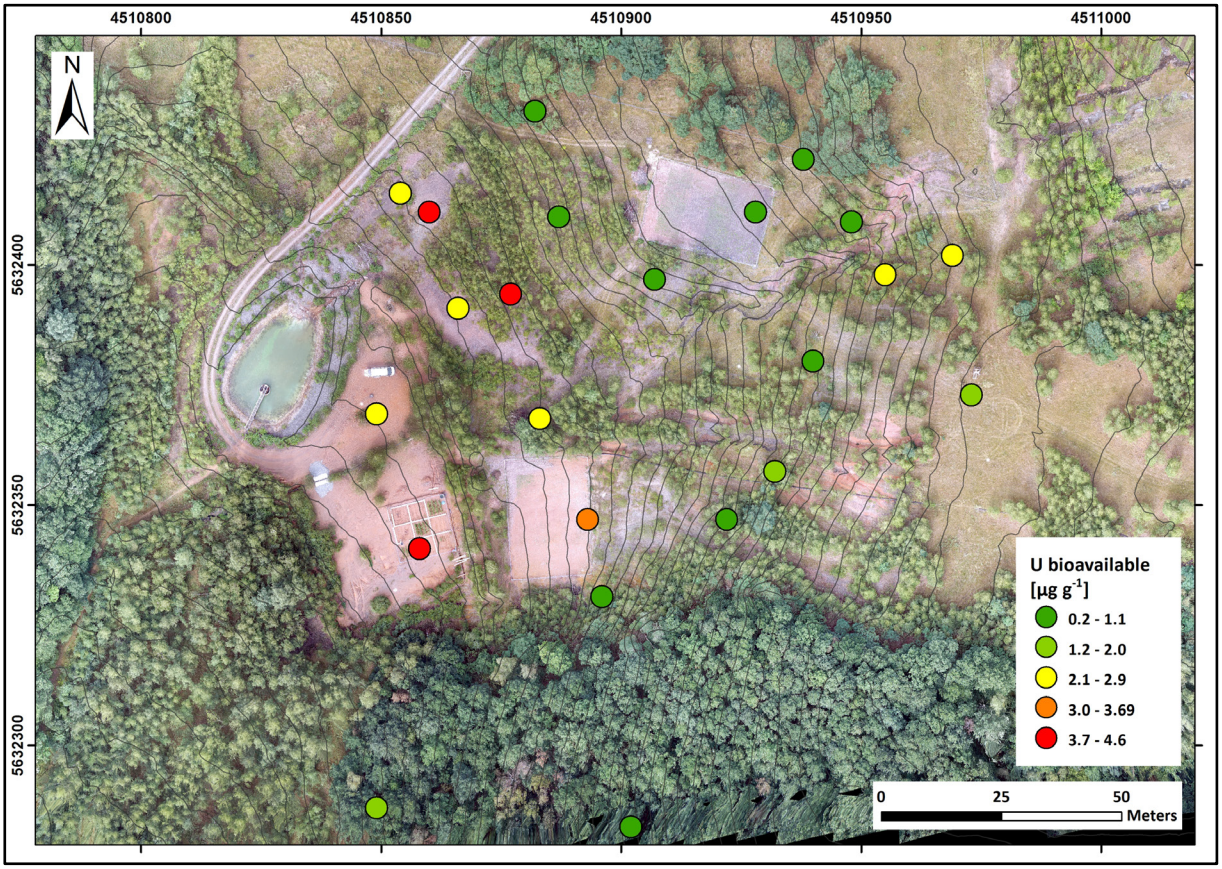

Figure 2–6 Results of the screening for the bioavailable U concentration at the study area by core sampling.

2.2 Substrate characterization: soil mapping, sampling, and preparation for analysis

Substrate representative for the study area was characterized pedologically in the course of a Bachelor's thesis (Männel, 2016). This substrate is following named as 'field substrate'. Freshly exposed substrate was characterized according to the German manual for soil mapping (Eckelmann & Ad-hoc Arbeitsgruppe Boden, 2005). The soil color was estimated using a color chart with standardized colors (Munsell Rock Color Chart, The geological society of America 1991). The carbonate content was estimated by observing the reaction (bubbling) of the substrate in the field with 10 % HCl. For chemical characterization by X-ray fluorescence (XRF) analysis, a sample of the exposed substrate from the field was taken and dried at 35 °C (following named as field-sample). Subsequently big aggregates were broken up with a mortar and the homogenized sample was then sieved to the fraction of fine soil (grain size < 2 mm; sieve: Nylon DIN 4197, Nr. 336958, Linker Industrie-Technik; mesh size: 2000 µm). A sub-volume of the sieved field-sample was milled to powder (grain size < 63 µm) using a mixer mill lined with zircon ('MM 400', Retsch).

Substrate used for a mesocosm pot experiment was removed from the study area close to a population of young birch trees (Easting: 4,510,914; Northing: 5,632,350; coordinate system: Gauss-Krüger zone 4; middle part of the slope). It was air-dried, sieved to a grain size < 2.8 mm, and homogenized several times. The homogenized substrate sieved to < 2.8 mm is following named as 'initial substrate'. The particle size distribution was determined by wet-sieving (analytical sieves, Co. Retsch, mesh widths: 63 µm, 125 µm, 0.2 mm, 0.4 mm, 0.63 mm, 0.8 mm, 2 mm) for the fraction > 63 µm, the fraction < 63 µm was analyzed using a laser particle sizer ('Analysette 22', Fritsch; possible measuring range: 0.31-300.74 µm). The parameters oven-dry density (ODD, determined for the fine soil fraction < 2 mm), the coefficient of permeability (k_f-value), the effective field capacity (FC_{eff}), and the water contents at different soil moisture tensions (suction pressure, pF-value) were distinguished according to VDLUFA, 1991. The measurements of these parameters were performed in 'undisturbed' samples, wherefore the initial substrate was filled into soil sampling rings (Co. Eijkelkamp) and compacted in the same manner as in the setup of the pot experiment.

2.3 Design and setup of the mesocosm pots

The four mesoscale pots (mesocosms) used for the experiment were designed based on laboratory lysimeters (ecoTech Bonn, Germany). Their mantle was made of transparent plastic (PVC) with an inner diameter of 30.5 cm by a height of 50.0 cm. The bottom of the lysimeters consisted of a membrane-filter-plate (material: polyamide; pore-size: 0.45 µm; delivery capacity: c. 1.1 l min^{-1}; bubble point: min. 1000 hPa) with a high hydraulically conductivity and a minimal sorption, which was covered with a polyamide-net for protection against mechanical damage. The membrane allows a free water-flow to study the migration of nutrients and pollutants without the formation of backwater and ensures unsaturated conditions in the soil column. The mantle tube had six stacked bores with fittings for redox probes and six bores with fittings for mini suction cups on the opposite side. Both stacks of bores were evenly spread over the full height of the lysimeter. The plastic mini suction cups

used are assigned to extract soil solution for the analysis of inorganic solutes including heavy metals (diameter: 2.5 mm; length: 100 mm; tube material: PVC; stiffening of the tube: glass fiber; filter material: porous polymer; pore size: 0.2 µm). The Pt-redox-electrodes used consist of a Pt-rod (Material: 99.95 % Pt, hard drawn; length: 5 mm; diameter: 1 mm; measuring range: -1 to + 1 V; resolution: 1 mV) which is mounted into a carbon-fiber shaft (length: 100 mm; diameter: 5 mm). An Ag/AgCl-electrode connected to soil by a salt bridge (KCl-Gel) served as a control. The setup measures the potential difference between the redox-electrodes (plus-pole) and the reference (minus-pole). The Pt-electrodes were designed by Prof. Dr. Mansfeldt (University of Cologne), the setup is proper for a permanent measurement of the redox potential in soils, even under wet and reducing conditions (Mansfeld, 2003). The redox potential-difference of each electrode against the reference was logged hourly by the data logger system 'enviLog Maxi' (Software: GP-Shell2, V1.14). All specifications of the lab lysimeters and measuring equipment refer to the product specifications (ecoTech, 2017); a scheme and a photograph are displayed in **Figure 2–7**.

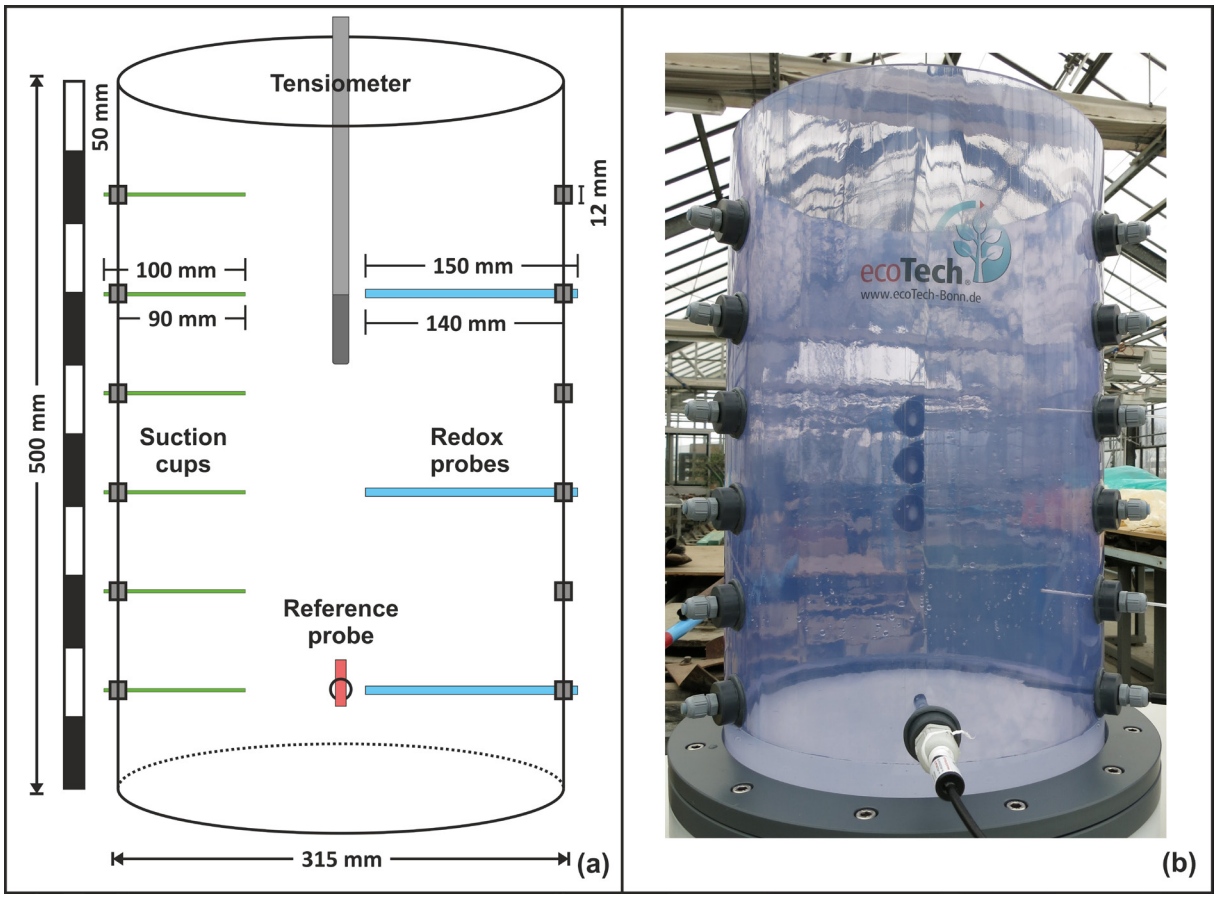

Figure 2–7 (a) Construction scheme of the laboratory lysimeters used for the mesoscale pot experiment illustrating the dimensions. The inner diameter of the tube is c. 30.5 cm, it is made from transparent plastic (PVC) with a wall thickness of c. 5 mm. The blue horizontal bars represents the dimensions of the redox probes installed, the green those of three suction cups (for installation depths see following Figure 2–8). The reference probe (red) serves as the minus pole for the redox probes. A manual tensiometer (grey) allows the determination of the soil moisture tension. **(b)** Photograph of a laboratory lysimeter before filling with substrate. Clearly visible are the vertically stacked fittings for the probes and suction cups (sideways left and right) as well as the inserted redox reference probe (middle low part) of the lysimeter. The grey flange ring at the bottom of the lysimeter contains the membrane filter plate with minimum sorption, preventing backwater formation.

The soil moisture tension was measured in each pot in a depth of 10-15 cm using tensiometers constructed of porous water-permeable ceramic cap (5 cm length) connected with a plastic tube filled with de-gassed water as measuring-volume and sealed air-tight by a rubber-septum. The pressure condition in the inside the tensiometers are connected via the water-permeable ceramic-cap to that in the soil. During soil drying-out water flows out of the tensiometers generating an underpressure that corresponds to the soil moisture tension. That was measured manually with a digital manometer by piercing a needle connected with the sensor through the septum.

The pots were filled up to a height of 45 cm layer-wise (5 cm layers) with the dried, homogenized, and sieved substrate from the study area. For each layer 5.55 kg air-dry substrate (remaining moisture: 4 wt%; corresponds to 5.33 kg oven-dry mass) moistened with 445 ml of deionized (DI) water was filled in the pots and compacted uniformly to a thickness of 5 cm. The surface was loosened subsequently gently before filling in the next layer to avoid the formation of density related horizons. In total 49.95 kg of air-dry substrate were used per pot (corresponding to 47.96 kg oven-dry mass) that had a volume of 0.13 m^3 pot^{-1}. The hydraulic contact to the membrane-filter plate at the bottom of the pots was ensured by sluicing using slurry substrate. The same was applied to connect the redox-reference probes and the tensiometers hydraulically with the substrate. The redox-reference probes were placed horizontally in a depth of 38 cm below substrate surface. The tensiometers were placed vertically in the middle of each pot; placing the ceramic head in a depth of 10-15 cm. In three pots each three birch trees (*Betula pendula* L., age: 1-3 yrs.) bedded out as a whole from a naturally grown population at the study area were planted. Therefore, the roots were washed with DI-water first and then buried in the uppermost 15 cm of the substrate. One pot remained unplanted and served as a control.

After filling-in the substrate and planting the trees the substrate was watered with DI-water to c. 15 vol% (considering the air-dried substrate as 0 vol% water-saturated), corresponding to c. 50 % FC_{eff} (determined from pF-water saturation-curves of the substrate; see **Figure 3–1**). This water saturation was re-adjusted frequently by weighting of the pots and replenishing water-loss due to evaporation and transpiration. This ensured a constant sufficient water supply and uniform moisture conditions in the substrate of all pots.

After a substrate-settling time of two weeks (c. 0.5 cm settlement), three redox probes and six suction cups per pot were inserted in 10, 24, and 38 cm depth below substrate surface (b.s.s.) or 3, 10, 17, 24, 31, and 38 cm depth (b.s.s.) respectively. The holes were pre-drilled using long screws with a slightly smaller diameter than the probes and suction cups to ensure a hydraulic connection to the substrate. A scheme of the setup of the pots equipped with suction cups and redox-probes and planted with birch trees is shown in **Figure 2–8**.

The pot experiment was conducted in a greenhouse with ambient air temperature to exclude the input of elements by rainwater. In the dormancy, the temperature in the greenhouse was kept above the freezing point to protect the pots and the probes from frost damage. The air temperature and air humidity were logged hourly using a temperature desktop station ('KLIMA LOGGER', TFA Dostmann) with an external remote sensor. The intervals of watering with DI-water were dependent on the temperature and therefore from the evaporation and transpiration (e.g. in summer the pots were

watered daily whereas in the winter weekly). The tensiometer measurements allowed the estimation of the soil moisture tension and therefrom the need for watering.

The pot experiment lasted 495 days and comprised two growing seasons and the intermediate dormancy. Begin of the dormancy was defined by the fall of the last leaf, the end by the first burst of buds.

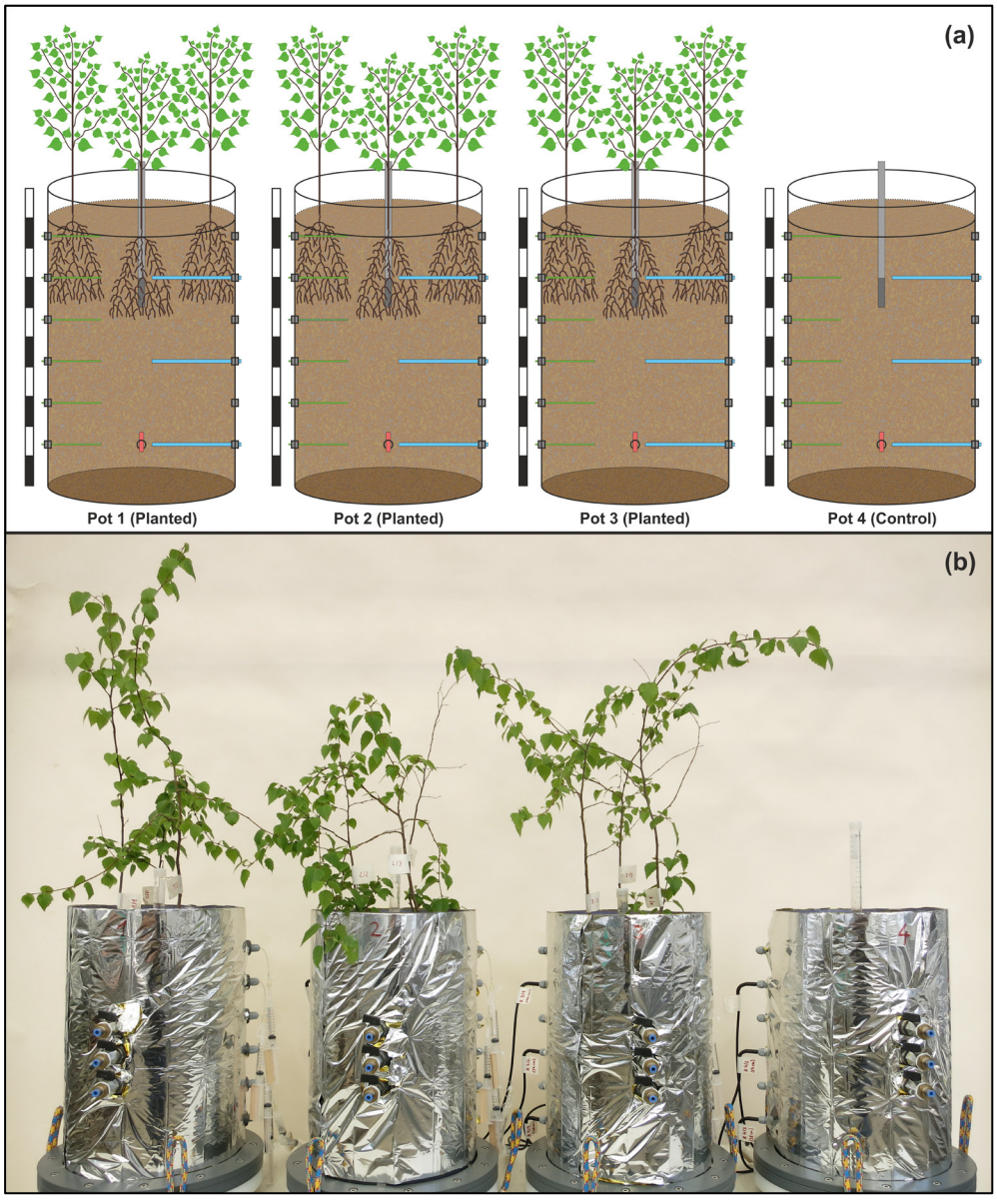

Figure 2–8 (a) Schematic setup of the mesocosm pot experiment. The pots were filled with sieved homogenized substrate from the U mining affected study area up to a height of 45 cm (substrate volume: 0.13 m³). The planted 1-3 yrs. old birch trees (*B. pendula*) were transplanted from a population grown naturally at the study area. The suction cups (green horizontal bars) were inserted in each pot in 3, 10, 17, 24, 31, and 38 cm depth (below substrate surface - b.s.s.). The redox-probes (blue horizontals bars) were inserted in each pot in 10, 24, and 38 cm depth (b.s.s.). One reference probe per pot (red) was installed in 38 cm depth, the porous measuring head of the tensiometers (grey) covered the depth range of 10-15 cm b.s.s. The scale left side of each pot shows sections of 5 cm. **(b)** Photograph of the pots taken at the end of the first growing season. The pots were wrapped into silver foil for the protection of soil and roots against solar radiation and for reduction of algal growth at the transparent lysimeter walls.

2.4 Soil water sampling and measurement of physico-chemical parameters

During the whole duration of the experiment, the substrate solution was regularly sampled via the suction cups. For the extraction of the solution from the substrate on each sampling date, syringes were connected via Luer-Locks with the suction cups. A vacuum was applied by pulling up the syringe and fixing the plunger with a wooden block. Per pot and sampling date a total volume of max. 10 ml solution was extracted from each sampling depth. Thereby the filling of the syringe lasted 5-8 h depending on the temperature, the depth of the suction cups, and on whether the pots were planted or not. The EC and the pH of the solution were measured directly after the extraction from the substrate. Therefore, two separate measuring-instruments were used: the pH-meter 'pH 320' (WTW) combined with the pH-electrode 'blue line' (SI-Analitics) or 'SenTix 81' (WTW) and the EC-meter 'MultiLab 540' (WTW) combined with a 'TretraCon 325' (WTW) probe. Later the multi-parameter instrument 'pH/Cond 3320' (WTW; same probes as before) replaced the separate devices. The pH-meter was calibrated on each measuring day using standards with pH of 4.01 and 7.00 (WTW and Mettler-Toledo). A small volume (min. 2 ml) was diverged from extracted substrate solution before measuring the physico-chemical parameters for the analytical determination of cation-concentrations. This samples were chemically stabilized against precipitation of elements from the solution using one drop of HNO_3 (65 %, subboiled, Merck) per sample and were then stored at 5 °C until analysis by ICP-MS/-OES. Sometimes, mostly in the case of sampling the uppermost suction cups in the planted pots at high temperatures, the volume of extracted substrate solution was to small to diverge an adequate volume for the cation determination. In this case, only the EC and pH of the solution were measured.

2.5 Substrate sampling and preparation for analysis

Three representative samples of the homogenized substrate used for the mesocosm pot experiment (initial substrate) were taken, dried at 40 °C, and then sieved to the fraction of fine soil (grain size < 2 mm; sieve: Nylon DIN 4197, Nr. 336958, Linker Industrie-Technik; mesh size: 2000 µm). A sub-volume of the fine soil fraction was milled to powder (grain size < 63 µm; mill: 'MM400' (zircon lined), Retsch).

After the ending of the experiment from each mesocosm pot the substrate was sampled separately in layers of each 5 cm. Material of each layer was extensively mixed and a sub-volume was sampled. The samples were then dried slowly at 35 °C in a dryer until a constant weight was reached. Afterwards aggregates were broken up with a mortar and the homogenized sample was then sieved to the fraction of fine soil (< 2 mm). Again, a sub-volume was milled to powder (< 63 µm).

2.6 Biomass sampling and preparation for analysis

After the ending of the mesocosm pot-experiment, the trees were harvested as a whole. They were kept fresh by storing the rhizosphere in a small volume of moist substrate until the sampling of mycorrhizal roots was finished. Afterwards the trees were separated into their compartments (roots, stem, branches, and leaves), washed each three time with deionized water, dried at 60 °C, and then weighted to determine their dry mass. The dried compartment samples were subsequently milled to powder using an ultra-centrifugal rotor mill ('ZM 200', Retsch; material of grinding tools: titanium). Thereby the root samples were pre-cut using a rotor beater mill ('SM 100', Retsch; material of grinding tools: steel).

2.7 Analytical procedure for substrate, soil water, and biomass samples

XRF-analysis was applied to determine the total concentrations of SiO_2 and sulfur (S) in the field-substrate. 6 g of powdered sample (grain size < 63 µm) were mixed with 1 g of pure paraffin wax and pressed in a pellet (pressure: 130 bar), which was then measured by XRF ('PW 2400', Phillips). The total carbon content (TC) was quantified by thermal combustion of 25 g powdered sample (< 63 µm) with a TC-analyzer ('multiN/C 2100 S', Analytik Jena) in 5 replicates. These measurements were conducted in the course of a Bachelor's thesis by Männel, 2016.

For the mineralogical characterization of the initial substrate used for the pot experiments a powdered sample (< 63 µm) was measured by X-ray diffraction (XRD) analysis ('D8 Advance DaVinci', Bruker; parameters: Cu Kα-radiation, energy 40 mA at 40 kV, 5-80° 2-theta angle in 0.02° steps, 0.5 s measuring time per step). The computation of the acquired diffraction spectra was performed using 'DIFFRAC Evaluation' software (version 3.0.0.8; Bruker AXS 2010-2013) using the ICDD PDF-2 database (release 2011).

The EC and the pH of the initial substrate were distinguished in the context of a Master's thesis (van Laaten, 2015) based on the German standards DIN ISO 11265-06 (EC) and DIN ISO 10390-05 (pH). 5 g of dried fine soil (< 2 mm) were suspended in 25 ml ultrapure water and shaken several times within one hour. Afterwards the suspension was left for 24 h and shaken at the end of this period again. After an additional hour the EC was measured ('Multi 340i', WTW). Subsequently the suspension was shaken again and the pH was measured instantly (same instrument). The measurements of EC and pH were performed in five replicates each. The determination of the effective cation exchange capacity (CEC_{eff}) was carried out according to the German standard DIN EN ISO 11260. Therefore 2.5 g of dried substrate (< 2 mm) were washed 3 times with 30 ml $BaCl_2$-solution (0.1 mol L^{-1}) to occupy all ion exchange sites of the substrate with Ba. Afterwards 30 ml of $MgSO_4$-solution (0.02 mol L^{-1}) were added causing the precipitation of both adsorbed Ba and Ba in solution and the occupation of all exchange sites by Mg. The Mg concentration in the supernatant as well as in the blank solution was then analyzed by ICP-OES ('725 ES', Varian). The adsorbed Mg, which corresponds to the sum of exchangeable cations, was calculated from the difference of the initial Mg concentration in the solution and the Mg content in the supernatant.

The sequential extraction method (Zeien & Brümmer, 1989) was applied to estimate the concentrations of metals bound in different forms to soils. Therefore, substrate samples (grain size < 2 mm) were sequentially suspended with different extracting agents and the extracts were subsequently analyzed. The sum of the concentrations of the first two fractions, named as 'mobile' and 'easily deliverable' is considered reflecting the bioavailable (potentially accessible by organisms - bioaccessible) metal concentration in soils. The 'mobile' fraction was extracted using NH_4NO_3 (1 M), for the 'easily deliverable' fraction NH_4Ac (1 M) was used. The other fractions are listed following (extracting agents in brackets): 'Occluded in Mn-oxides fraction' (0.1 M NH_2OH-HCl + 1 M NH_4Ac), 'Organically bound fraction' (0.025 M NH_4-EDTA), 'Occluded in poor-crystalline Fe-oxides fraction' (0.2 M NH_4-oxalic buffer), and the 'Occluded in crystalline Fe-oxides fraction' (0.1 M ascorbic acid in 0.2 M oxalate buffer). The residual bound fraction was calculated by subtracting the sum of the concentrations of fractions I-XI from the total concentrations. Total contents were determined after digestion by a method modified from Grawunder *et al.* (2014). 100-150 mg of the powdered sample (< 63 µm) was digested in a pressure digestion system ('DAS', PicoTrace). The ground material was put in PTFE (TFM™) vessels and 2 ml 65 % HNO_3 (subboiled, Merck), 3 ml 40 % HF and 3 ml 70 % $HClO_4$ (both suprapur, Merck) were added. This mixture was then heated up to 180 °C within 6 h. After maintaining the temperature for 12 h the samples were cooled down. For evaporating the acids, the system was heated up again to 180 °C for 4-5 h in a special evaporating hood maintaining the temperature again for 14 h. The remaining solids were dissolved again after adding 2 ml HNO_3 (subboiled, Merck), 0.6 ml HCl (suprapur, Roth) and 7 ml pure water ('GenPure UV-TOC', Thermo Fisher Scientific) at 150 °C within 8 h. The cooled samples were transferred to calibrated 25 ml flasks ('PMP', Vitlab) and replenished to 25 ml by addition of pure water. The analyses of the soil samples were carried out both with ICP-MS ('X-Series II', Thermo Fisher Scientific) and ICP-OES ('725 ES', Varian) each in triple determination.

The soil water samples, diluted with ultrapure water, were analyzed using with ICP-MS and ICP-OES (same instrumentation as mentioned before).

The biomass samples were analyzed after microwave digestion using heat, over-pressure, and concentrated HNO_3 as solvent. The protocol comprises the following steps: Approximately 200 mg of sample (ground and dried) is suspended with 5 ml concentrated HNO_3 and left for reaction 20 min in open vessels. Then the vessels are closed and heated up to 180°C in a microwave oven ('MARS', CEM Corporation) within 15 min., this temperature is maintained for further 15 min. Afterwards, the samples are cooled down within 30 min. The sample is transferred to a graduated 25 ml PMP flask and filled with deionized water to 25 ml. The sample is then transferred to 50 ml centrifuge tubes and centrifuged at 3000 rpm to get rid of undissolved parts such as silicates. The clear supernatant is then transferred and analyzed by ICP-MS and ICP-OES (same instrumentation as mentioned before).

2.8 Abundance of ECM short root morphotypes and identification of fungal species

2.8.1 Counting, morphotyping, and determination of ECM short root morphotypes

To estimate the degree of mycorrhizal infection (abundance) and the morphologically identification of the ECM fungi short roots, root specimens from the rhizosphere of the trees of each pot as well as from the field site (one pooled sample from the rhizosphere of each pot and one from the field) were taken. After rinsing with deionized water they were densely draped in big water-filled Petri dishes. The mycorrhization rate was estimated by counting short roots and non-mycorrhizal root tips via a binocular microscope that was used for photo-documentation as well (microscope: 'Stemi 2000-C', Zeiss; light source: 'KL1500 LCD', Zeiss; camera: 'Insight 4', Modell 14.2 Color Mosaic, SPOT; image capture software: 'SPOT Advanced' v. 5.1.23, Build 10906). The characterization and identification of short roots morphotypes was carried out following the standard procedure for determination of ectomycorrhizae in the 'Colour Atlas of Ectomycorrhizae' (Agerer, 2012).

2.8.2 DNA isolation, amplification, and sequencing

For genetically identification from each short root morphotype samples were taken and stored in PBS-buffer (per 100 ml: 8.0 g NaCl, 0.2 g HCl, 1.448 g Na_2HPO_4, 0.24 g KH_2PO_4; pH: 7.4) at 4 °C till further processing. For DNA isolation, the PowerSoil DNA Isolation Kit (MO BIO Laboratories Inc.) was used according to the protocol 12888 (MO BIO Laboratories Inc., 2016). To avoid DNA-degradation in the DNA-isolation product (diluted DNA, following named as samples) by DNases the samples were pre-washed with 500 µL Na-EDTA (0.5 M; pH: 8.5). Additionally the samples were incubated at 60 °C for 10 min in a water bath and afterwards stored frozen at -20 °C. To increase the amount of DNA-fragments of the highly conserved ITS region in the rDNA it was amplified with the general primers ITS-1 and ITS-4 by Polymerase chain reaction (PCR). Therefore in each case a 1 µL aliquot of the sample was combined with 33.25 µL distilled water (nuclease free) and 15.75 µL of PCR-mix containing 0.5 µL dNTPs (10 mM), 5 µL Primer ITS-1 (10 mM), 5 µL Primer ITS-4 (10 mM), 5 µL Taq-Polymerase-Buffer and 0.25 µL Taq-Polymerase. Amplification of DNA fragments was carried out using a programmable thermo block (PCR machine: 'UNI II', Biometra,). An initial denaturation step of 5 min at 95 °C was followed by 35 amplification cycles (denaturation: 30 s at 95 °C, annealing: 30 s at 56 °C, extension: 50 s at 72 °C). After the 35 cycles were finished the samples were incubated for additional 10 min at 72 °C and finally cooled down to 4 °C for storage. After amplification the samples were removed from PCR machine and stored at -20 °C. Gel electrophoresis was used to check the PCR product for the amount of amplified DNA. Therefore 1 µL of the PCR product and 5 µL of blue marker were mixed and loaded into the pockets of a 1.8 % Agarose gel. The gel electrophoresis ran 1 h at 100 V, 58 mA (electrophoresis chamber: Cleaver Scientific, Ltd.; power supply: Scie-Plas, PSU 400/600). A size marker (ladder: λ Pst I) was added additionally to the samples separately in one gel pocket. After dying the gel in an ethidiumbromid-bath it was checked for bands in the range of 600-800 bp (base pairs). In the case of a single band in this range each 20 µL of the relative PCR-product sample were sent without any further preparation to a company for purification (PCR-purification

SUPREME, GATC Biotech) and sequencing (Sanger sequencing ABI 3730xl, GATC Biotech). The sequences were then loaded into the BLASTN tool (v. 2.2.29, reference: Altschul *et al.*, 1997) at the UNITE website (database for DNA based fungal species linked to the classification, https://unite.ut.ee/). The sequences were compared with sequences from the databases UNITE (fungi), GenBank, EMBL, and DDBJ. The sequences producing the most significant alignments were listed by score with the attributed species name.

2.9 Sampling and specimen preparation of short root cross-sections

For the µ-PIXE investigations additional short root specimens were collected from the rhizosphere of the test birches (from pot experiment and field site). Each short root morphotype of each tree was sampled separately. Therefore, the roots were washed three times with tap water and following three times with DI-water. The separation of the SR and the determination and differentiation of the morphotypes was carried out under a binocular microscope ('SMZ-143', Motic). They were then stored for the further preparation in droplets of DI-water in petri dishes.

All steps of the specimen preparation were performed after the procedure developed by and described in Vogel-Mikuš *et al.* (2009). After sampling the short roots were transferred to small beds made from aluminium (Al) foil. The beds were filled with tissue freezing medium ('Tissue-Tek O.C.T. Compound', Sakura Finetek) and the short root were placed in the freezing media in an upright position. Following the cups were rapidly frozen in an Al thermo-block that contained liquid propane cooled with liquid nitrogen (LN_2). Thereupon they could be stored for transport or until further processing in a LN_2-cooled Dewar-vessel. For cross-sectioning a cryostat (Leica, 'CM 3050') was used (section thickness: 30 µm, chamber temperature: -25 °C, object temperature: -30 °C). After cutting the cryo-sections were then transferred to special designed stainless steel cups, wherein they were placed between small discs of filter paper and weighted down with a stainless steel cap. From each short root several cross-sections were produced and stacked in the holders between filter papers. For lyophilization (-100 °C; 0.001 mbar) the stainless steel cups with the short roots cross-sections were transferred into a freeze-dryer ('CoolSafe 100-9 Pro', SCANVAC) and left there for 2 days. The freeze-dried specimens were sorted under a binocular microscope ('MZ8', Leica) regarding quality issues like the presence of cracks. Optimally preserved cross-sections of each sample were mounted between 2 Al sample holders with windows that were covered with a c. 200 nm thin foil of Pioloform (SPI Chem). The sample holders were then agglutinated with a 2-component epoxy adhesive ('Araldite').

2.10 Light microscopy and scanning electron microscopy (SEM)

The freeze-dried cross-sections in the Al sample holders were photographed using a fluorescent microscope ('Axioskop 2 mot plus', Zeiss; Camera: 'AxioCam MRc', Zeiss). Images were captured using the program 'Axio Vison' (Rel. 4.8, Zeiss) with 2.5x, 10x and 10.6x magnification, both with reflected visible light source ('KL 750', Schott) and a transmitted UV-light source ('HBO 50', Zeiss). The latter causing an excitation of the sample with two different wavelengths (365 nm and 450-490 nm).

Highly resolved images were captured from one freeze-dried short root cross-section (fungal species: *Melioniomyces bicolor*) using a scanning electron microscope (SEM). Therefore, a tabletop SEM-microscope was used ('TM-1000', Hitachi), the electron beam had an acceleration voltage of 15000 V and an emission current of 59.6mA. Back-scattered electrons (BSE) were detected as the signal.

2.11 Micro-PIXE measurements

The micro-PIXE measurements were performed with a nuclear microprobe at the Institute 'Jožef Stefan' (IJS) in Ljubljana (Slovenia). In the setup at the IJS a hydrogen proton (H^+) beam with an energy of 3 MeV is used as proton source. The whole setup of the micro beam station at IJS with a schematic view is described in Vavpetic *et al.* (2013). The beam is generated in a tandem accelerator from H^--Ions that are accelerated to 1.5 MeV in the middle of the accelerator where a leak valve introduces nitrogen. The H^--Ions collide with the nitrogen molecules and lose 2 electrons. Subsequently the beam is accelerated a second time to an energy of 3 MeV. The proton beam with size of 1 µm is scanned over the sample surface. In total 17 samples were measured (see **Table 2–1**) For the measurements a stage was loaded with the samples and introduced in the vacuum sample chamber (pressure: 6.7 x 10^{-8} mbar). The focusing of the beam on the sample surface is coupled to the focus of a zoom-microscope, which has the same focal plane. The stage could be moved in X-, Y- and Z-direction to position the sample area of interest. The proton beam is scanned over a square-shaped area and 5 detection systems are detecting the induced X-ray and scattered ion events, stamped with the beam position. Two detectors detect the X-ray fluorescence in an angle of 45° against the sample: a silicon drift detector (SDD; Peltier-cooled) for the lighter elements (X-ray energies: from 0.7 to 12 keV) and a high-purity germanium detector for the heavier ones (X-ray energies from 3 to 23 keV, LN_2-cooled). Rotating frequently into the beam, a beam-chopper allows the determination of the proton dose that is necessary for the off-line quantification of elemental concentrations. For scanning transmission ion microscopy (STIM), a modified beam stopper with a 400 nm Al-foil is placed in the beam behind the sample, and scattered protons are detected with silicon detector to determine the energy loss in the sample (Pallon *et al.*, 2009). The measured energy loss allows the determination of the sample thickness. The fifth detector is an elastic BSE-detector which gives information on the carbon-nitrogen-oxygen-ratios in the sample. The individual measurement frames consist of 256x256 pixels. The size of each pixel in the element map depends on the size of the selected area of interest on the sample. The average limits of detection (LODs) calculated from particular LODs of the particular measurements are given per element in **Table 2–2**.

Ectomycorrhiza fungal species	Growing site	Sample number
Meliniomyces bicolor	Pots	8
	Field	2
Cenococcum geophilum	Pots	4
	Field	1
Pisolithus tinctorius	Pots	0
	Field	2

Table 2–1 List of 17 samples analyzed by micro-PIXE. The samples differed regarding the fungal species colonizing the mycorrhizal roots and the growing site of the birch trees.

Table 2–2 Mean detection limits (LOD) in of the micro-PIXE measurements calculated from particular LODs of the single measurements. n represents the number of single values introduced into the mean; n differs because not all elements were detected in each sample.

	Al	Ca	Cu	Fe	K	Mg	P	S	Si	Ti	Zn
Average LOD [µg g^{-1}]	64	39	10	9	47	54	44	46	58	13	21
n	17	17	17	16	17	16	15	17	17	17	16

2.12 Data processing, data analysis and statistics

The XRD data (provided as data matrix of 2theta angle vs. count-rate) were plotted using the program OriginPro (v. 9.0.0, OriginLab Corporation) as a line diagram. The physico-chemical data, the in-situ redox, as well as the metal concentrations of the substrate solution were displayed as depth resolved plots for each sampling date separately using the freeware PanPlot (PANGEA, Alfred Wegner Institute for Polar and Marine Research). Afterwards plots of eight representative sampling dates evenly spread over the duration of the pot experiment were compiled for each metal using the graphic suite CorelDRAW X6 (v. 16.4.1.1281, Corel Corporation). The means given in this work were calculated as arithmetical means in any case, the data processing and plotting of bar and column diagrams was done by the spreadsheet program Microsoft Excel 2010. The data obtained from the pot-experiment monitoring were transformed before plotting: The hourly logged temperature data as well as the irregularly measured water use and soil moisture tension were merged to weekly means to fit the same time axis. The standard deviations (SD) of the ICP-MS and ICP-OES analyses (biomass and post-experiment substrate samples) were calculated from triple determination of the same sample using the following formula (function 'STABW.S' in Microsoft Excel 2010):

$$SD\ (sample) = \sqrt{\sum (x - \bar{x})^2/(n-1)}$$ (x … *arguments,* $\bar{x}$ … *mean of a sample,* n … *sample size*)

The standard deviations of the analyses of separate samples measured as replicates (triplicate samples of the initial substrate; biological replicates of three birches per pot) were calculated using the following formula (function 'STABW.N' in Microsoft Excel 2010):

$$SD\ (population) = \sqrt{\sum (x - \bar{x})^2/(n)}$$ (x … *arguments,* $\bar{x}$ … *mean of a population,* n … *sample size*)

All acquired analytical data of the metal concentrations in the substrate solution, in the biomass, and in the substrate samples are provided digitally as Excel-files on the data carrier attached to this work (inside of back cover).

The acquired data of the micro-PIXE measurements were analyzed by the program GeoPIXE (CSIRO Earth Science and Resource Engineering). First the spectra of the chopper were used to calculate the proton dose. The thickness and the matrix composition are deduced from STIM and EBS spectra. The X-ray intensity maps are then transformed into quantitative elemental maps. Na was not considered for the maps due to high background by the overlap of the weak Na-signal with the Bremsstrahlung-Peak in the spectra. Furthermore an overlap of the Na K-line with the Zn L-line in the spectra is another possible interference, so only X-ray fluorescence lines above 1.3 keV were taken into account. The elemental concentration maps were saved then as concentration matrices in CSV-file format. Quantitative element distribution maps were produced for each element and individual sample by GeoPIXE software.

For the extraction of average concentrations from the short root tissues hyphal mantle, cortex with Hartig net, and the central cylinder from the concentration matrices the program ImageJ v1.49 (National Institute of Health, USA) was applied. With the tool 'ROI manager' it is possible to distinguish the tissues from each other by masking (**Figure 2–9** illustrates the ROI masking using a STIM density map). Besides the Si concentration distribution maps also microscopic images with different light sources and the STIM density maps were used to distinguish between the different compartments.

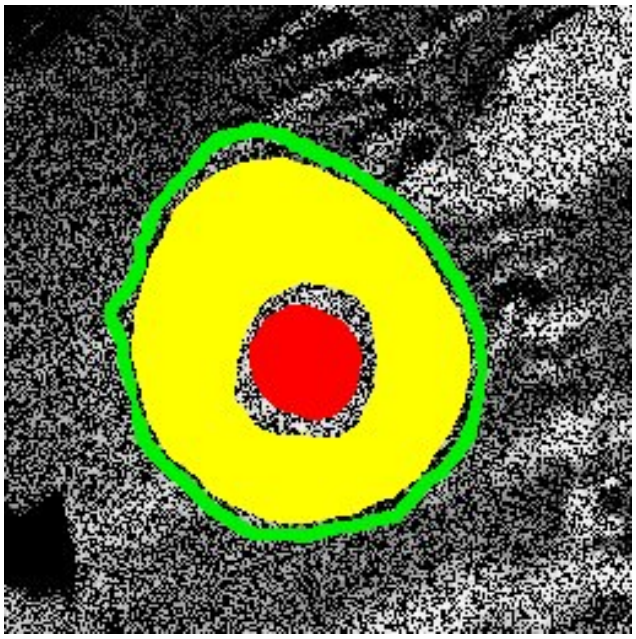

Figure 2–9 Selection and masking of the regions of interest (ROI) using the STIM density map: hyphal mantle - green, cortex with Hartig net - yellow, central cylinder- red; Image size: 200 x 200 µm

From all data points lying within the masked areas the average concentrations were calculated (tool 'Measure' in 'ROI Manager'). The results were saved as a matrix-dataset: the elemental concentrations (columns) of the different tissues for each single sample (rows). In the cases that concentrations were below the detection limit (average LODs; see **Table 2–2**) the missing values were replaced with a random number between 0 and the LOD assigned to the particular measurement of the sample. Variables (elements) with more than 25 % lacking data due to concentrations below the LOD were excluded from the dataset. As pre-preprocessing for the following statistics, the concentration data were Z-standardized (column wise per element) using the following formula:

$$Z = (X - \mu) \cdot \sigma^{-1}$$ (*Z: standardized concentration; X: concentration of an individual sample; µ: mean concentration of all samples*; σ: *absolute standard deviation of all samples*)

All pre-processing of micro-PIXE concentration data was performed in Excel 2010 (Microsoft). The dataset after pre-processing was plotted as box-plots using OriginPro, that illustrates graphically different statistics and the range of the dataset. Enhanced heat mapping combined with cluster analysis was performed with the program RStudio v0.99.902 with R v3.3.0 as socket (The R Foundation of Statistical Computing). For the cluster analysis the squared Euclidean distance measure and the clustering method of Ward were chosen. The variables (elements) and observations (standardized concentrations of the different tissues of each sample) were reordered regarding their similarity (the more similar the closer together). The calculated clusters were plotted as dendrograms above and sidewise the heatmap. Color coded row side bars were assigned which allow the characterization of each sample regarding growing site, ECM species, and short root compartment. Furthermore two discriminant analyses (DA) were performed using the non-standardized compartment concentrations extracted from the quantitative elemental PIXE-maps by ROI-masking. Again variables with more than 25 % lacking data were excluded from the dataset and otherwise replaced by values between 0 and the LOD. Both DAs were performed by XLSTAT software (Version 2014.5.03, Addinsoft SARL). Within-class covariance matrices were assumed to be different, confirmed each by Box tests (Chi-square asymptotic approximation, Fisher's F asymptotic approximation). Prior probabilities were not taken into account, the significance level was 5 %, and the classes' weight correction was set to 'Automatic'.

3 RESULTS

3.1 Soil properties, mineralogy, physico-chemistry, and element concentrations of the study site substrate

The substrate from the 'Kanigsberg' study area was described as anthropogenic topsoil. It originated not from the pristine intact soil surface but from the basement of the removed heap. It was carbonate free, low to moderate humic, and had a moderate yellowish brown color. The soil type was classified as sandy loamy silt, with a high percentage of gravel and blocks originating from the coarsely weathered Paleozoic slate (base rock) as well as representing relicts of the waste rock deposited on the former heap. The TC content was 0.27 ± 0.14 g kg^{-1}, the SiO_2-content and S concentrations, both analyzed by XRF, were rounded 80 % and 1800 mg kg^{-1}. The k_f-value of the undisturbed substrate from the field was 4.9 10^{-5} m s^{-1} and the ODD (determined for the fine soil fraction < 2 mm) was 1.51 g cm^{-3}. The pF-water saturation-curve in **Figure 3–1** shows the relationship between the water content and the matric potential for the initial substrate used in the pot experiment (after sieving < 2.8 mm and homogenization). The standard pF-ranges for field capacity (FC), FC_{eff}, and permanent wilting point (PWP) as parameters characterizing the water supply properties of substrate were adapted from Blume *et al.* (2016).

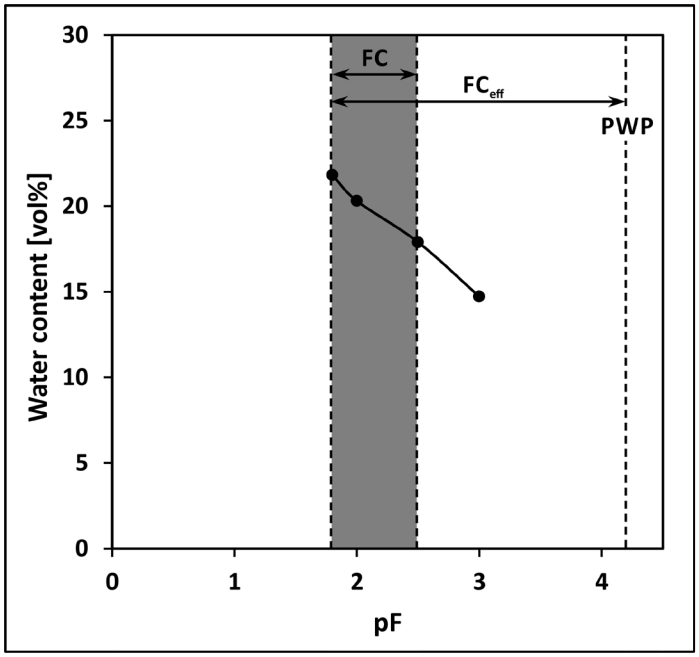

Figure 3–1 The pF-water saturation-curve shows the relationship between the water content and the matric potential for the initial substrate used in the pot experiment (< 2.8 mm). The pF-value corresponds to the logarithmic total value of matric potential (in hPa or cmH_2O). The standard pF-ranges for FC, FC_{eff}, and PWP were adapted from Blume *et al.*, 2016. FC - field capacity, FC_{eff} - Effective field capacity, PWP - permanent wilting point.

The initial substrate (< 2.8 mm) consisted mainly of the mineral quartz (high peak at 27 ° 2θ and several smaller peaks, **Figure 3–2**) as expected from the XRF analysis that revealed a SiO_2-concentration of almost 80 %. Furthermore, lower percentages of illite and muscovite (which cannot be distinguished from each other in the XRD-spectrum) and feldspars were abundant in the sample.

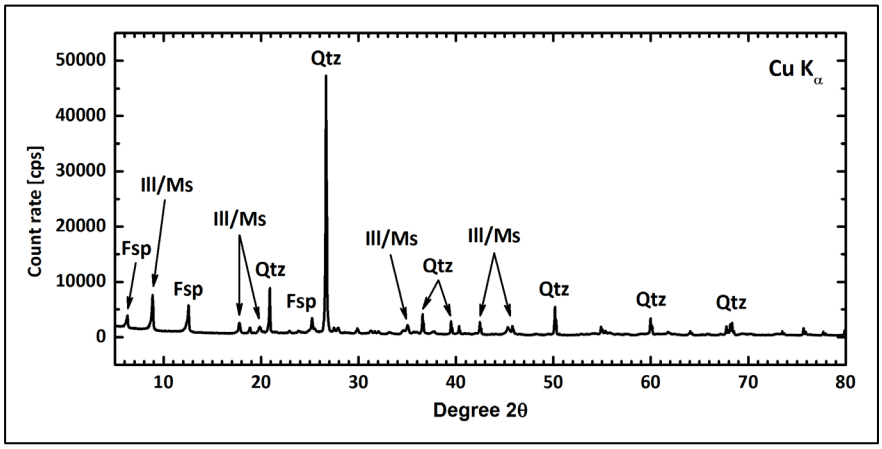

Figure 3–2 XRD-spectra of a sample from the substrate (sieved < 2.8 mm and homogenized) that was used in the pot experiment; mineral name abbreviations: Fsp - feldspars, Ill/Ms - illite/muscovite (peaks cannot be separated), Qtz - quartz; XRD-parameters: Cu Kα-radiation, Energy 40 mA at 40 kV, 5-80° 2θ (2-theta angle) in 0.02° steps, 0.5 s measuring time per step.

The field substrate from the study area before sieving consisted to c. 66 wt% of coarse-grained particles (> 2 mm) and to 34 wt% of fine soil fraction (< 2 mm). After sieving (< 2.8 mm) the initial substrate used for the pot experiment consisted to c. 9 wt% of fine gravel, 46 wt% of sand, and c. 45 wt% of silt/clay (see **Figure 3–3**, upper diagram). The fraction of silt/clay consists to c. 86 vol% of silt and c. 14 vol% of clay as determined volumetrically by laser particle sizer (**Figure 3–3**, lower diagram with blue background).

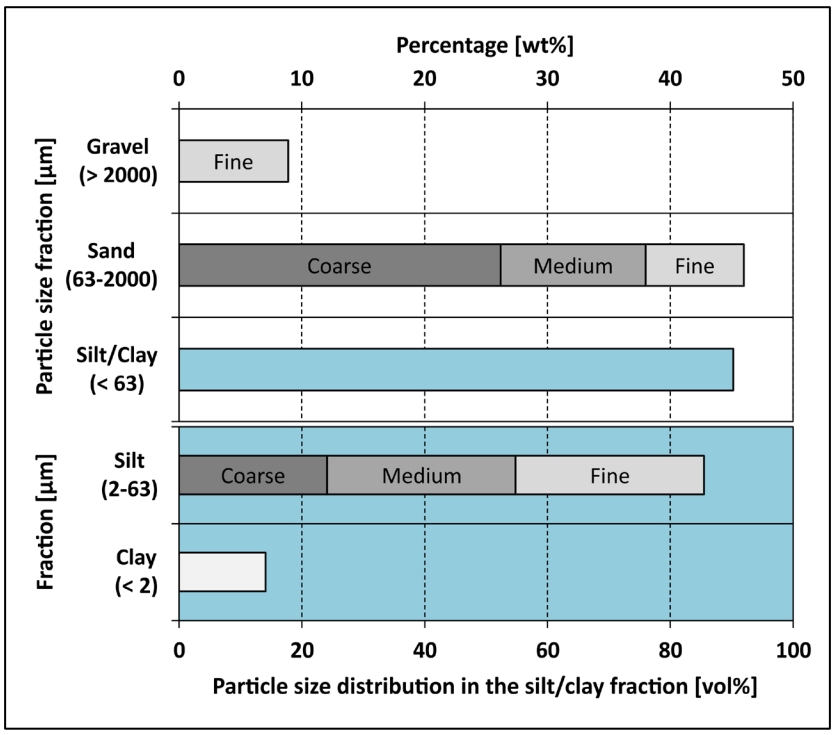

Figure 3–3 Diagram of the particle size fractions of the initial substrate (< 2.8 mm) as determined by wet sieving and weighting (upper diagram, assigned to the upper X-axis). The classification by particle size into the fractions gravel, sand, silt, and clay and their sub-classes was conducted according to the German nomenclature (Blume *et al.*, 2016). The particle size distribution within the silt/clay fraction was determined volumetrically by laser particle sizer and is displayed in the lower diagram with blue background (referred to the fraction < 63 µm from wet sieving, assigned to the lower X-axis)

The substrate had an acidic pH (measured in ultrapure water: 4.17 ± 0.01) and a low electrical conductivity (EC: 77.7 ± 0.5 µS cm^{-1}), the CEC_{eff} was 4.22 cmol kg^{-1}. The total concentrations (**Table 3–1**) of Ni, Ti, and Zn were at least as high or double the mean concentrations in European subsoils (Salminen *et al.*, 2005). The levels of Al, Fe, K, P, and U were between three and four times higher and Cu had almost fivefold the concentration of the reference value from the literature (same reference as before). Cr, Cu, and Ni exceeded the precaution values for silt soil type of the German soil protection regulation (BBodSchV, 1999). The bioavailable concentrations were low except for Al and Cu.

Table 3–1 Total concentrations of selected elements in the initial substrate (used for the pot experiment) and reference values; bioavailable (potentially bioaccessible) concentration: sequential extraction of the mobile and specifically adsorbed elements (together considered as bioavailable fraction in soils) of the substrate samples with NH_4NO_3 and NH_4Ac (method by Zeien & Brümmer, 1989); Total concentration: total digestion of substrate samples with HNO_3 (65 %), HF (40 %), and $HClO_4$ (70 %) (modified from Grawunder *et al.*, 2014); Mean values of European subsoils: digestion of soil samples with HNO_3 (65 %), HF (40 %), and $HClO_4$ (70 %); for Cu and Ni analysis the digestion was carried out without $HClO_4$ (Salminen et al. 2005); Metal precaution values for silt soil type from the German soil protection regulation after aqua regia digestion (HNO_3 and HCl) of soil samples (BBodSchV 1999); n.a. no regulation value available.

[µg g^{-1}]	Al	Ca	Cr	Cu	Fe	K	Mg	Na	Ni	P	Ti	U	Zn
Bioavailable concentration	276	87	0.1	14	6.1	27	10	< 7.5	0.5	< 12	< 0.4	0.8	5.1
Total concentration	85142	455	62	86	54884	29753	8345	1387	91	724	6606	6.8	115
Mean values of European subsoils	29639	31732	87	17	14164	8841	8504	9273	39	253	3531	2.5	61
Precaution values for Germany	n.a.	n.a.	60	40	n.a.	n.a.	n.a.	n.a.	50	n.a.	n.a.	n.a.	150

3.2 Temporal developing of soil moisture tension and water use

The soil moisture tensions measured by the manual tensiometers represent absolute values of the substrate matric potentials. They showed high fluctuations over the period of the pot experiment in all pots (measured in a depth of 10-15 cm b.s.s.; see **Figure 3–4**). Especially in the period between the weeks 35 and 48 the minima and maxima tensions differed strongly by c. 400-450 cmH_2O. This might be referred to the longer intervals between the watering events due to the reduced water use in the dormancy period (weeks 25-44). Typical tensions were between c. 50-200 cmH_2O, corresponding to the range of field capacity (pF 1.8-2.5). Generally the values are lower in the control pot compared to the other three pots, especially in the second growing season (week 45-67). Comparing the planted pots Pot 1 frequently reached the highest tensions and the discrepancies between the values increased within the second growing season. The measurements were not conducted continuously but scheduled directly before watering of the pots. Therefore the curves represent the maximum tensions under the driest soil moisture conditions of the distinct date.

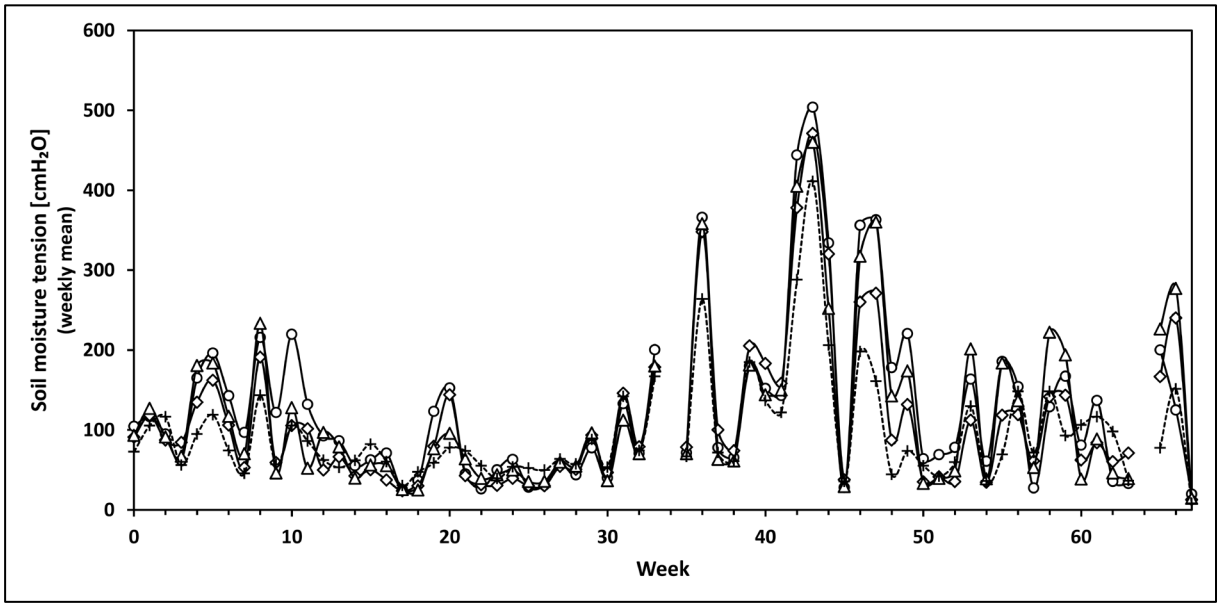

Figure 3–4 Soil moisture tension curve of the substrate in the four pots within the duration of the pot experiment including two growing seasons (week 0-24 and 45-67) and one dormancy (week 25-44). The continuous lines with the symbols display weekly means of maximum values of the planted pots (circles: Pot 1, diamonds: Pot 2, triangles: Pot 3) while the dotted line with crosses represents the data of the control pot. The non-continuously measurements were scheduled always before watering and reflect therefore the lowest water saturation conditions of the distinct date. The soil moisture tension was determined indirectly by forming absolute values from the negative pressure measured in the mechanical tensiometers. The porous ceramic cells of the tensiometers were installed with hydraulically connection to the substrate (depth: 10-15 cm b.s.s.). Lacking data points are due measuring gaps in the weeks 34 and 64. The lines connecting the data points were smoothed by the software (Microsoft Excel 2010).

The water use of the pots depended strongly on the air temperature in all pots. The water use was higher during the growing seasons than in the dormancy due to higher air temperatures that cause an increase of the transpiration of the planted birch trees of Pot 1-3 as well the evaporation of all pots including the control. In the growing seasons the planted pots have clearly a higher water use than the control, in the dormancy there is no obvious effect of the plantation and the water use curves of all four ports overlay each other. The water use of the planted pots in the second growing season is higher than in the first one whereas that of the control pot is equal or even slightly lower. Moreover in the second growing season the water usages of the planted pots deviated more distinct from each other than in the first one. Comparing the three planted pots Pot 3 had the highest water demand.

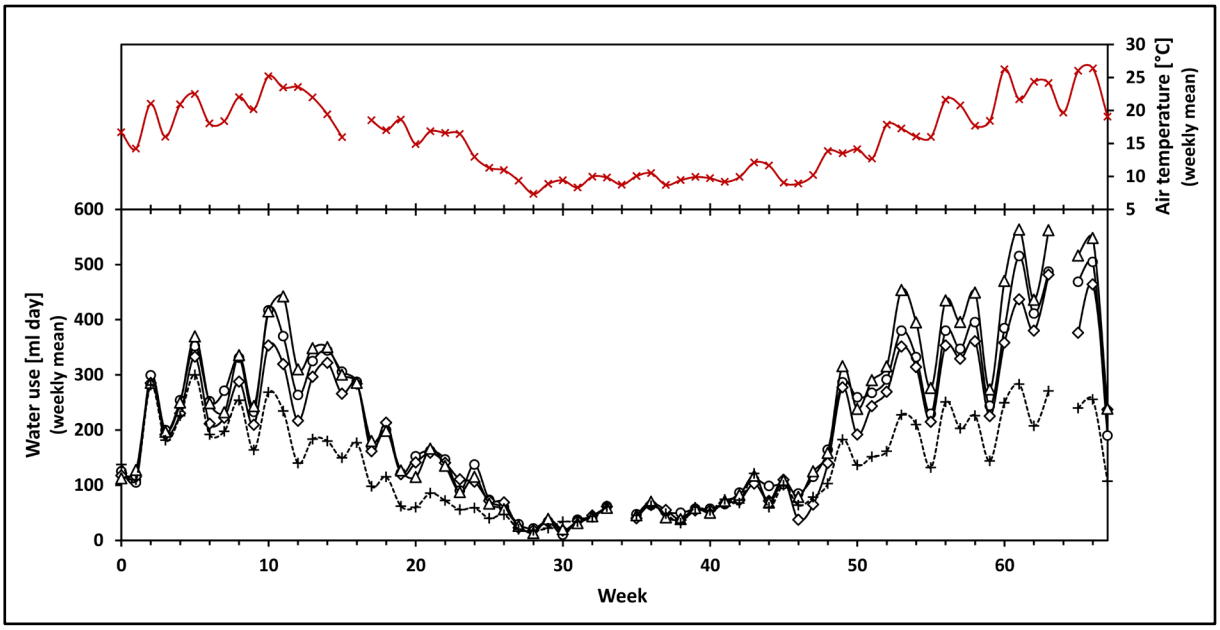

Figure 3–5 Mean water use and mean air temperature of the four pots within the experimental duration including two growing seasons (week 0-24 and 45-67) and one dormancy (week 25-44). The continuous black lines with symbols display weekly means of the water use of the planted pots (circles: Pot 1, diamonds: Pot 2, triangles: Pot 3) while the dotted black line with crosses represents the data of the unplanted control pot. The continuous red line with the diagonal crosses in the upper part of the diagram indicates air-temperature weekly means. The water use was measured 1-2 times the week by weighting; the air temperature was logged hourly. Those data were used to calculate the weekly means which may cause a shift of the non-continuous measured water use against the continuously-logged temperature curve. All lines connecting the data point were smoothed by the software (Microsoft Excel 2010).

3.3 Temporal developing of physico-chemistry and concentrations of metals and plant macro-nutrients in the substrate solution

The physico-chemistry of the substrate solution showed depth dependent alterations with ongoing duration of mesocosm pot experiment and differed strongly between the three planted pots and the unplanted control. The pH at the beginning of the pot experiment (week 0, see diagram **(a)** in **Figure 3–6**) was around 4.1 over the entire depth of the pots with no significant differences between the planted pots and the control. In the further progress of the experiment (week 9, diagram **(b)**) the pH decreases with increasing depth in all pots to minimum 3.7 in 38 cm b.s.s. From week 18 until the end of the experiment in week 67 (diagrams **(c)**-**(h)**) the pH in the planted pots is higher than in the control except in 38 cm depth. In this depth, the pH is equal between all pots or minimally higher in the planted ones. In the control pot the pH decrease with greater depth is more linear, whereas in the planted pots the pH is buffered and decreases slower. From the beginning of the dormancy until the start of the second growing season (week 28-47, diagrams **(d)**-**(f)**) the curves of the two treatments converged again: Over the entire depth the pH in the Pot 4 increased slightly and decreased in the planted pots 1, 2, and 3. Then, with the beginning of the second growing season until the end of the experiment (week 47-67, diagrams **(f)**-**(h)**), this effect is reversed again and the lowest pH of c. 3.6 is reached in the control pot in 31 cm depth in week 67. Furthermore, the curves of the planted pots start to diverge from each other, showing a more individual pH trend. During this last period of

the experiment Pot 1 had the highest pH of all planted pots (maximum 0.2 units higher than in the other two pots).

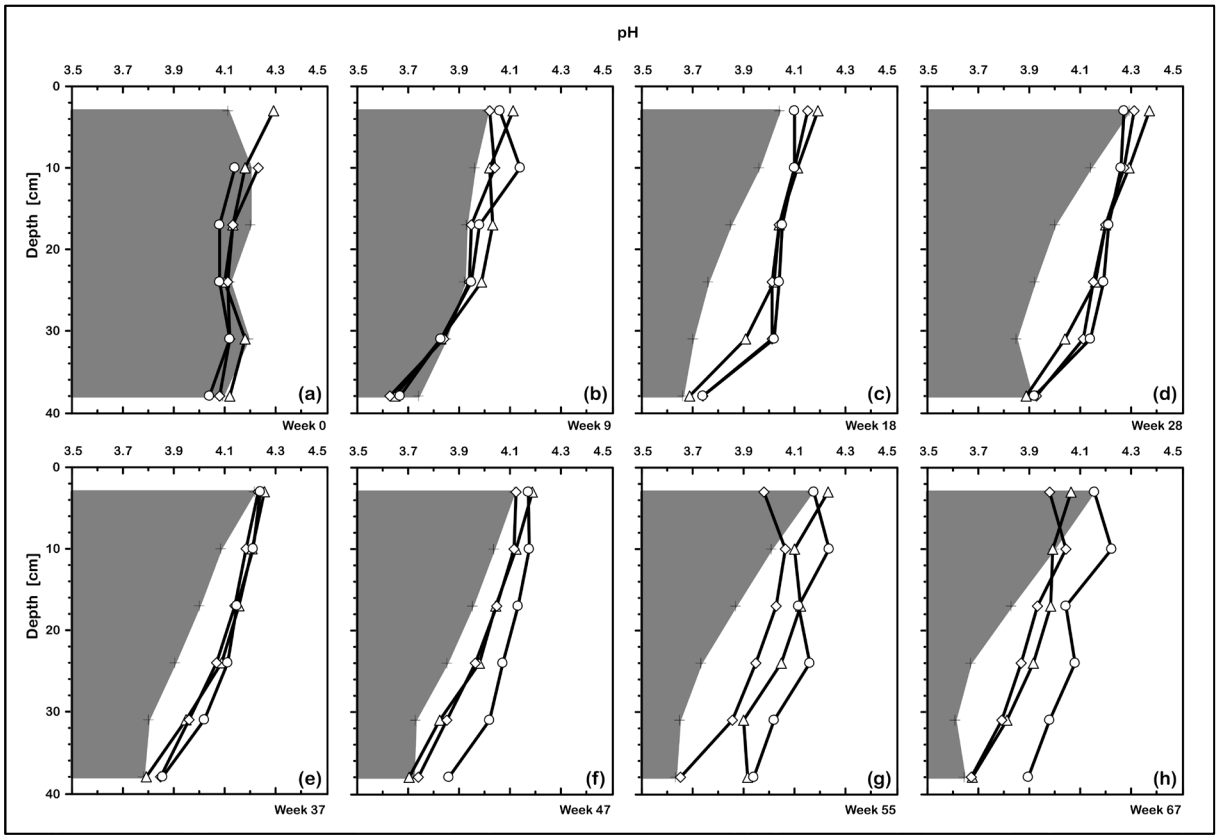

Figure 3–6 Temporal development of the substrate solution pH in the pots planted with birch and the unplanted control pot in different depths (3, 10, 17, 24, 31, and 38 cm b.s.s.). Symbols connected by lines indicate the data points of the planted pots: *Circles* - Pot 1, *Diamonds* - Pot 2, *Triangles* - Pot 3. C*rosses margining the grey colored area* indicate the data of the unplanted control (Pot 4). The diagrams **(a)**-**(h)** display representative time slices of the substrate solution monitoring during the pot experiment (week 0 to week 67) including two growing seasons and one dormancy. The first growing season lasted from week 0 to 24 (diagrams **(a)**-**(c)**), the dormancy from week 25 to 44 (diagrams **(d)**-**(e)**), and the second growing season from week 45 to week 67 (diagrams **(f)**-**(h)**). Lacking data points (e.g. Pot 1 and Pot 3 in 3 cm b.s.s.) are due to too less substrate solution volume gained on the particular sampling day. Backwater formation was avoided due to not exceeding a water saturation corresponding to 50 % effective field capacity. Small volumes of leachate formed in each pot within the duration of the pot experiment were drained of by the lysimeter bottom with minimally sorption.

Weekly means of the redox potential (Eh) logged hourly in-situ in the substrate in three different depths per pot (10, 24, and 38 cm b.s.s) are displayed in **Figure 3–7**. The figure shows six representative time slices covering the duration of the pot experiment. At the beginning of the pot experiment (week 0, diagram (a)) the Eh was constantly between 700-750 mV, independent from the depths and irrespective whether the pots were planted. In the further progress of the experiment (week 9-67), diagram (b)-(h)) the Eh decreased in 24 cm b.s.s. in Pot 2 to c. 625 mV as well as in 38 cm in Pot 3 to 600 mV whereas the Eh values in Pot 1 and Pot 4 remained constant over the entire depth. The trends described for Pot 2 and Pot 3 intensified with ongoing duration of the pot experiment whereas the Eh in the other two pots just slightly decreased with greater depths. An influence of the tree plantation on the Eh of the substrate solution was not recognizable. The deviating redox-values in

the Pot 2 (38 cm b.s.s.) and Pot 3 (24 cm b.s.s.) might be related to oxygen-consuming processes taking place on a small scale in the direct vicinity of the redox probe's tip. These could be locally occurring pyrite oxidation of a pyrite rich substrate grain, root respiration, or decomposition of soil organic matter by microorganisms. These data points are therefore considered as outliers.

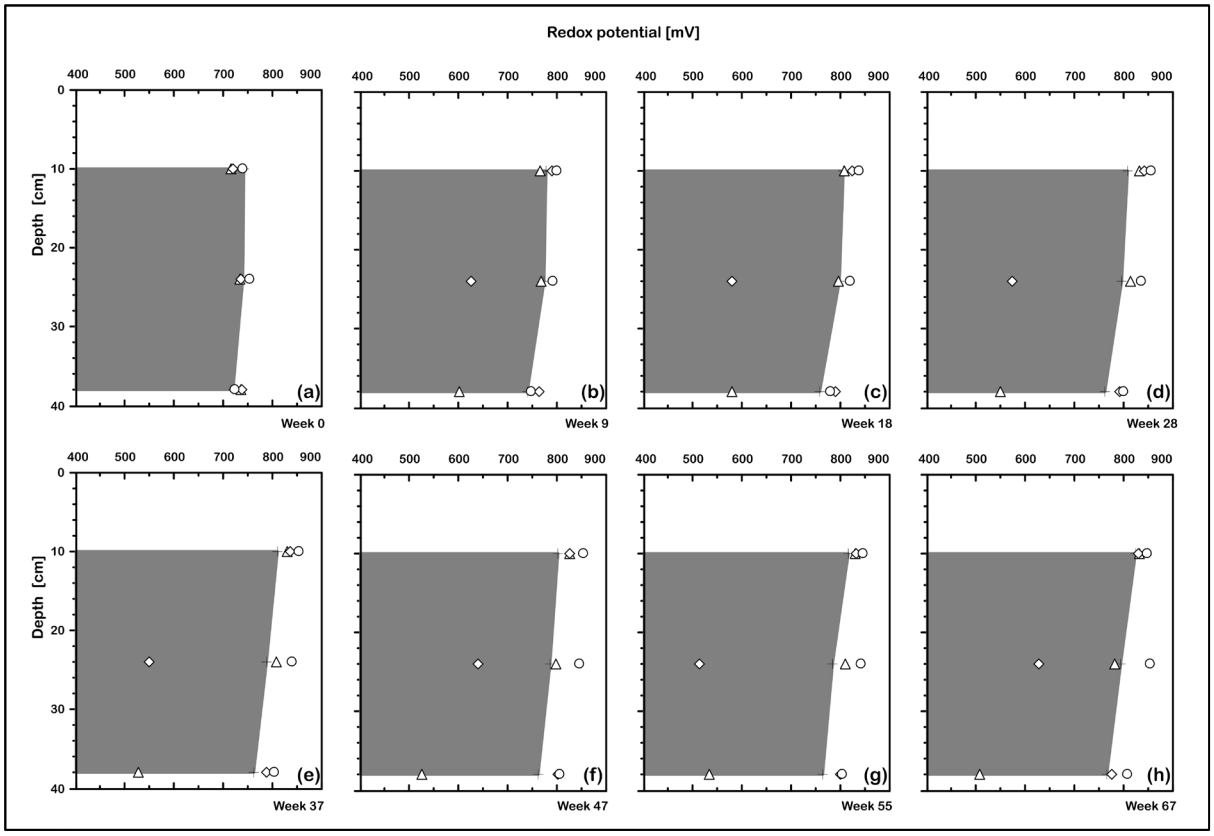

Figure 3–7 Temporal development of the redox potential (Eh) measured in-situ in three different depths (10, 24, 38 cm b.s.s.; the Ag/AgCl-reference electrode was installed in 38 cm b.s.s.) in the substrate of pots planted with birch (*Circles* - Pot 1, *Diamonds* - Pot 2, *Triangles* - Pot 3) and the unplanted control pot (*Crosses margining the grey colored area* -Pot 4). The diagrams **(a)**-**(h)** show representative time slices of Eh weekly means calculated from the Eh data logged hourly during the pot experiment including two growing seasons (first: diagrams **(a)**-**(c)**; second: diagrams **(f)**-**(h)**) and one intermediate dormancy (diagrams **(d)**-**(e)**). The measured Eh-values were referred on standard hydrogen electrode by adding a correction factor of +207 mV.

The Al concentrations in the substrate solution at the beginning of the pot experiment ranged from 500 to 2000 µg L^{-1} with a slightly trend to higher concentrations with greater depths (**Figure 3–8**, diagram **(a)**). With ongoing duration of the first growing season and the beginning of the dormancy (week 9-28, diagram **(b)**-**(d)**) the Al concentrations in greater depths increased strongly especially in the control pot. Therein the highest levels of c. 25,000 µg L^{-1} were reached in 38 cm b.s.s. (week 28, diagram **(d)**).During the dormancy and the beginning of the second growing season the Al curves of the planted pots and the control converged: While the Al levels in the planted pots increased in shallow depths, those of the control decreased (week 37-47, diagrams **(e)**, **(f)**). With the beginning of the second growing season until the end of the experiment the Al concentrations in the control pot stayed relatively constant with a strong increase from smaller to greater depths. In the same period the concentration curves of the planted pots diverge from each other. Compared to the Pots 2 and 3

Pot 1 shows the lowest Al levels over the entire depth, similar to the initial concentrations at the beginning of the experiment. In the control the concentration range covered more than two orders of magnitude (c. 2,000-24,000 µg L^{-1}) between the shallowest and the deepest measuring point.

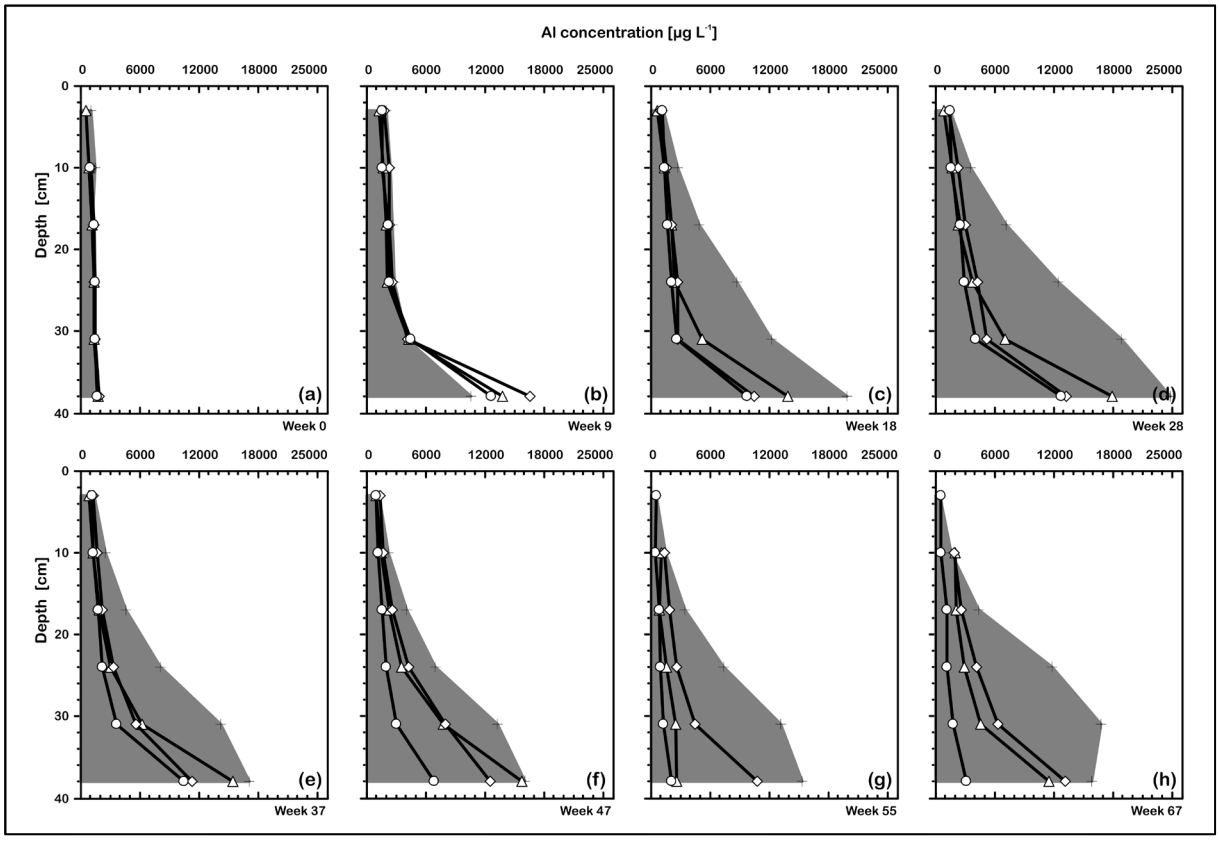

Figure 3–8 Temporal development of the substrate solution Al concentrations in different depths of the planted pots (symbols: *Circles* - Pot 1*, Diamonds* - Pot 2, *Triangles* - Pot 3) and the unplanted control pot (*crosses margining the grey colored area* - Pot 4). The diagrams **(a)**-**(h)** display representative time slices of the substrate solution monitoring during the pot experiment including two growing seasons (first: diagrams **(a)**-**(c)**; second: diagrams **(f)**-**(h)**) and one intermediate dormancy (diagrams **(d)**-**(e)**).

The Cu, Fe, Ni, and U concentrations in the substrate solution in different depths showed the same trends as described for Al over the duration of the pot experiment (Cu: **Figure 3–9**, Fe: **Figure 3–10**, Ni: **Figure 3–11**, U: **Figure 3–12**, Zn: **Figure 3–13**). The Cu concentrations in the control pot were about one order of magnitude higher (500-4,500 µg L^{-1}) compared to those of Ni (50-350 µg L^{-1}) and Fe (10-30 µg L^{-1}) comparing the extrema in the control pot from the shallowest to the greatest depth in week 28. The U concentration extrema in the control pot ranged from 2-10 µg L^{-1}, those of Zn were in the range of 500-5,000 µg L^{-1}. Like in the case of Al, the Cu, Fe, Ni, U, and Zn levels in the planted pots were constantly lower over the entire depth except in 38 cm b.s.s. in the first growing season. During this period of the experiment their concentration curves plotted closely together and then diverged from the end of the dormancy onwards. The Cu, Fe Ni, and U concentrations were the lowest in Pot 1 compared to the other two planted pots during the last part of the experiment. Fe showed some outliers at the beginning and at the end of the experiment in some depth of the planted pots. It was assumed that this could have been contaminations occurred during sampling.

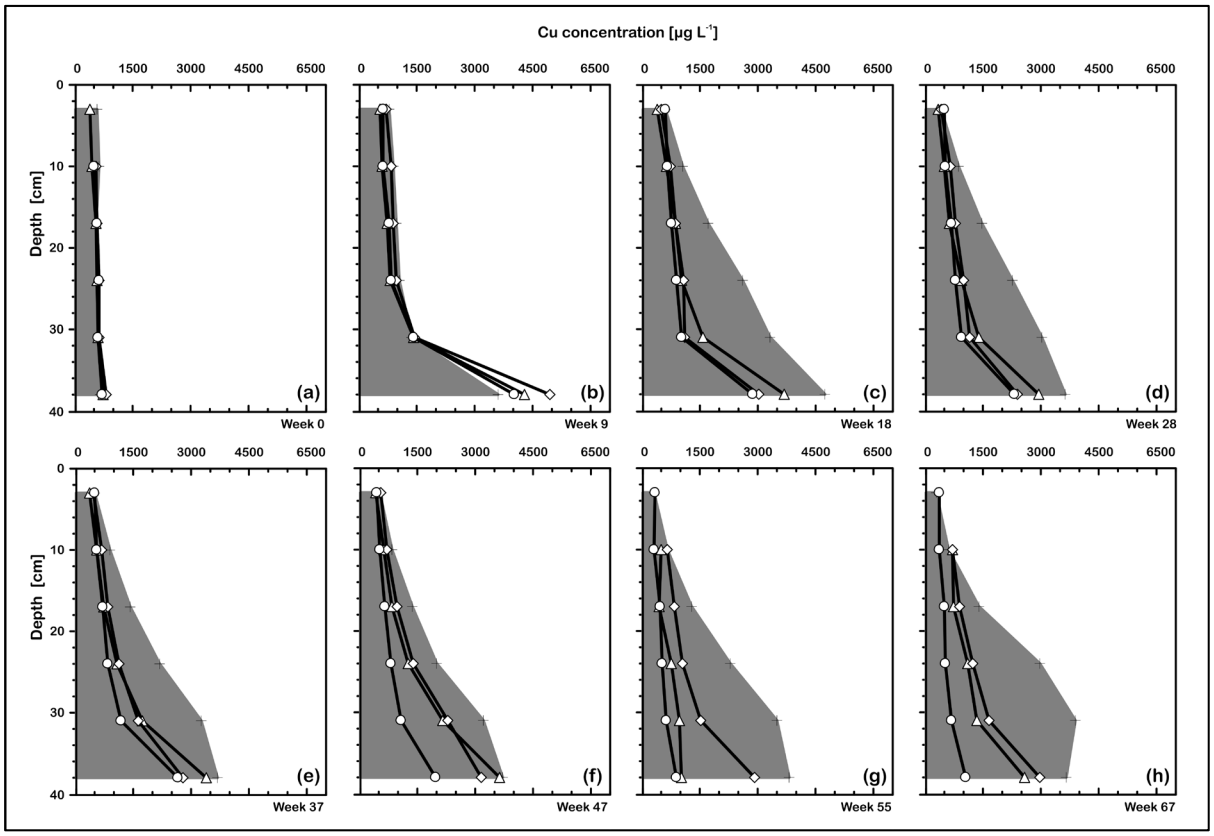

Figure 3–9 Temporal development of the substrate solution Cu concentrations in the four pots in different depths (*Circles* - Pot 1*, Diamonds* - Pot 2, *Triangles* - Pot 3, *Crosses margining the grey colored area* - Pot 4).

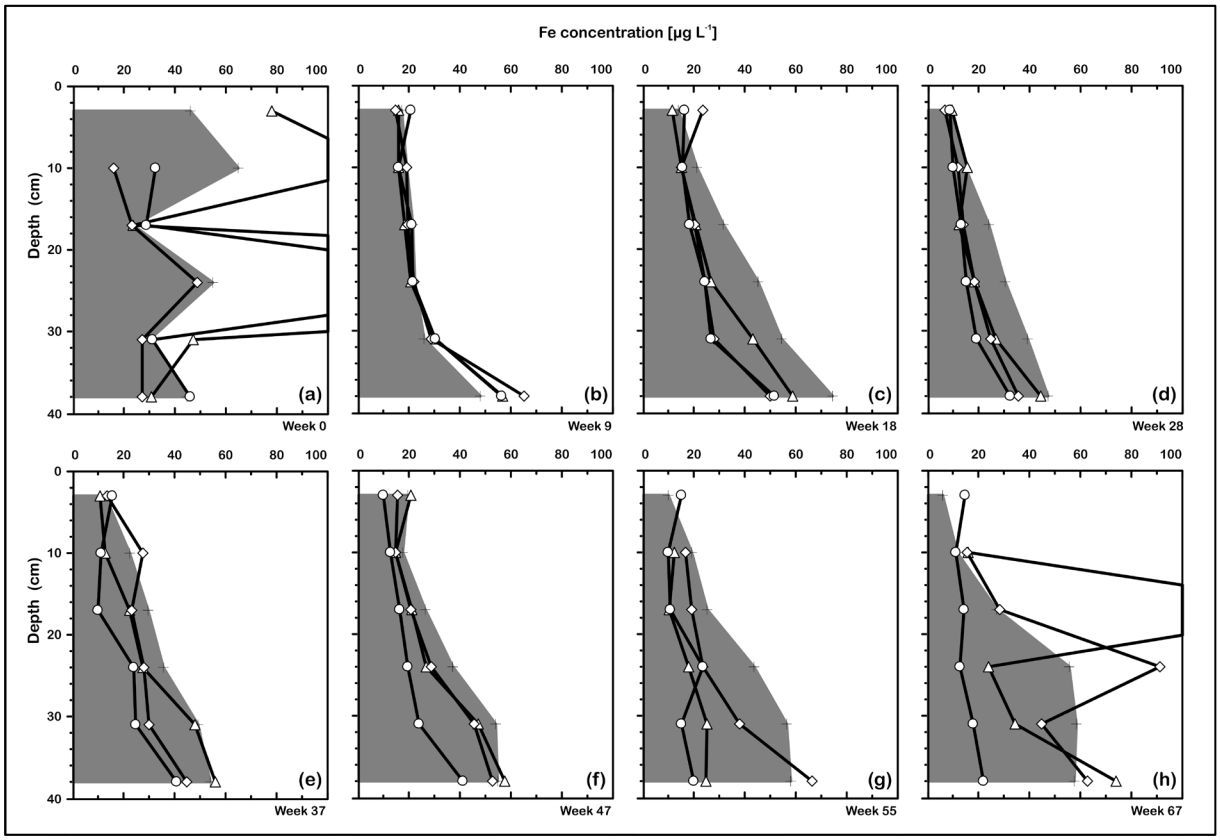

Figure 3–10 Temporal development of the substrate solution Fe concentrations in the four pots in different depths (*Circles* - Pot 1*, Diamonds* - Pot 2, *Triangles* - Pot 3, *Crosses margining the grey colored area* - Pot 4).

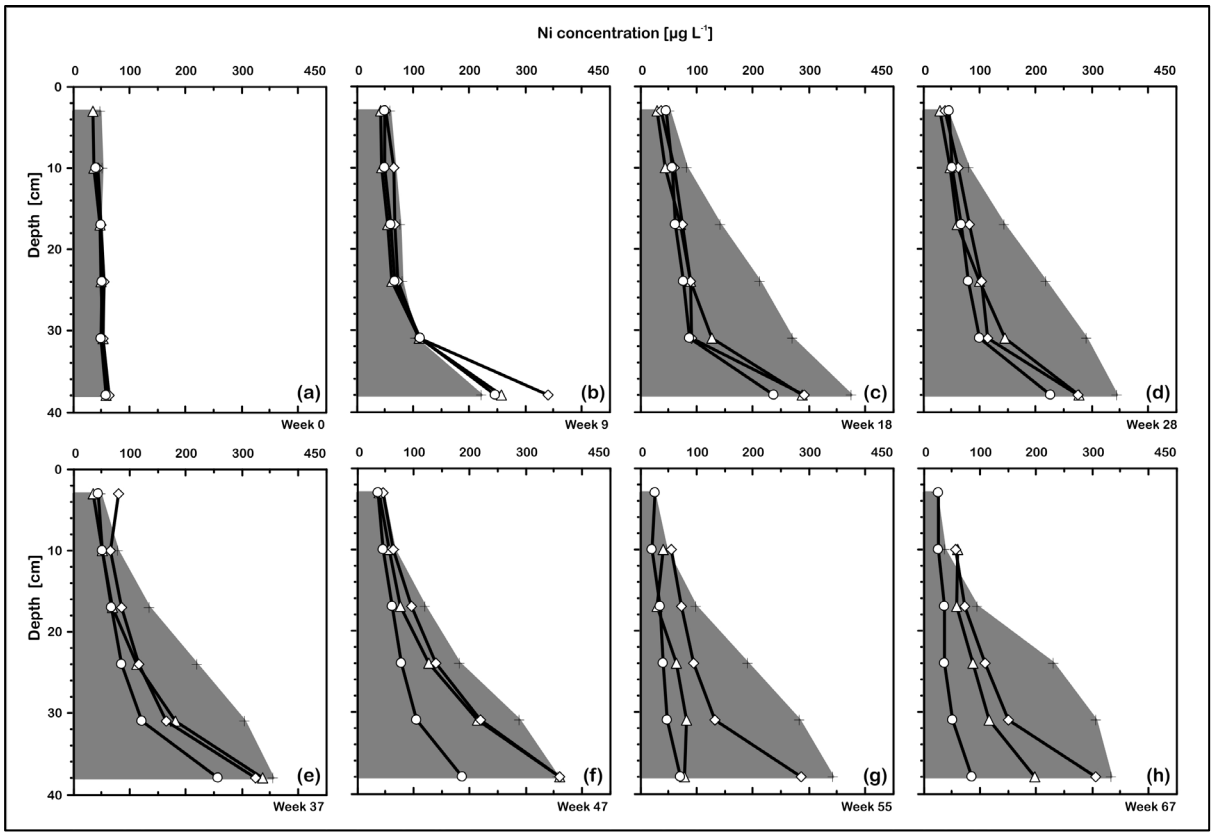

Figure 3–11 Temporal development of the substrate solution Ni concentrations in the four pots in different depths (*Circles* - Pot 1*, Diamonds* - Pot 2, *Triangles* - Pot 3, *Crosses margining the grey colored area* - Pot 4).

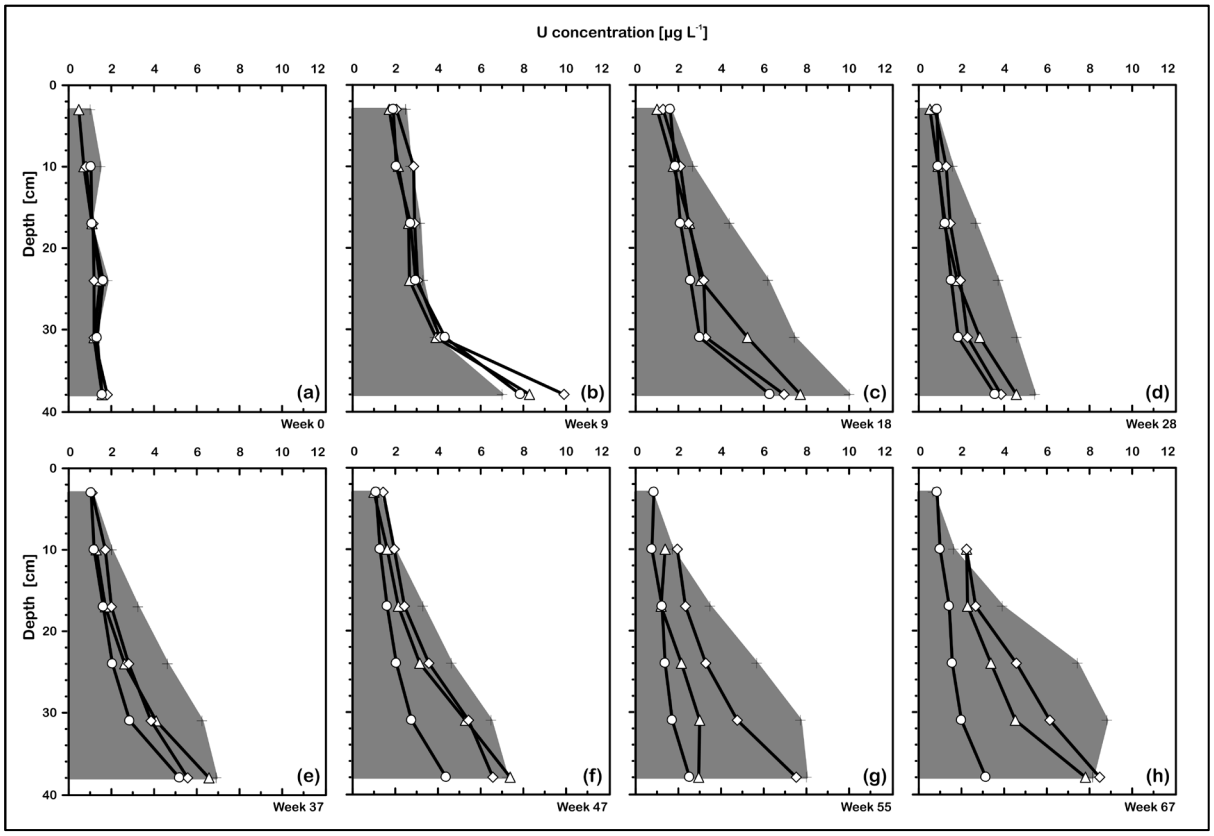

Figure 3–12 Temporal development of the substrate solution U concentrations in the four pots in different depths (*Circles* - Pot 1*, Diamonds* - Pot 2, *Triangles* - Pot 3, C*rosses margining the grey colored area* - Pot 4).

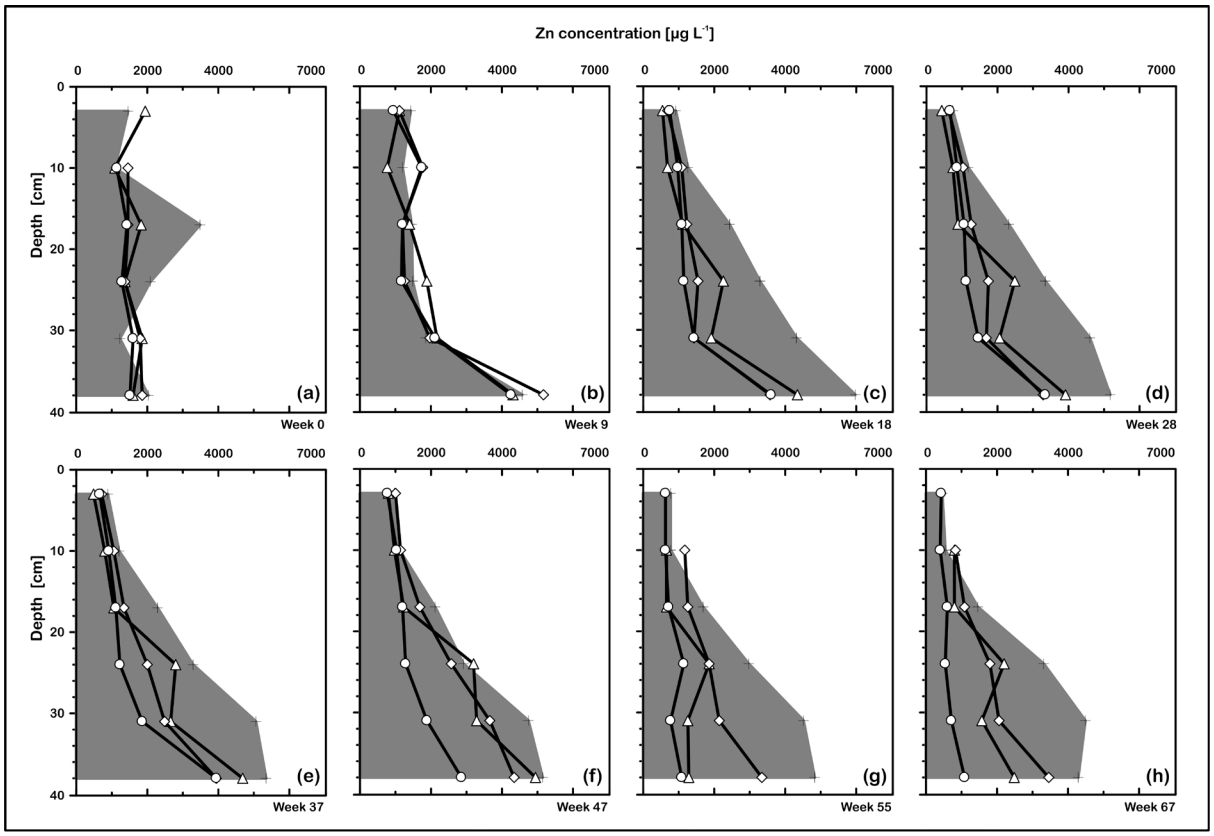

Figure 3–13 Temporal development of the substrate solution Zn concentrations in the four pots in different depths (*Circles* - Pot 1*, Diamonds* - Pot 2, *Triangles* - Pot 3, *Crosses margining the grey colored area* - Pot 4).

Similar concentration trends to those described for Al, Cu, Ni, U, and Zn are valid for Ca and Mg in the substrate solution over the time-span of the pot experiment. The aforementioned elements were correlated to the EC trend. K was strongly reduced in the planted pots and constant over the entire depths of the pots except in 38 cm b.s.s. The concentrations were temporary even below the detection limits. The diagrams of Ca, Mg, K, and of the EC are shown in the appendix (see **Figure A 4**, **Figure A 5**, **Figure A 6**, **Figure A 7**).

The S concentrations of the substrate solution show distinct different trends in all pots during the run-time of the experiment compared to the aforementioned elements (see **Figure 3–14**). The S levels are higher in the planted pots than in the control during the first growing season and the dormancy. Furthermore the concentrations in these pots increase with greater depth until 31 cm b.s.s. and decrease then again. At the end of the second growing season (week 67, see diagram **(h)**) the S concentrations in Pot 1 decreased to the level of the control pot while the levels in the substrate solution of the other two pots remained higher. Moreover the S concentrations in the control pot did not show a distinct increase with greater depths but reach the highest values in the shallow to middle depths. In general, the overall concentrations in the planted pots increased while decreased in the control over the duration of the experiment.

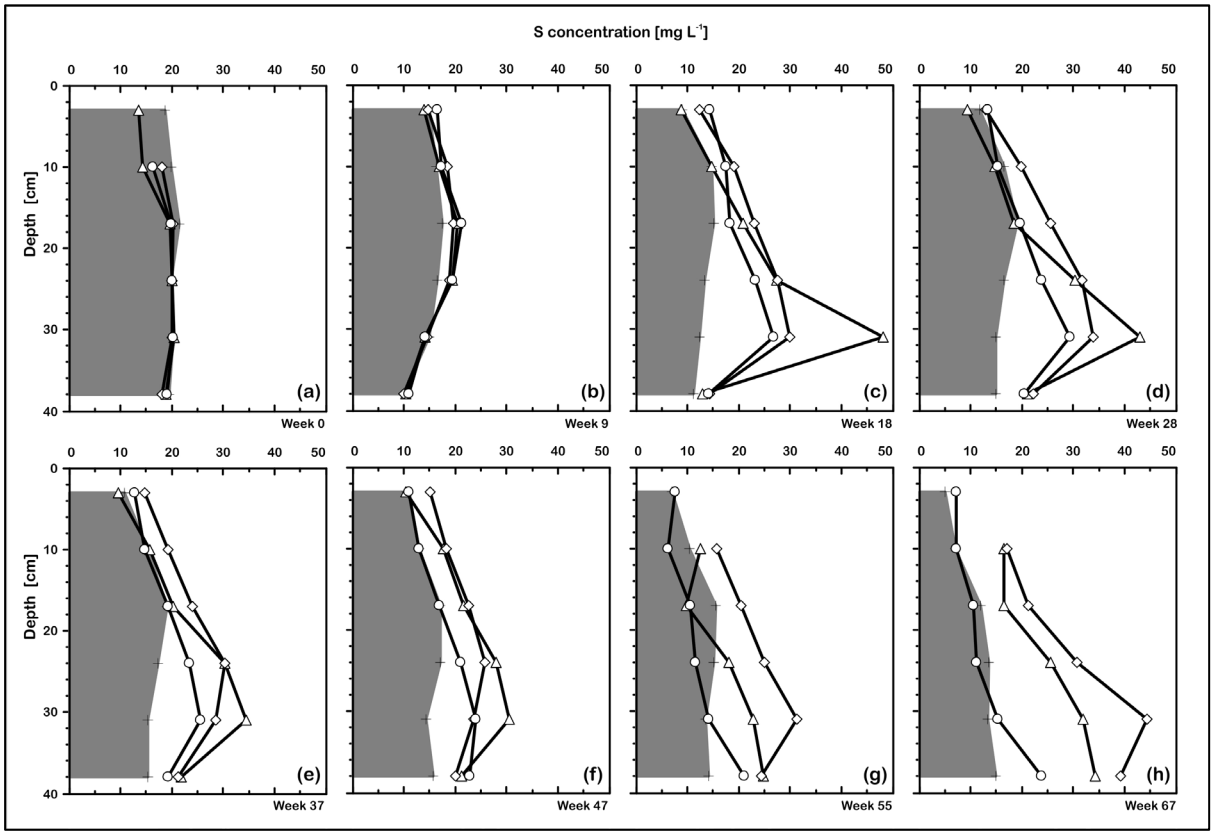

Figure 3–14 Temporal development of the substrate solution S concentrations in the four pots in different depths (*Circles* - Pot 1*, Diamonds* - Pot 2, *Triangles* - Pot 3, *Crosses margining the grey colored area* - Pot 4).

The balance of the output and input volumes of sampling water, leachate, and DI-water for watering (see **Table 3–2**) shows that the output by leachate was two orders of magnitude lower than the total volume of DI-water that was used to maintain in the anticipated substrate FC_{eff} of 50 %. The output volume by water taken during the regular sampling of the substrate solution was one order of magnitude higher than the leachate volume. The highest output volume of both sampling water and leachate occurred in the unplanted control pot, which had on the one hand the lowest water use (DI-water) of all pots and on the other hand the highest leachate volume. The highest water use had Pot 3.

	Pot 1	Pot 2	Pot 3	Pot 4
Total volume of sampling water [L]	2.12	2.05	2.07	2.18
Total volume of leachate water [L]	0.26	0.26	0.15	0.46
Total volume of DI-water used for watering of the pots [L]	93.91	86.65	98.45	62.40

Table 3–2 Total volumes of outputs by sampling water and leachate as well as input by watering with deionized (DI) water in the duration (495 days) of the mesocosm pot experiment.

3.4 Tree growth, biomass production, and metal concentration in tree tissues

The birches (*B. pendula*) planted in the pots at the beginning of the pot-experiment were taken from the 'Kanigsberg' field site and originate from one stand. The trees were chosen in the field regarding similar heights and diameter, assuming them also to have a similar age. Nevertheless, the initial heights of the trees varied between 31 and 58 cm and the diameter differed between 3 and 5.1 mm (see **Figure 3–15**). In each pot one tree of at least 50 cm initial height and 4 mm initial diameter was planted. Regarding the average height and diameter the trees in Pot 1 had initially after set-up of the pot experiment the poorest physiology of all planted pots. The actual initial tree ages were determined after the experiment by counting the tree rings at the base of the stem and correcting the age for 2 vegetation periods (experiment duration). Most of the planted trees were between 1 and 2 years old, singly tree 1/3 was initially already 3. The age of tree 2/1 was not distinguishable because the old stem died off in the first growing season. These age differences were not assessable or distinguishable from the heights and diameters during their selection at the field site.

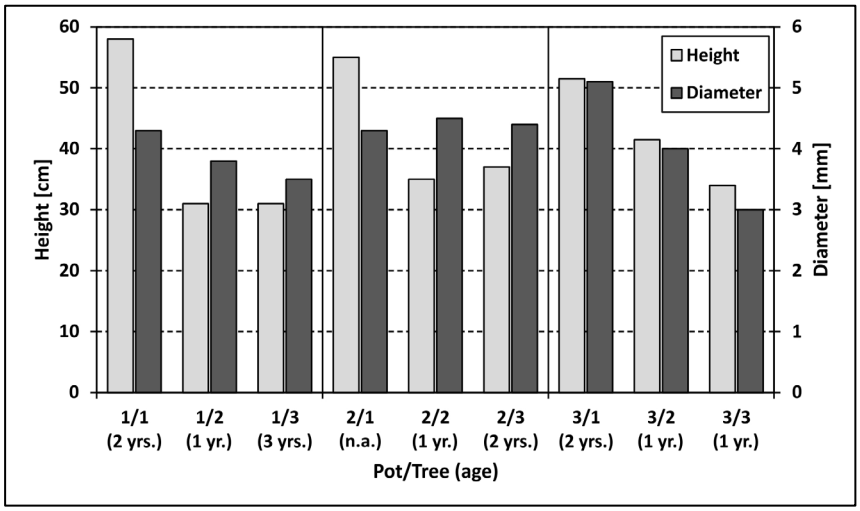

Figure 3–15 Initial heights and diameters of birches planted in the pots. The initial ages are given in brackets below the labels. The trees originated from one grove at the study site and were chosen regarding similar physiological parameters. The plant roots were planted in the pots in a depth of 0-15 cm b.s.s. Growth and diameter were measured from the reference point at 5 cm above the substrate surface at any time.

The growth of the birches differed strongly between the distinct individuals (see **Figure 3–16**). The highest growth in height had tree 3 in Pot 1 with 43 % in the first growing season and 22 % in the second one. The highest growth in diameter had tree 3 in Pot 2 with 24 % in the first and 32% in the second growing season. The growth parameters of tree 1 in Pot 2 could not be determined because the main shoot died off in the first growing season. Afterwards new shoot sprouted at the base of the old stem. On average the highest growths regarding height occurred in Pot 3, regarding diameter in Pot 1.

The biomass, determined separately for each compartment after harvesting the trees, differed heavily between the individual birches (see **Figure 3–17**). The biomass after harvest did not refer necessarily to the linearly to the initial fresh weight of the trees: Tree 3 in Pot 1 had the highest biomass of all birches planted but the lowest fresh weight at the beginning of the pot experiment. On average the highest biomass was produced by the trees of Pot 1.

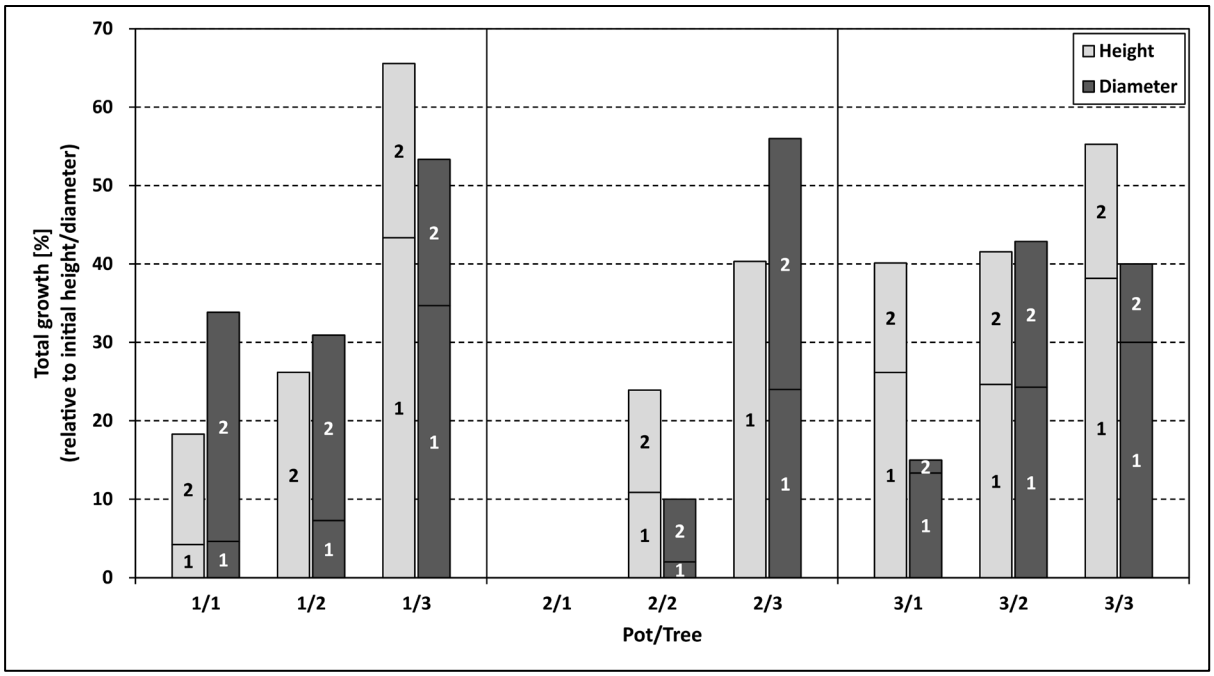

Figure 3–16 The diagram shows the growth of the trees in height and diameter after the first and the second growing season on the base of the initial parameters. The numbers in the subsections of the columns indicate the growing season; the entire column shows the total growth within the duration of the pot experiment.

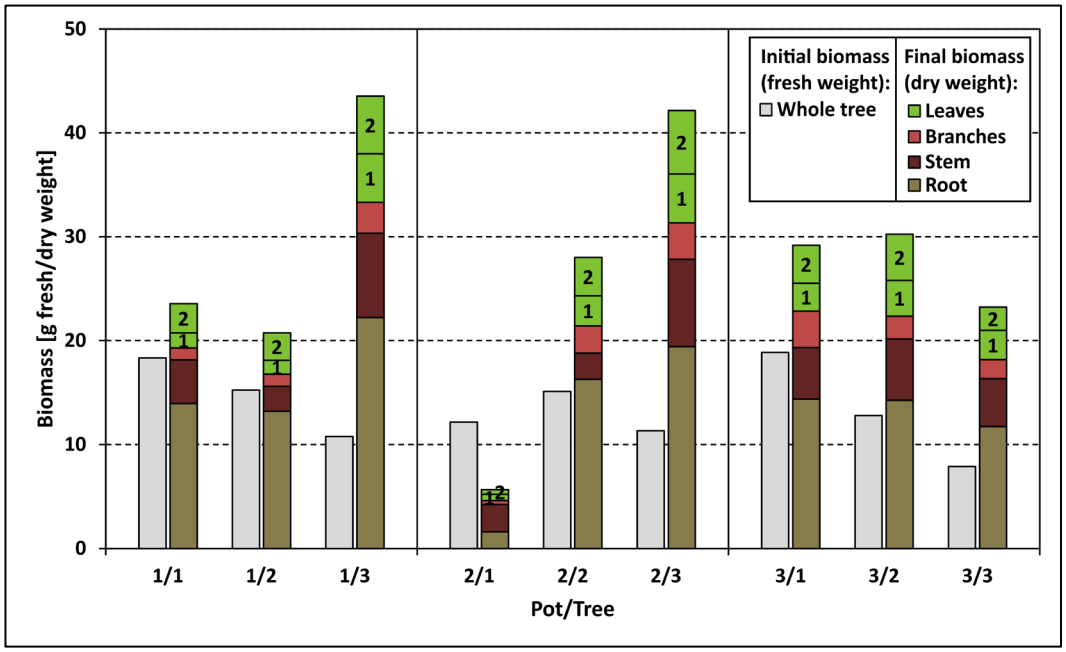

Figure 3–17 The total biomasses of the trees planted in the pot experiment are displayed by the columns: The initial biomass is given as fresh weight of the whole tree whereas the biomass of the trees after the harvest is given as dry mass separately for each compartment (sub-sections of the colored columns). The leave-fall of the two vegetation periods was weighted separately, which is indicated by numbers within the leave-subsections.

The highest concentrations of the metals Al, Cu, Fe, and U were found in the roots of the birches harvested at the end of the pot experiment (maximum concentrations in dry matter rounded to whole numbers - Al: 1419 ± 260 µg g^{-1} see **Figure 3–18**, Cu: 131 ± 21 µg g^{-1} see **Figure 3–19**, Fe 1514 ± 450 µg g^{-1} see **Figure 3–20**, U: 4 ± 1 µg g^{-1} see **Figure 3–22**). The levels of those elements in the aerial

parts of the trees stem, branches and leaves were about one order of magnitude lower, in the case of U even about two orders of magnitude. In contrast for Ni and Zn the highest concentrations were determined in the leaves (maximum concentrations in dry matter rounded to whole numbers - Ni: 9 ± 2 µg g^{-1} see **Figure 3–21**, and Zn: 388± 10 µg g^{-1} see **Figure 3–23**). Additionally Zn had higher concentrations in in the other compartments of the aerial biomass than in the roots. Regarding the individual biomass concentrations, the highest values in all compartments were reached in trees from the pots and the lowest in reference trees sampled at the field site 'Kanigsberg'. Comparing the plants' biomass concentrations between the three pots the maximum concentrations were reached for almost all elements except Cu in Pot 3 (highest root Cu concentrations of Pot 1 trees).

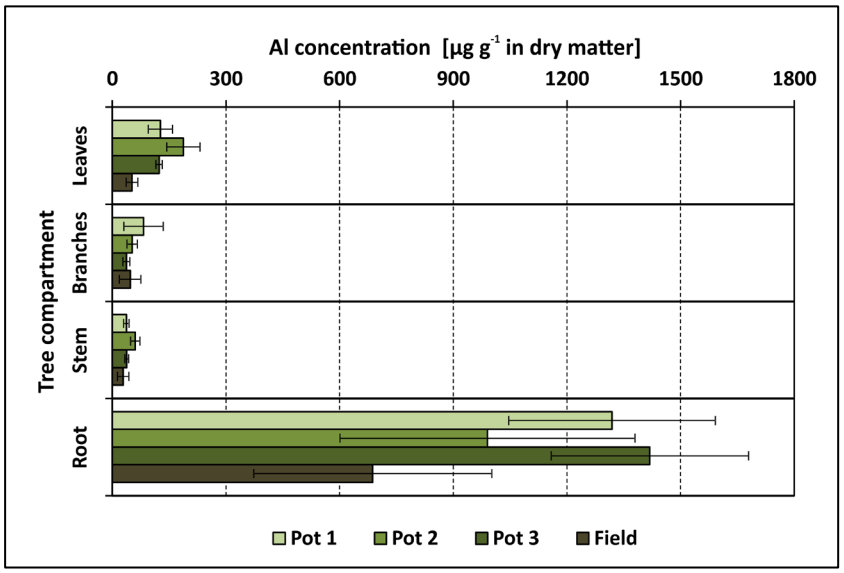

Figure 3–18 Mean Al concentrations in powdered dry matter of samples from aerial compartments and root of birches grown in the three pots and at the reference field site. The plants were harvested and sampled in the end of the pot experiment. The color code indicates the growing site of the samples. The means were calculated from three individuals per pot/field site. The whiskers indicate the standard deviations between the three biological replicates per growing site.

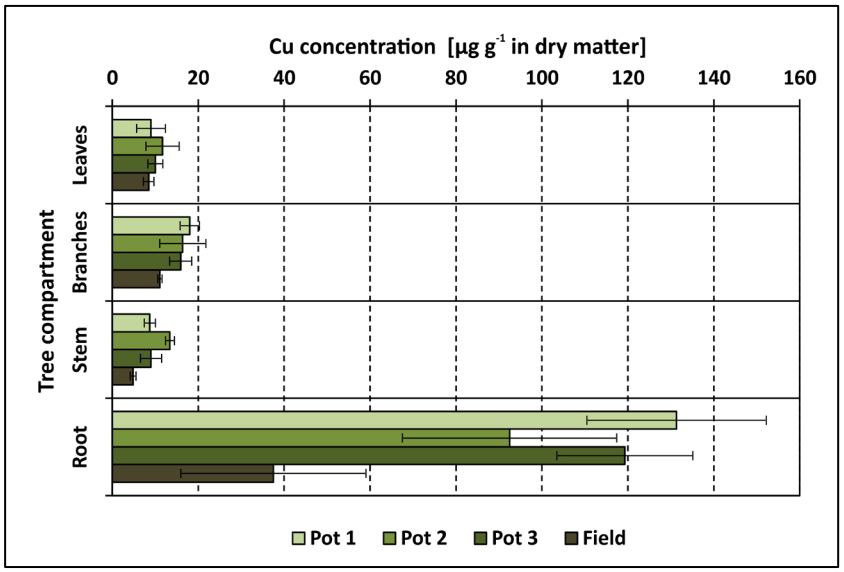

Figure 3–19 Mean Cu concentrations in four different compartments of birches grown in the three pots and at the reference field site.

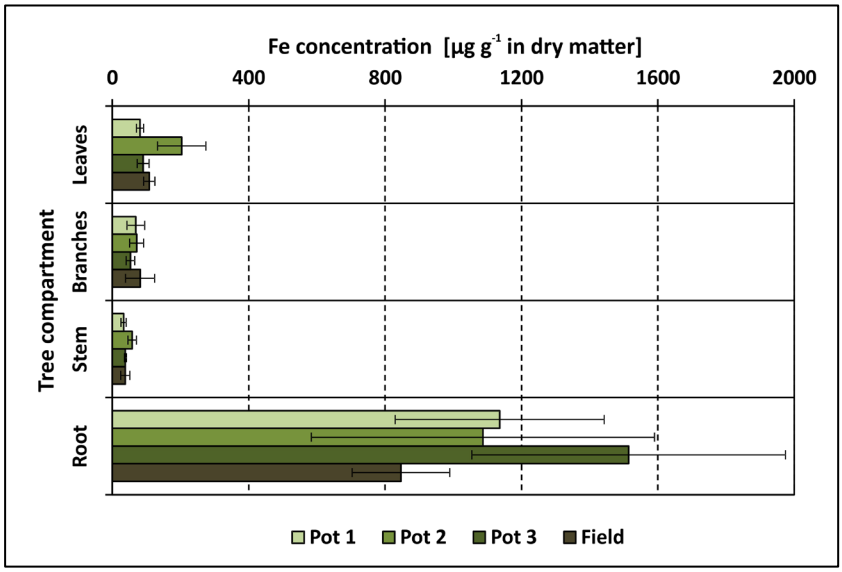

Figure 3–20 Mean Fe concentrations in four different compartments of birches grown in the three pots and at the reference field site.

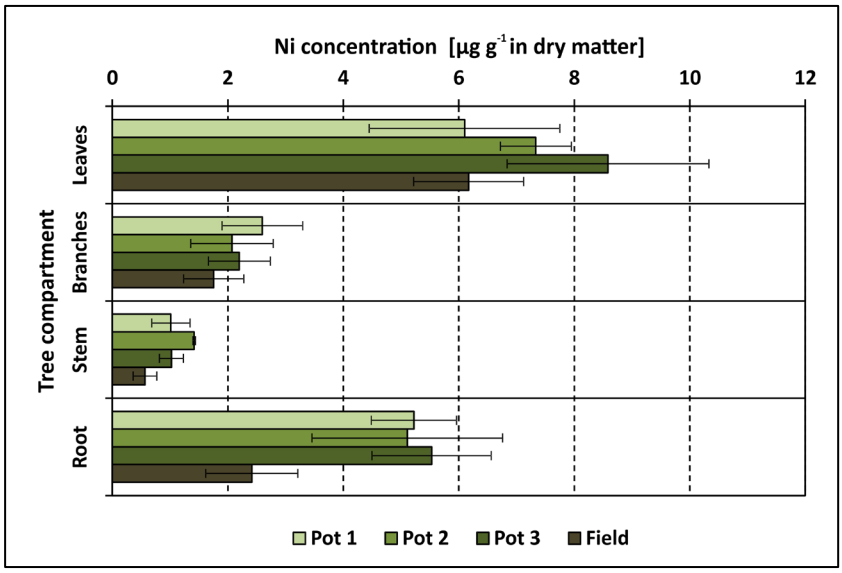

Figure 3–21 Mean Ni concentrations in four different compartments of birches grown in the three pots and at the reference field site.

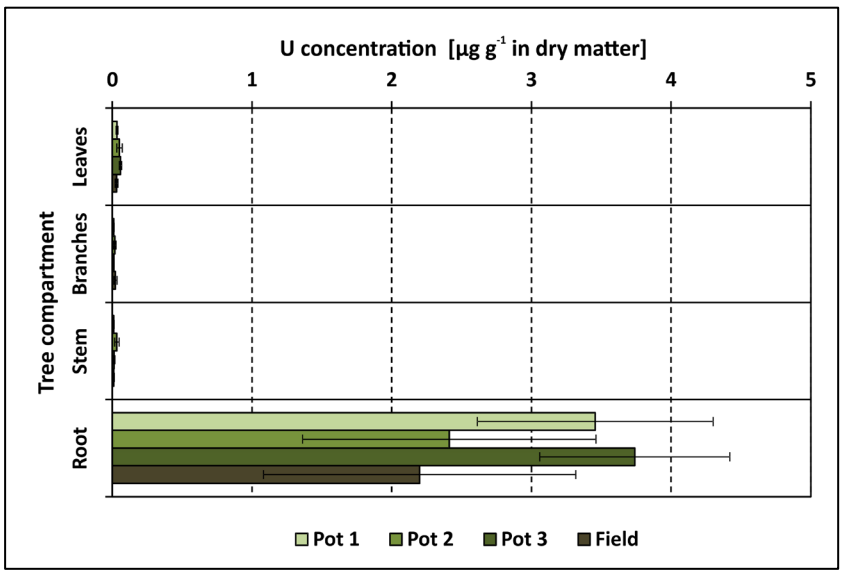

Figure 3–22 Mean U concentrations in four different compartments of birches grown in the three pots and at the reference field site.

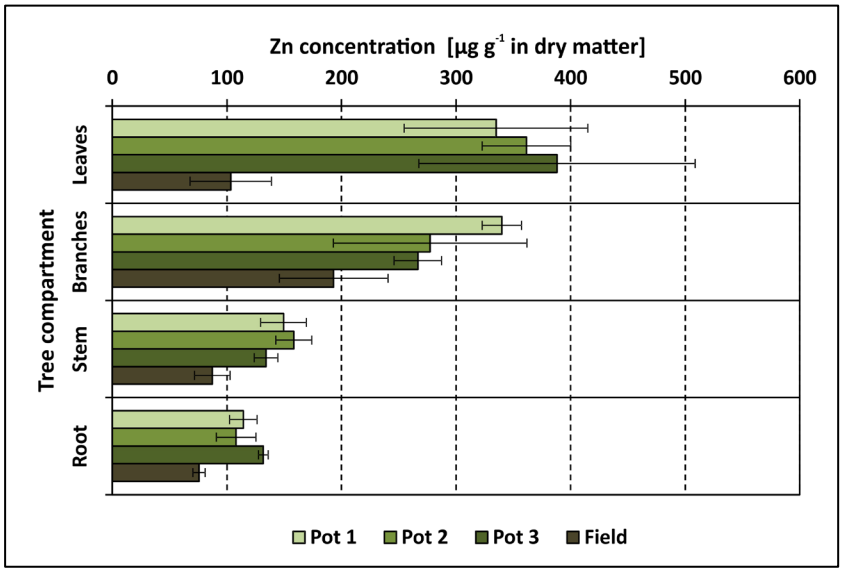

Figure 3–23 Mean Zn concentrations in four different compartments of birches grown in the three pots and at the reference field site.

The metal concentrations in the biomass were used to calculate mean biomass concentrations for the roots and the above-ground biomass. Therefore the individual tissue concentrations of the nine birch trees grown into the pots were used to calculate the ratios between the bioavailable concentration in the substrate (sum of first two fractions of the sequential extraction method; mean calculated from the layer-resolved data of the three planted pots) and the concentration in the roots, expressed by the transfer factor soil-root (TF_{root}). The ratio between the substrate bioavailable concentration and the mean concentration in the above-ground biomass is expressed by the TF_{shoot}. The translocation factor $TLF_{root\text{-}shoot}$ indicates the tree internal migration of the metals from the roots to the aerial parts of the birches. Factors > 1 indicate always a migration and accumulation of the metal to the compartment in the denominator of the ratios. TF_{root} values are > 1 for all metals; high factors are reached for Fe, Ni, and Zn (in descending order). TF_{shoot} values are > 1 only for Zn, Fe, and Ni. Translocation from roots to the aerial tissues of the trees occurred only in the case of Zn.

Table 3–3 Transfer factors (TF) for different metals expressing the ratio between the bioavailable substrate concentrations (sum of the fractions I and II) and the levels in biomass, either in roots of the birch trees (TF_{root}) or in their above-ground biomass (TF_{shoot}). The metal translocation from the roots to the shoots within the trees is reflected by their ratio as translocation factors ($TLF_{root\text{-}shoot}$). The bioavailable concentrations in the substrate relate to the sum of the concentrations extracted in fraction I and II. Means of bioavailable concentrations were calculated from the layer-resolved levels of the three planted pots. The concentrations in the roots and shoots are means calculated from the tissue concentrations of the 9 tree individuals grown in pots.

	Substrate conc. bioavailable [µg g^{-1}]	$Conc_{root}$ [µg g^{-1}]	$Conc_{shoot}$ [µg g^{-1}]	TF_{root}	TF_{shoot}	$TLF_{root\text{-}shoot}$
Al	283.99	1242.66	82.84	4.38	0.29	0.07
Cu	13.90	114.35	12.46	8.23	0.90	0.11
Fe	6.19	1245.78	77.56	201.39	12.54	0.06
Ni	0.49	5.29	3.59	10.81	7.35	0.68
U	0.89	3.20	0.03	3.61	0.03	0.01
Zn	3.84	118.06	267.83	30.72	69.70	2.27

3.5 Metal mass output from the mesocosm pots by water and biomass

The metal mass output by water (sampling water and leachate) as well as by the biomass of the birch trees harvested after the pot-experiment is represented by the bar diagrams in **Figure 3–24** and **Figure 3–25**. Even though the pots were watered carefully to c. 50 % FC_{eff} to maintain the mesocosm pots as a closed system, little leachate in the range of a few hundred ml was produced (compare **Table 3–2**). The mass output of all elements besides Ni by biomass was higher than that by water. Fe was the element with the lowest output by water in the range of c. 20 µg, in Pot 2 and Pot 4 the Fe input by watering with DI-water was even higher than the output by water (see negative output-values in **Figure 3–24**). The summed-up mass output by water and biomass is set in relation to the total mass balance in the substrate for each metal is given in the following section (see **Figure 3–35**, diagram **(a)**-**(f)**).

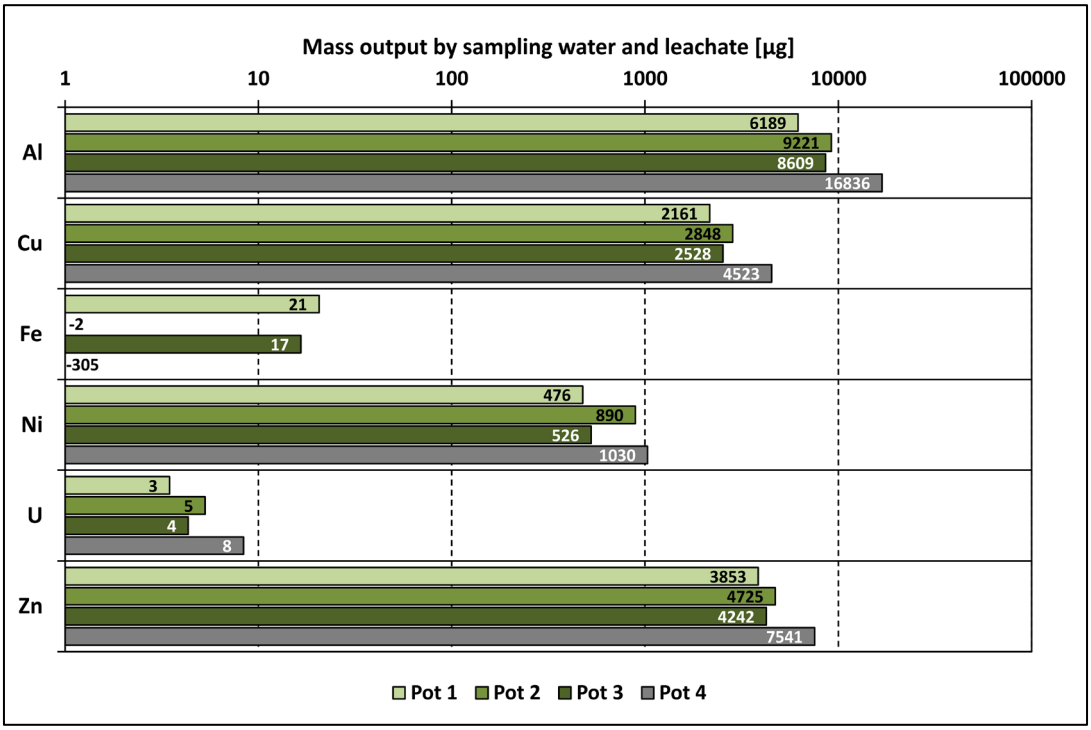

Figure 3–24 Metal output from the mesocosm pots by sampling water and leachate within the duration of the pot experiment (495 days) corrected by the input by watering with deionized (DI) water. The output was calculated by referring the measured concentrations of each sampling date on the total volumes of sampling water, leachate, and DI-water that was used for watering. The input by the DI-water was higher than the output in Pot 2 and 4 for Fe, which is why the values were negative.

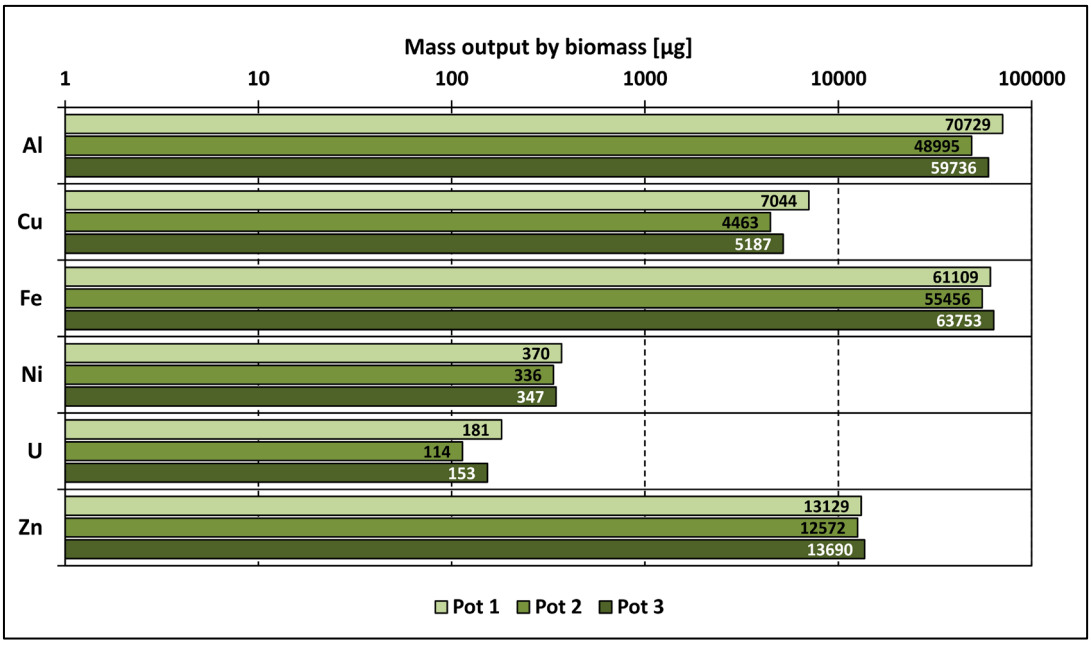

Figure 3–25 Metal output from the mesocosm pots by the biomass of the birch trees growing in the pots 1-3. The output masses were calculated by referring the measured concentrations of the tree compartments (roots, stems, branches, and leaves) after harvesting on the relative dry weights and summing up the resulting metal masses.

3.6 Soil physico-chemistry and metal concentrations of post-experiment substrate

The pH of the post-experiment substrate decreased with greater depths in the case of the planted pots (Pot 1-3) whereas it first decreased and then increased again below 25 cm b.s.s. in the control pot (see **Figure 3–26**). Pot 1 had the highest pH values of all pots in most of the depths. The strongest decrease occurred in Pot 2 from 4.16 to 3.89. The highest differences in pH between the pots occurred in the greatest depth of 40-45 cm b.s.s. where the pH of the control pot reached the highest values (4.13). Comparing the pH values of the post-experiment substrate with that of the initial in the most cases a lowering of the pH occurred, a trend that intensified in greater depths. Up to 30 cm b.s.s. the pH decrease was always the highest in the control pot, whereas below that depth the trend inverted and the planted pots showed the strongest pH decline. On average Pot 1 showed the lowest decrease of the pH, in the shallow depths even a slightly elevation of max. 0.05 pH units.

The EC of the post-experiment substrate distinctly increased with greater depths in the planted pots (Pot 1-3) to approximately twice the values of the shallowest depths (from 50-60 µS cm^{-1} in 0-5 cm to 120-140 µS cm^{-1} in 40-45 cm b.s.s.). In the control, the decrease is less significant, furthermore the highest EC occurred in 0-5 cm depth (see **Figure 3–27**). Compared to the initial EC the post-experiment EC was reduced in the three planted pots within the depth range of 0 to 25 cm b.s.s. Below 30 cm the substrate EC in those pots was enlarged and increased with greater depths. The described trends were less significant in the control, in contrast to the planted pots the EC shift was positive in the shallowest depth.

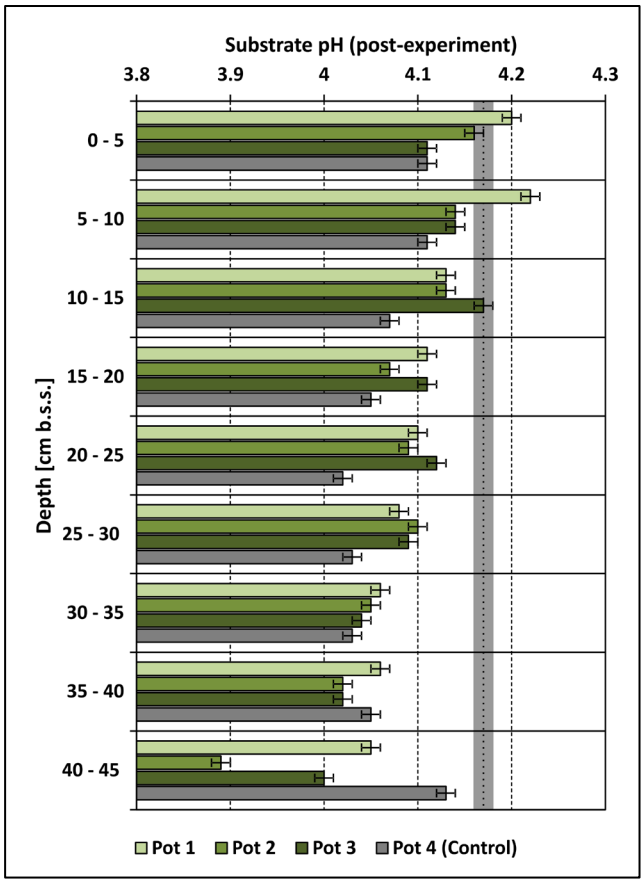

Figure 3–26 Depth resolved pH of the post-experiment substrate in the four pots (indicated by the color-coded bars). The pH of the initial substrate was 4.17 ± 0.01 (determined from 5 replicates) and is displayed as reference in the diagram by the dotted vertical line with the grey background (indicating the standard deviation). The standard deviation of the initial substrate was assumed as the error of measurement and therefore taken over as error whiskers of the post-experiment samples (those were measured without replicates). The substrate pH was determined in ultrapure water suspension according to DIN ISO 10390-05.

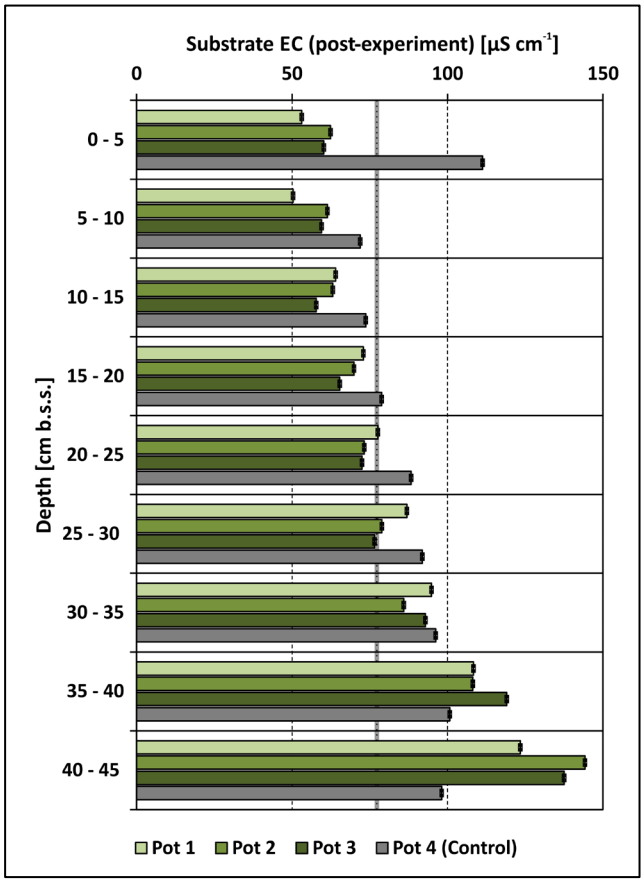

Figure 3–27 Depth resolved specific electrical conductivity (EC) of the post experiment substrate in the four pots (indicated by the color-coded bars). The EC of the initial substrate was 77.4 ± 0.5 µS cm^{-1} (determined from 5 replicates) and is displayed as reference in the diagram by the dotted vertical line with the grey background (indicating the standard deviation). The standard deviation of the initial substrate was assumed as the error of measurement and therefore taken over as error whiskers of the post-experiment samples (those were measured without replicates). The substrate EC was measured in ultrapure water suspension according to DIN ISO 11265-06.

The CEC_{eff} of the post-experiment substrate did not show clear trends with greater depth in any pot and only marginal differences between the different pots (see **Figure 3–28**). The CEC_{eff} values ranged from 2.4 cmol kg^{-1} (Pot 1 in 30-35 cm b.s.s.) to 4.34 cmol kg^{-1} (Pot 4, 5-10 cm b.s.s.). Especially in the planted pots there was a trend of decreased CEC_{eff} of the post-experiment substrate compared to the initial values. However, this trend is not significantly due to the overlap of the error whiskers and the standard deviation of the initial value.

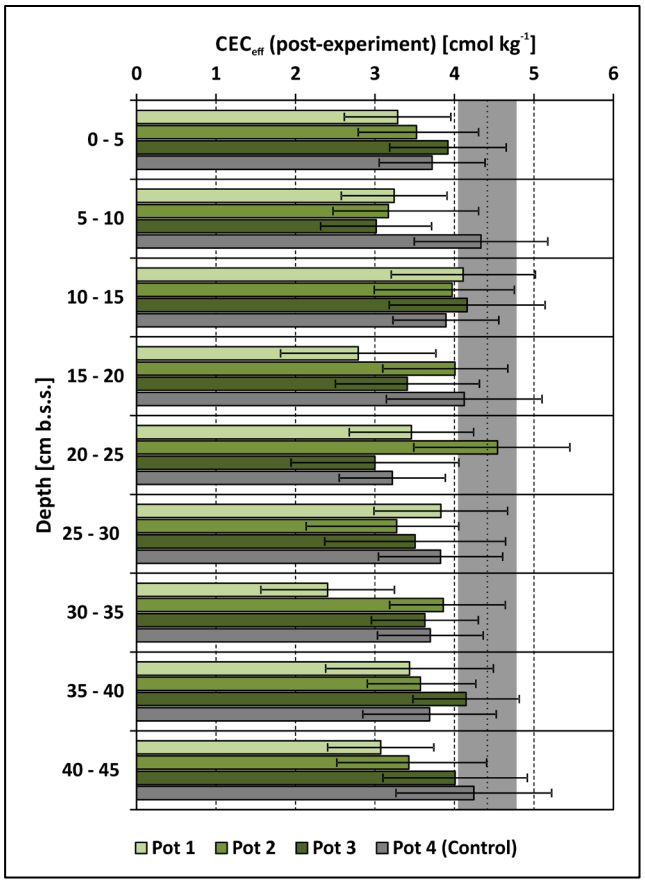

Figure 3–28 Depth resolved effective cation exchange capacity (CEC_{eff}) of the post-experiment substrate in the four pots (indicated by the color-coded bars). The CEC_{eff} of the initial substrate was 4.42 ± 0.36 cmol kg^{-1} (determined by triple measurement of the same sample) and is displayed as reference in the diagram by the dotted vertical line with the grey background (indicating the standard deviation). The CEC_{eff} was measured according to DIN EN ISO 11260.

The Al concentrations of the initial substrate as well as (depth resolved) of the post-experiment substrate in the four pots are displayed in **Figure 3–29** in the diagrams **(a)**-**(d)**. Comparing the Al concentrations bound to the first six fractions the highest amounts of Al were occluded in (poor-) crystalline Fe-oxides (fractions V and VI) or are mobile (fraction I). Nevertheless the sums of the six fractions were on average 50 times lower than the total concentrations. In all pots the sum of the six fractions was higher in the initial substrate than in the post-experiment substrate. There were marginal differences between the different pots in the depth resolved Al concentrations of the post-experiment substrate. Furthermore no consistent depth-related trends were observable, neither in the different fractions, nor in the total contents. Comparing the Al concentrations between the post-experiment and the initial substrate (indicated for the total concentrations by the vertical dotted lines with the grey-shaded background corresponding symmetrical standard deviations) the sixth fraction as well as the total concentrations showed lowered concentrations in all pots and all depths, whereas the bioavailable fraction was slightly increased. In the control pot additionally the organical-

ly bound fraction was lowered, furthermore the sixth fractions were slightly higher than in the three planted pots. Nonetheless the mentioned trends of the total concentration as well as of the fractions I and V were oftentimes not significant due to an overlap of standard deviations. The Al mass balance (see **Figure 3–35**, diagram **(a)**), indicating the shifts of the Al masses of the post-experiment substrate compared to the initial (both referred on the total substrate mass per pot), revealed a decrease of the Al mass occluded in poor-crystalline Fe-oxides of 0.45-1 ± 0.25 g (largest decrease in the control). The decrease of the Al mass occluded in crystalline Fe-oxides was c. 5 ± 2 g in the planted pot and c. 3 ± 2 g in the control. Additionally the organically bound Al-mass in the control pot was slightly decreased (0.5 ± 0.04 g pot^{-1}). Trends appearing for the other fractions or total masses were not significant due to the fact that they are in range of the error. The output from the planted pots by leachate and biomass was marginal compared to the mass decreases in fraction V: it ranged from 0.6 to 0.8 g pot^{-1} whereas the output by leachate in the control was even smaller (0.02 g pot^{-1}).

The sum of the Cu concentrations of the first six fractions in the post-experiment substrate of all pots is negligible smaller in all pots and almost all depths than in the initial sample (see **Figure 3–30**, diagrams **(a)**-**(d)**). The highest Cu-concentrations in the first six fractions were (1) occluded in crystalline Fe-oxides and (2) were mobile (ordered anticlimactic). On average the sum of the six fractions contributed to at least 50 % to the total Cu concentrations. The total Cu concentrations in the post-experiment substrate in the different pots and depths thereby scattered in the error range of the initial sample. Compared to the initial Cu concentrations the concentrations of the mobile as well as the fraction occluded to crystalline Fe-oxides in the post-experiment substrate of the planted pots were decreased. These trends were less distinct in the control pot. The Cu mass balance (see **Figure 3–35**, diagram **(b)**) revealed a decrease of the Cu mass in fraction V in the post-experiment substrate compared to the initial one of c. 0.01-0.015 ± 0.06 g pot^{-1} in the planted pots and 0.08 ± 0.06 g pot^{-1} in the control. Compared to that trend the Cu output mass by leachate and, in the case of the planted pots, by biomass was negligible in all pots (below 0.01 g pot^{-1}). Apparent mass balance trends in other fractions were within the errors.

The sum of the Fe concentrations of the six fractions were lower in all pots and depths in the post-experiment substrate than in the initial one (see **Figure 3–31**, diagrams **(a)**-**(d)**). The fractions VI and V had percentaged the highest Fe concentrations, the concentrations of the other fractions were 1-3 orders of magnitude lower. The total Fe levels were c. 3 times higher than the cumulated concentrations of the six fractions which ranged between 52,000 and 55,000 µg g^{-1}). Compared to the initial substrate the concentration of Fe occluded in crystalline Fe-oxides (fraction VI) in the post-experiment substrate was lower in all pots and depths. The post-experiment total concentrations were in the range of the error, whether planted or not and irrespective of the depth. The mass balance revealed a significant decline of the Fe occluded in poor-crystalline Fe-oxides (fraction V) after the experiment in all pots (see **Figure 3–35**, diagram **(c)**). The apparent negative trends in the mass balances of fraction V and the total mass were in the error range. The Fe output by leachate, and in the case of the planted pots by biomass, was negligible low (rounded 60 mg pot^{-1} in the planted pots and 0.3 mg pot^{-1} in the control).

The cumulated Ni concentrations of the six fractions were lower in the post-experiment substrate than in the initial irrespective of the pots and the depths (see **Figure 3–32**, diagrams **(a)**-**(d)**). The

highest Ni concentrations were those in fraction VI. The total concentrations were approximately 5-6 times higher than the summed up concentrations of the fractions I-VI and ranged from rounded 84 to 94 µg g^{-1}. In the initial substrate the total concentrations were lower than in the post-experiment substrate in all pots and depths. The decrease of the Ni mass bound to fraction VI and the increase of the total Ni mass balance (see **Figure 3–35**, diagram **(d)**) was entirely in the range of the error. The Ni output of c. 0.001 g pot^{-1} did not significantly differ between the planted pots and the control and was negligible low in the Ni-balance of the post-experiment substrate.

The cumulated U concentrations in the initial substrate bound to the six fractions were slightly lower than in the post-experiment substrate in all pots and mostly all depths (see **Figure 3–33**, diagrams **(a)**-**(d)**). The fractions with the percentaged highest U concentrations were the easily deliverable fraction II, as well as the fractions V and VI. The total U concentration was 2-3 times higher than the cumulated ones of the six fractions (c. 7 µg g^{-1}). A depth related trend of the differently bound U concentrations as well as of the total levels was absent. Compared to the initial substrate the post-experiment-concentrations of the easily deliverable U fraction in the post-experiment were increased in the planted pots (range 0.07-0.13 µg g^{-1}) as well as to a lesser extend in the control pot. The same pattern applies to the U fractions bound to Mn oxides (fraction III). The mass balance revealed significant increases of the easily deliverable U mass and the U mass bound to Mn-oxides in the three planted pots (fraction II: +0.005 g pot^{-1}; fraction III: +0.001 g pot^{-1}) as well as a positive total mass balance in Pot 1 of 0.02 g pot^{-1} (see **Figure 3–35,** diagram **(e)**). The output by biomass and leachate in the planted pots was in the range of 0.0001-0.0002 g pot^{-1} and three orders of magnitude lower in the control.

The concentrations of Zn in the first six fractions were higher in the initial substrate than in the post-experiment; the percentaged highest Zn levels were bound to the fraction VI and I (see **Figure 3–34**, diagrams **(a)**-**(d)**). The Zn concentrations of the fractions II, II, and IV were almost always below the detection limit in the case of the planted pots. The cumulated Zn concentrations of the fractions I-VI after the experiment were lower than the initial substrate. Thereby depth related trends were absent. The total Zn concentrations did not show significant differences between the pots or depths (rounded 105-120 ± 5 µg g^{-1}). The Zn mass balance did not show any significant trend due to overlapping error whiskers (see **Figure 3–35**, diagram **(f)**). The output level was rounded 0.02 g pot^{-1} for the planted pots and 0.01 g pot^{-1} in the case of the control.

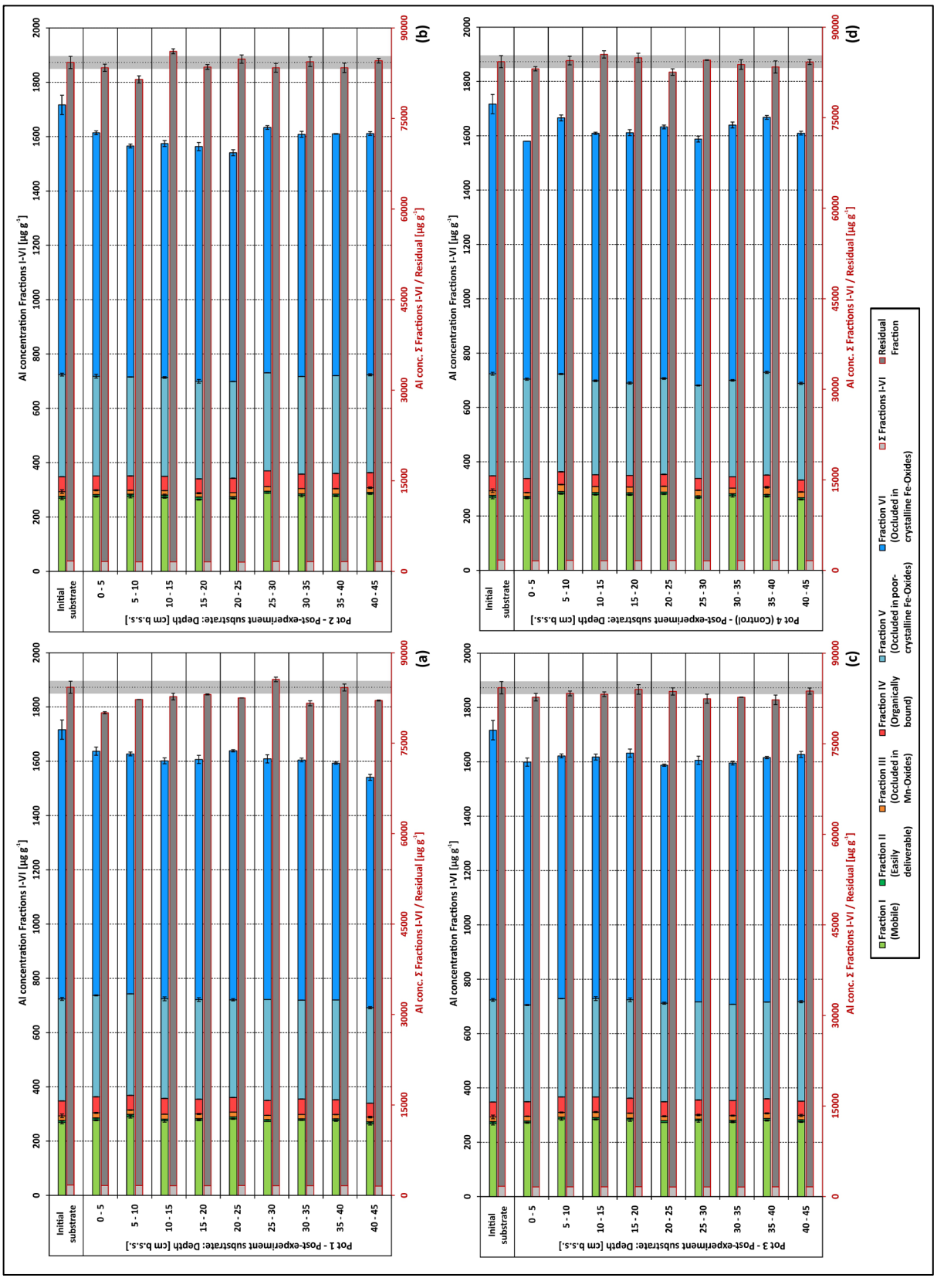

Figure 3–29 Depth resolved Al concentrations of the differently bound fractions and total concentrations of the post-experiment substrate in the four pots (diagrams **(a)-(d)**) opposed to the values of the initial substrate (the initial total concentration with standard deviation is highlighted as reference each by the vertical dotted line with grey background). Color-coded stacked bars assigned to primary X-axes (top of each diagram) represent the Al levels in the fractions I-VI (extracted according to Zeien & Brümmer, 1989). Grey red-framed bars assigned to secondary X-axes (bottom of each diagram, in red) indicate the total Al concentrations subdivided in the sum of the six fractions and the residual fraction (light and dark grey subsections). Whiskers at the end of the bars represent standard deviations of all fractions and total concentrations of (1) the post-experiment substrate (single samples, measured 5 times) and (2) the initial substrate (3 individual samples).

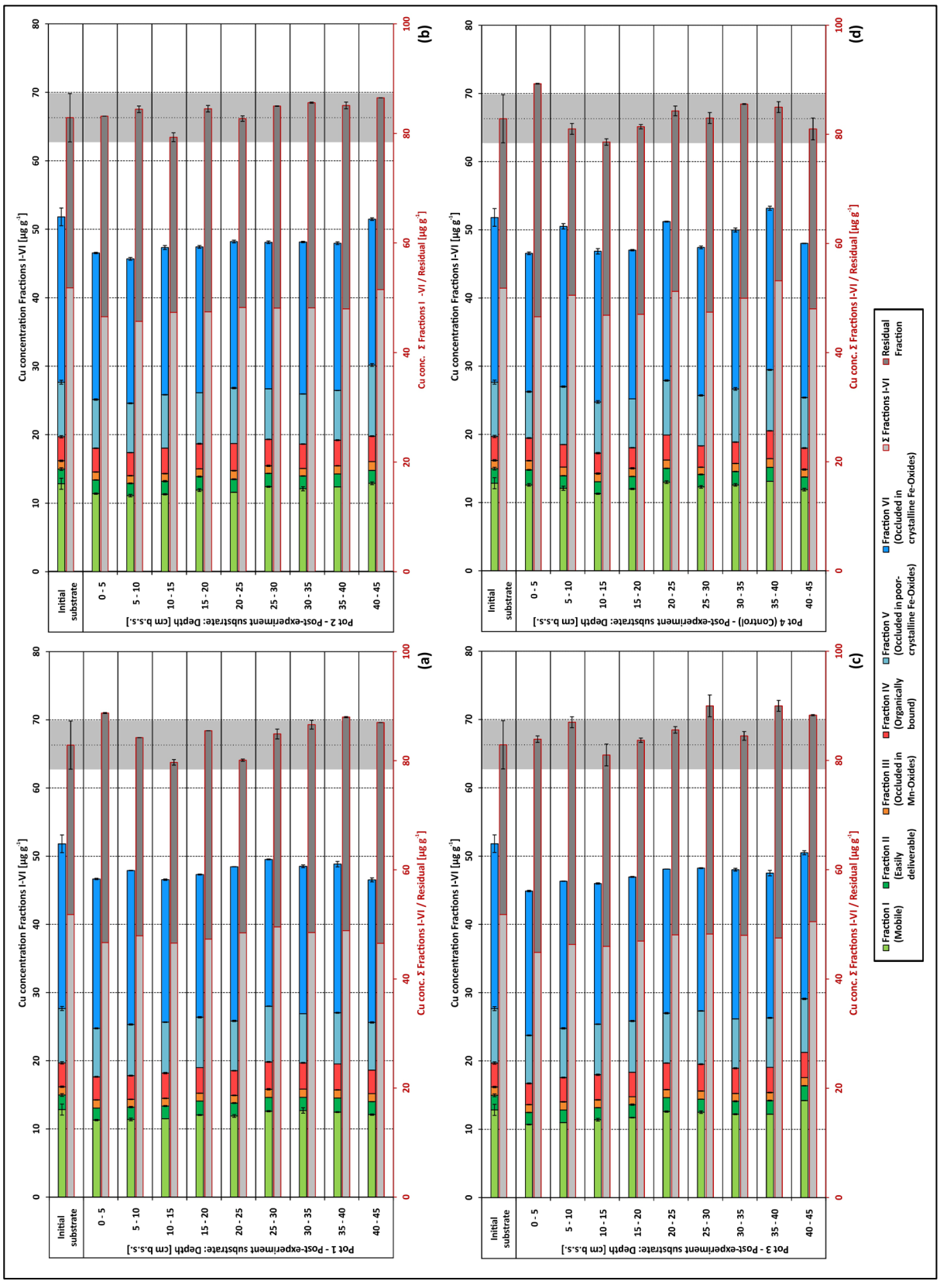

Figure 3–30 Depth resolved Cu concentrations of the differently bound fractions and total concentrations of the post-experiment substrate in the four pots (diagrams **(a)-(d)**) opposed to the values of the initial substrate.

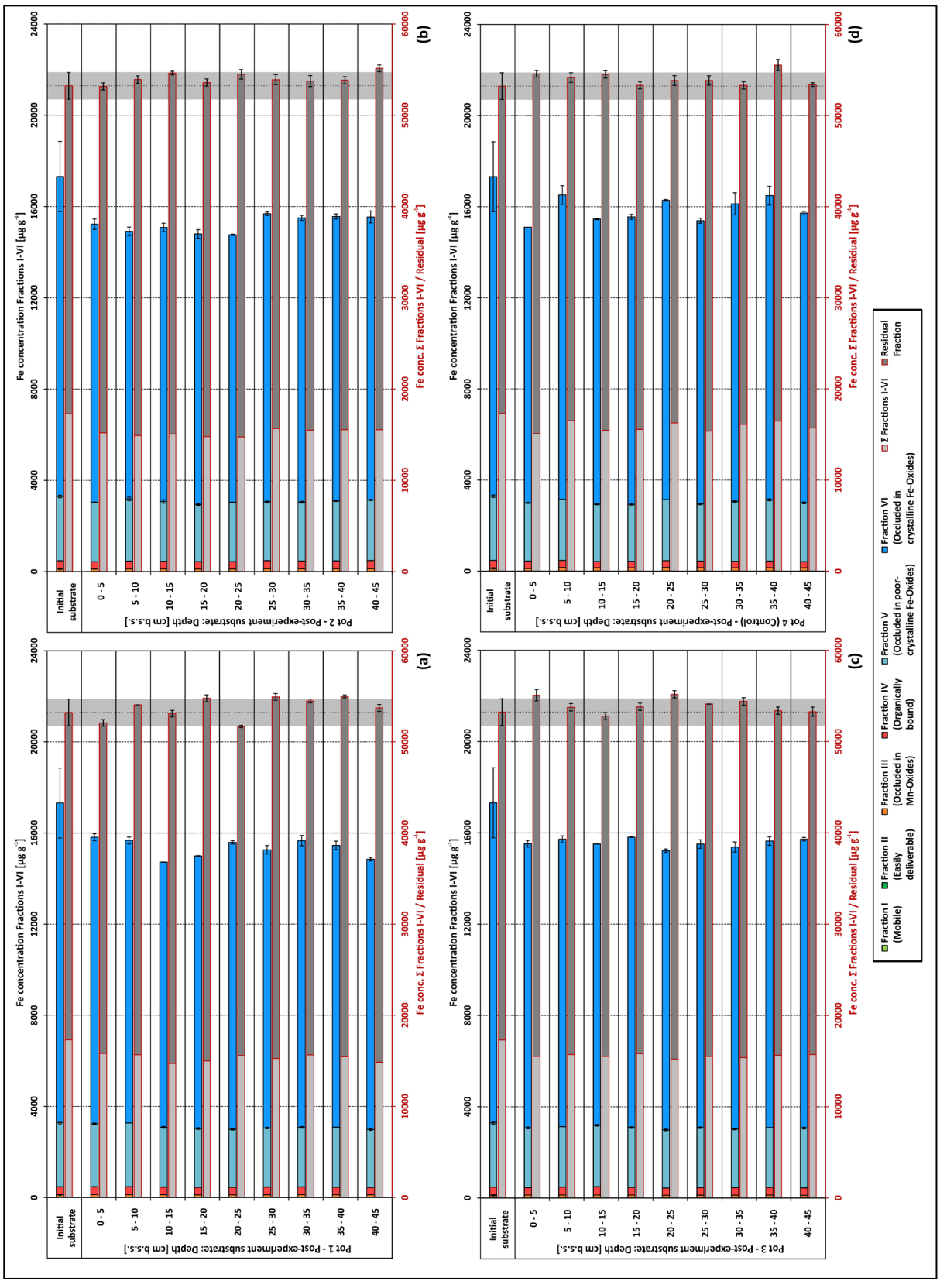

Figure 3–31 Depth resolved Fe concentrations of the differently bound fractions and total concentrations of the post-experiment substrate in the four pots (diagrams **(a)-(d)**) opposed to the values of the initial substrate.

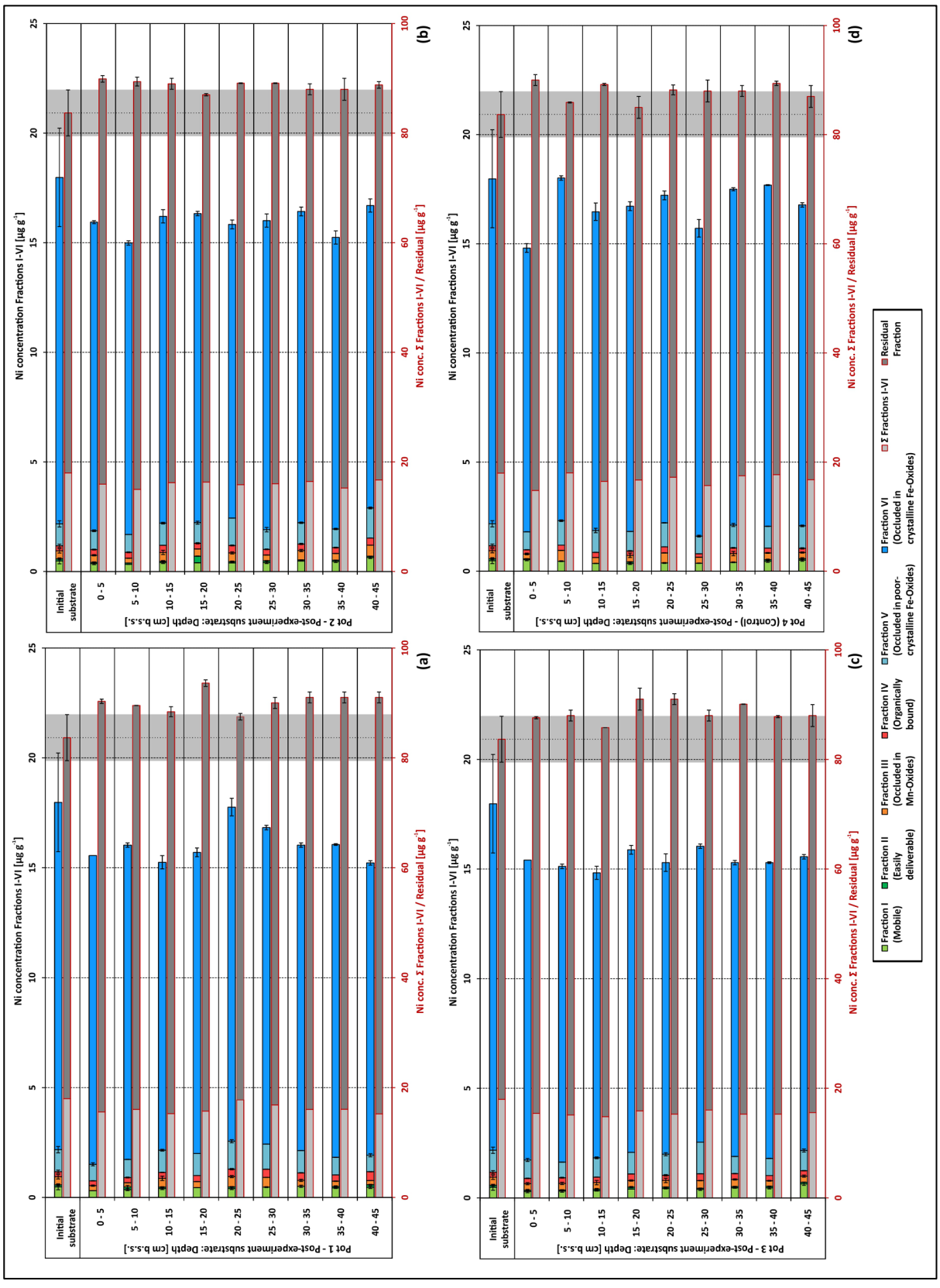

Figure 3–32 Depth resolved Ni concentrations of the differently bound fractions and total concentrations of the post-experiment substrate in the four pots (diagrams **(a)-(d)**) opposed to the values of the initial substrate.

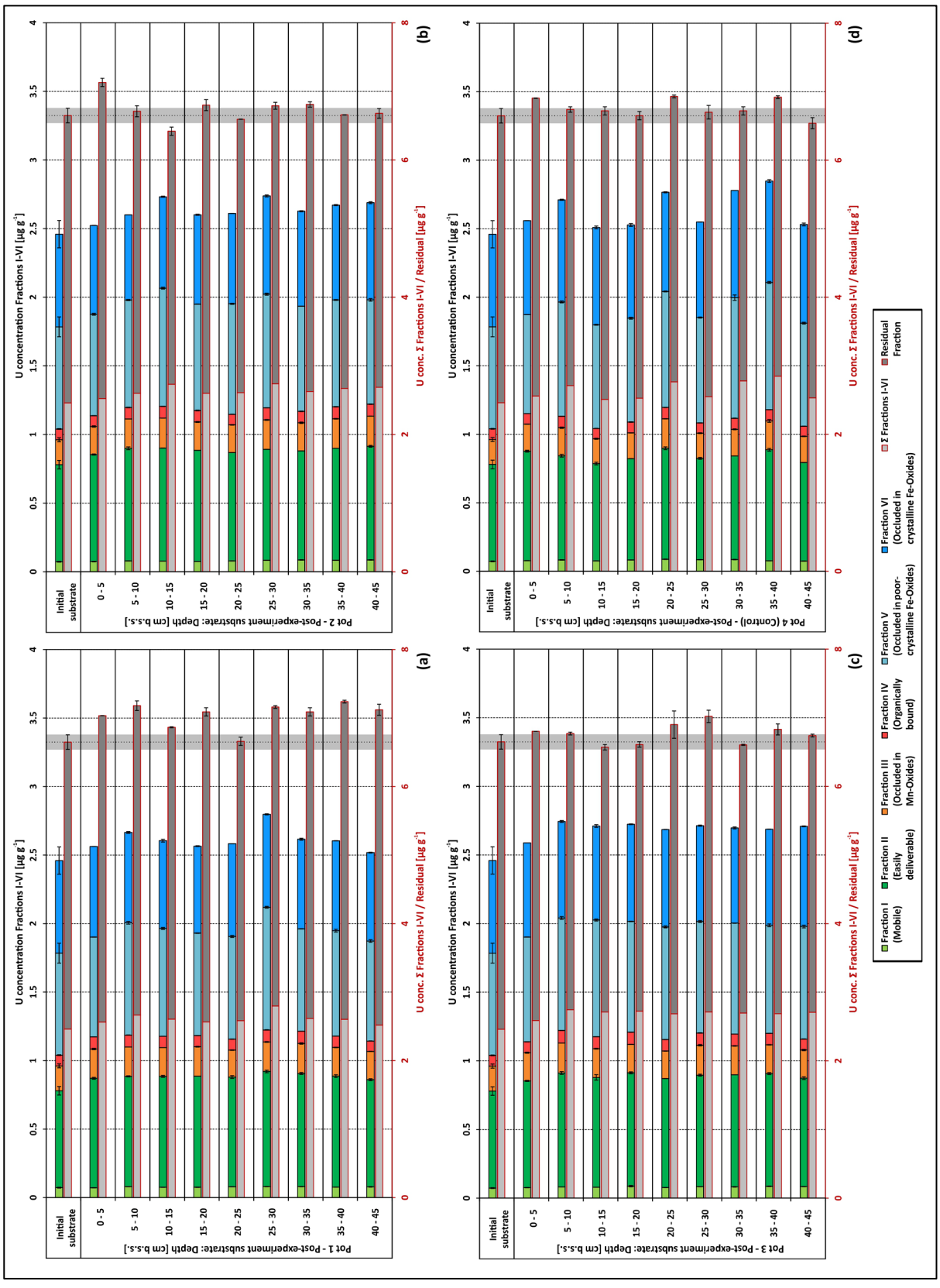

Figure 3–33 Depth resolved U concentrations of the differently bound fractions and total concentrations of the post-experiment substrate in the four pots (diagrams **(a)-(d)**) opposed to the values of the initial substrate.

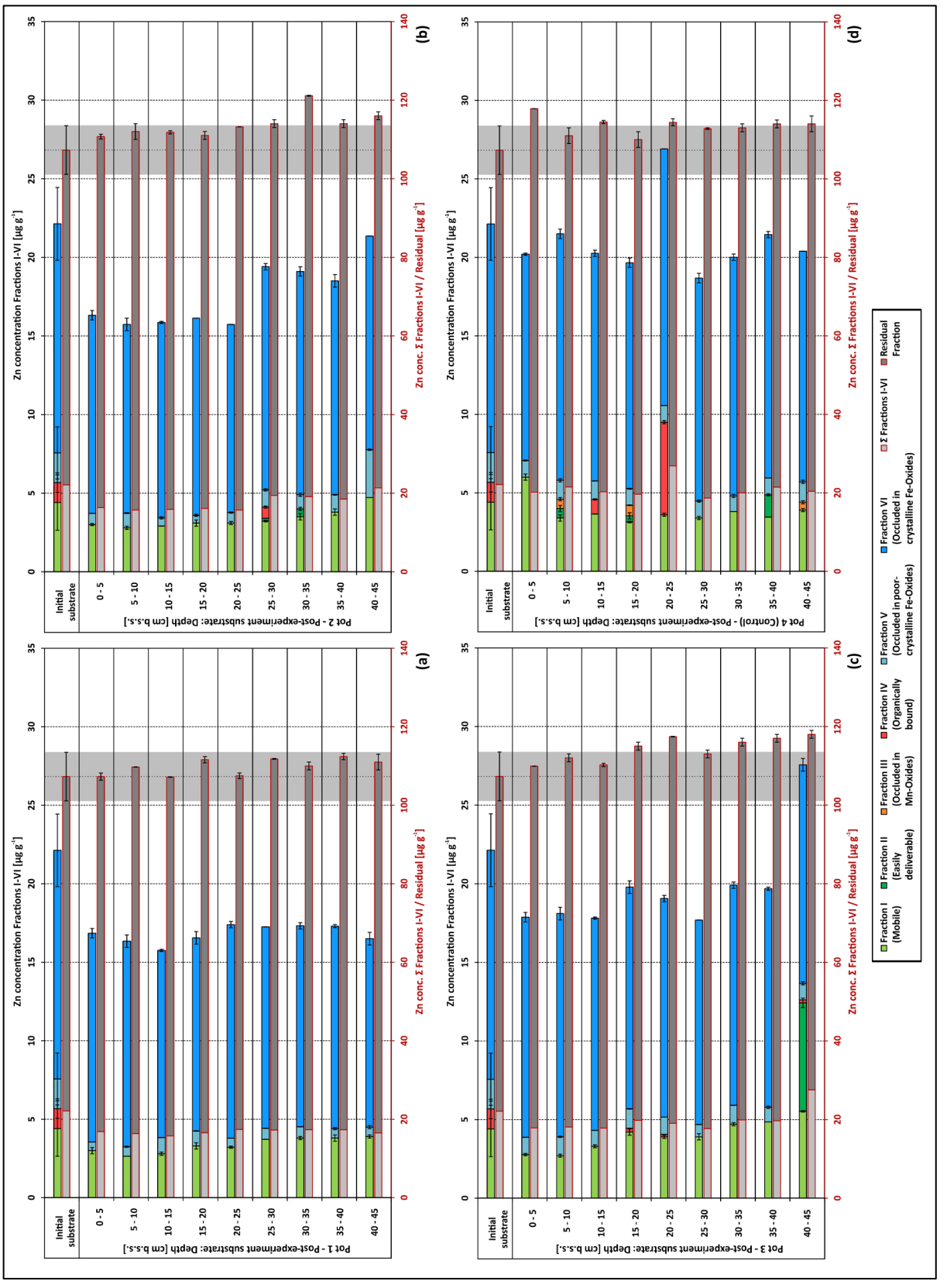

Figure 3–34 Depth resolved Zn concentrations of the differently bound fractions and total concentrations of the post-experiment substrate in the four pots (diagrams **(a)-(d)**) opposed to the values of the initial substrate.

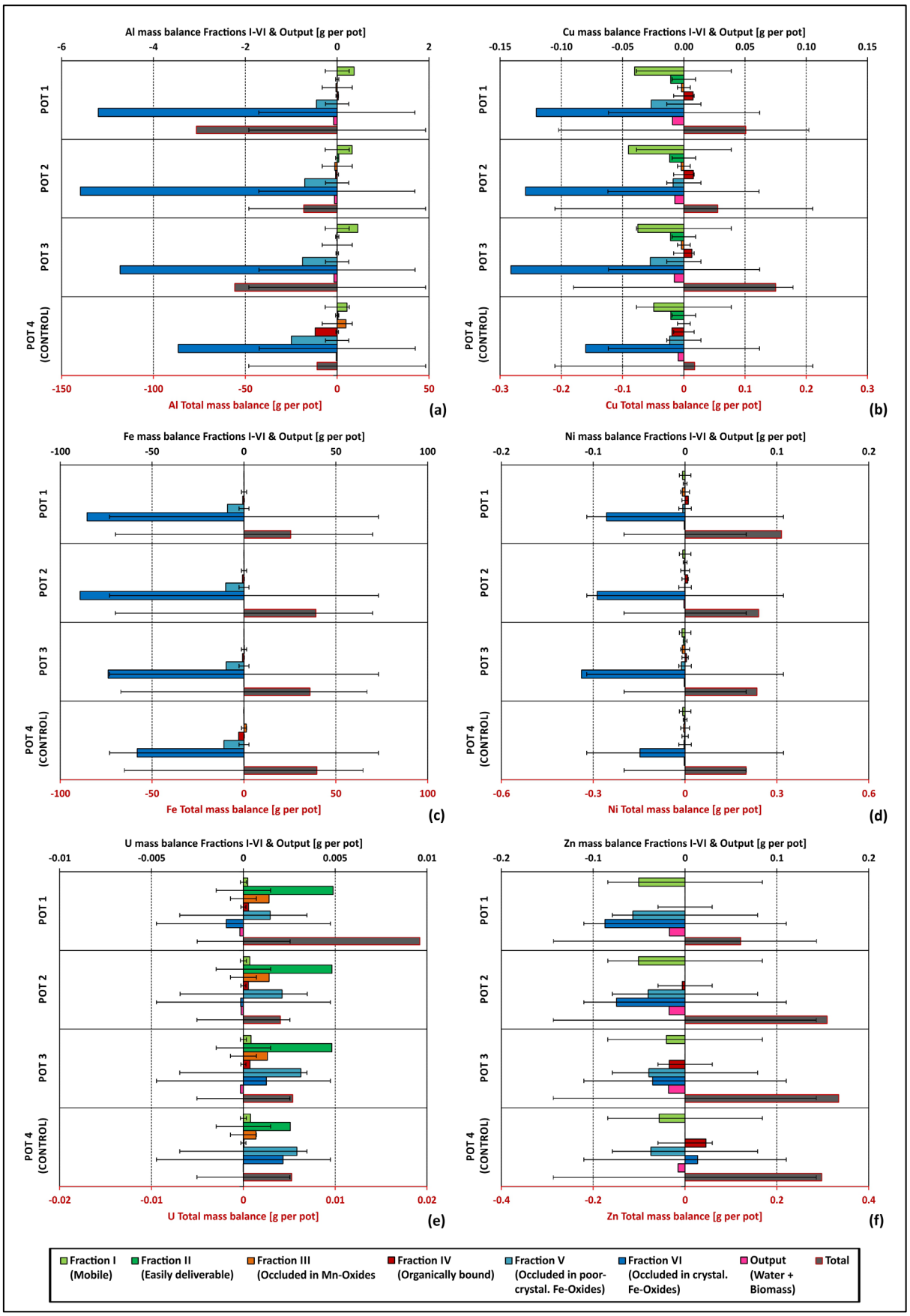

Figure 3–35 Mass balances of the elements Al, Cu, Fe, Ni, U, and Zn (diagrams **(a)**-**(f)**) in post-experiment substrate of the four pots compared to the initial substrate. The mass balances indicate the mass decrease or increase of the particular element in the total substrate mass per pot (47.961 kg) after the experiment. The color-coded stacked bars assigned to the primary X-axes (top of each diagram) represent the mass balances of the fractions I-VI. The grey red-framed bars assigned to the secondary X-axes (bottom of each diagram, in red) indicate the total element masses. The red-pink bars show the total output by water and biomass. The error whiskers were calculated from the standard deviations of the initial substrate (3 individual samples) for each fraction referred to the total mass per pot. This allows estimating the significance of the mass increases or decreases (therefore the whiskers were placed on the zero-point of the X-axes).

3.7 Abundance of ECM short root morphotypes and species identification

Both for the samples from the pots and the field site, three different types of short roots were distinguished morphologically (MT-1, MT-2, MT-3; see **Figure 3–36** for microscopic images). MT-1 was identified based on sequences similarities of the highly conserved ITS-region in the rDNA of a short root sample from POT-1 (sequences length: 397 bp) to published sequences in databases (UNITE, GeneBank, EMBL, DDBJ). The sequence with the most significant alignments to that of the sample refers to the ECM fungus *Meliniomyces bicolor* (INSD sequence: GenBank no. DQ273324; reference: Bergemann & Garbelotto, 2006). The sequence similarity was 98 % (360 of 367 bp). The two other short root morphotypes were clearly identified by their morphological features using the Color Atlas of Ectomycorrhizae (Agerer, 2012) as reference. MT-2 was identified as the ECM fungus *Cenococcum geophilum* while MT-3 was assigned to *Pisolithus tinctorius*, both forming typical short roots with the host tree *Betula pendula*. In general the degree of mycorrhization of birch roots was in almost twice as high (c. 80 %) in the field compared to that in the pots (c. 40 %). The dominating short root morphotype in the case of the pots was assigned to *M. bicolor*. In the field it was more diverse and tree dependent: While for two samples *M. bicolor* was the most abundant species (maximum 80 %) in one sample it was *P. tinctorius*. In the case of samples from the pots short roots of *P. tinctorius* were absent and in the field *C. geophilum* ECM was observed only sporadic.

Morphotype	**MT-1**	**MT-2**	**MT-3**
Species	*Meliniomyces bicolor*	*Cenococcum geophilum*	*Pisolithus tinctorius*
Phylum	Ascomycota	Ascomycota	Basidiomycota
Abundance in Pots (n = 9 trees)	30 - 40 %	5 %	0%
Abundance in Field (n = 3 trees)	5 - 80 % (tree dependent)	< 5 % (sporadic)	5 - 80 % (tree dependent)
Microscopic image	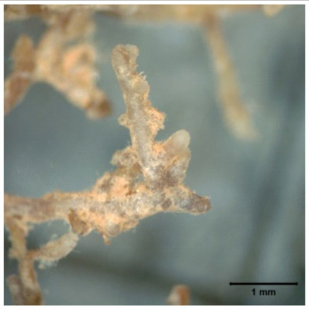		

Figure 3–36 Morphotypes (MT) of ectomycorrhizal short roots found on birch (*B. pendula*) growing in pots or at the field site. The fungal species were identified genetically or by their morphology (according to Agerer, 2012). The given abundances express the ratio of counted mycorrhizal short roots and non-mycorrhizal root tips. The scale bar in each microscopic image stand for to 1 mm on the sample.

The BSE-image captured by SEM (**Figure 3–37**) shows a representative sample of a freeze dried short root thin section (*M. bicolor* from the field site). The thick outer layer is the hyphal mantle consisting exclusively from hyphae of the ectomycorrhizal fungus. The larger cells in the intermediate layer are the cortical cells with apoplastic growing hyphae of the Hartig net (not clearly visible in the BSE-image). The contact area of the Hartig net in the apoplast of the cortex is the main interface in a short root between the fungus and the trees where the transfer of water, nutrients, and sugars between the symbionts tree and fungus takes place. The inner part is the central cylinder, consisting of tree related tissue without any fungal hyphae.

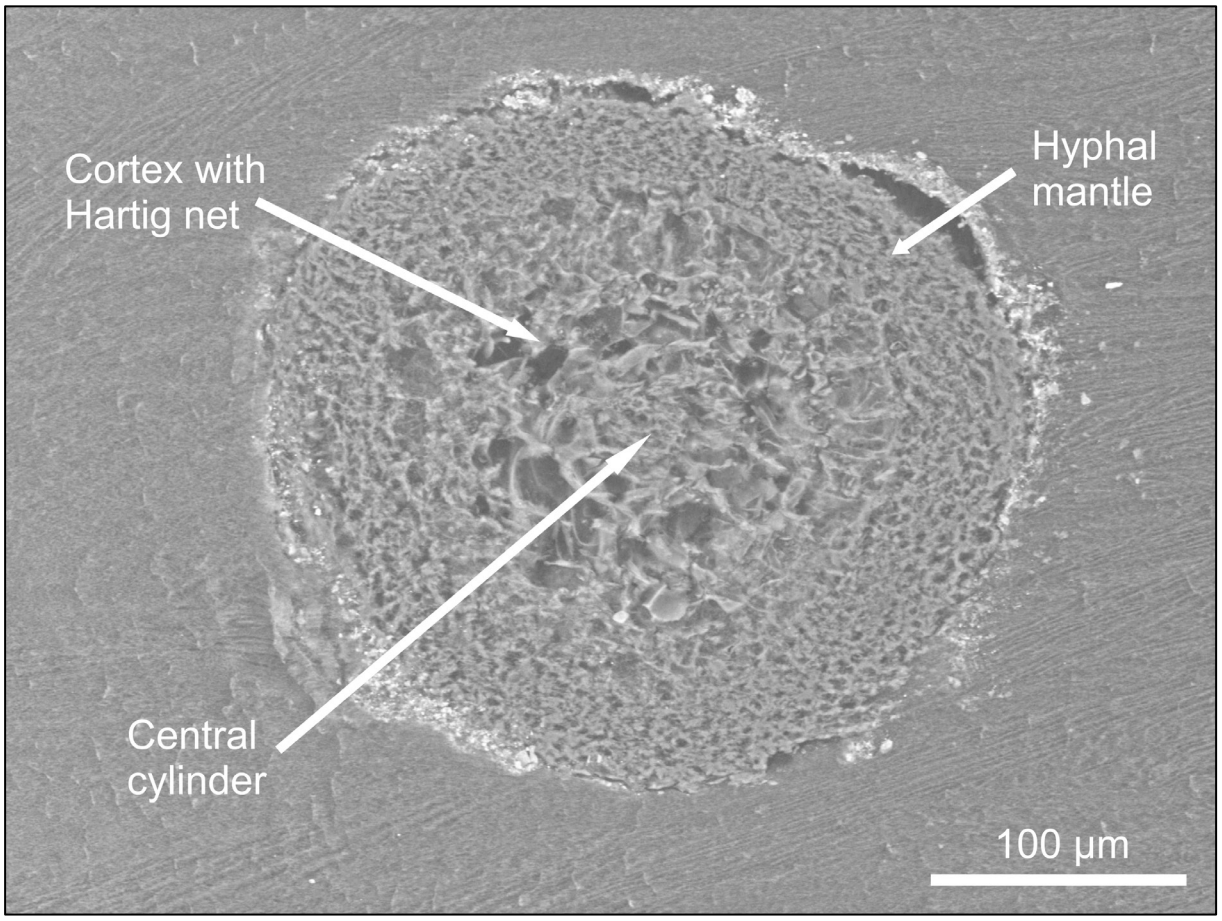

Figure 3–37 Image of a short root thin section (species: *M. bicolor* from field site) captured using a scanning electron microscope (SEM). The typical tissues of an ectomycorrhizal roots are marked by the arrows. The greyish material surrounding the circle shaped short root section is dried tissue freezing medium. The whitish particles coatings at the outer edge of the hyphal mantle are of unknown origin. The image was captured from detected back-scattered electrons (BSE-image, 400x magnification). The acceleration voltage of the electron beam was 15000 V, the emission current was 59.6 mA.

3.8 Mean elemental concentrations and their spatial distribution in ECM short roots

The concentrations of potentially phytotoxic metals as well as plant nutrients differed significantly between the three different short root tissues of mycorrhizal birch roots (**Figure 3–38**; individual sample statistics provided in the appendix, **Table A 1**). On average the highest total concentrations for the elements Al, Fe, K, Mg, Ti, and Si occured in the hyphal mantle. The levels of Al, Fe, Si, and Ti

were there one order of magnitude higher than in the other two compartments. The elements Ca, Cu, P, S, and Zn reached the highest concentrations either in one or in both of the inner tissues (central cylinder and cortex with Hartig net). Ca and Cu showed the highest mean concentrations in the cortex tissue whereas S and Zn were most concentrated in the central cylinder. P showed almost similar maximum mean concentrations in both inner compartments (± c. 50 µg g^{-1}). Within the central cylinder the plant nutrients Ca, K, Mg, P, S, and Si but also Al had the highest percentages. In contrast in the hyphal mantle the contents of Ca, Mg, P, and S were relative to Al, Fe, K, and Si lower. In this tissue Al, Fe, and Si had outstanding high mean concentrations of rounded 24,000 µg g^{-1} (Fe), 27,000 µg g^{-1} (Al), and 43,300 µg g^{-1} (Si). Nevertheless the total Ca, Mg, P, and S levels were in the same range as in the cortical cells and the central cylinder. The percentages of all elements in the cortical cells, which represent the transition between fungal hyphae and tree related tissue, were between that of the central cylinder and the hyphal mantle. Cu, Ti, and Zn had in all compartments the lowest percentages compared to the other elements.

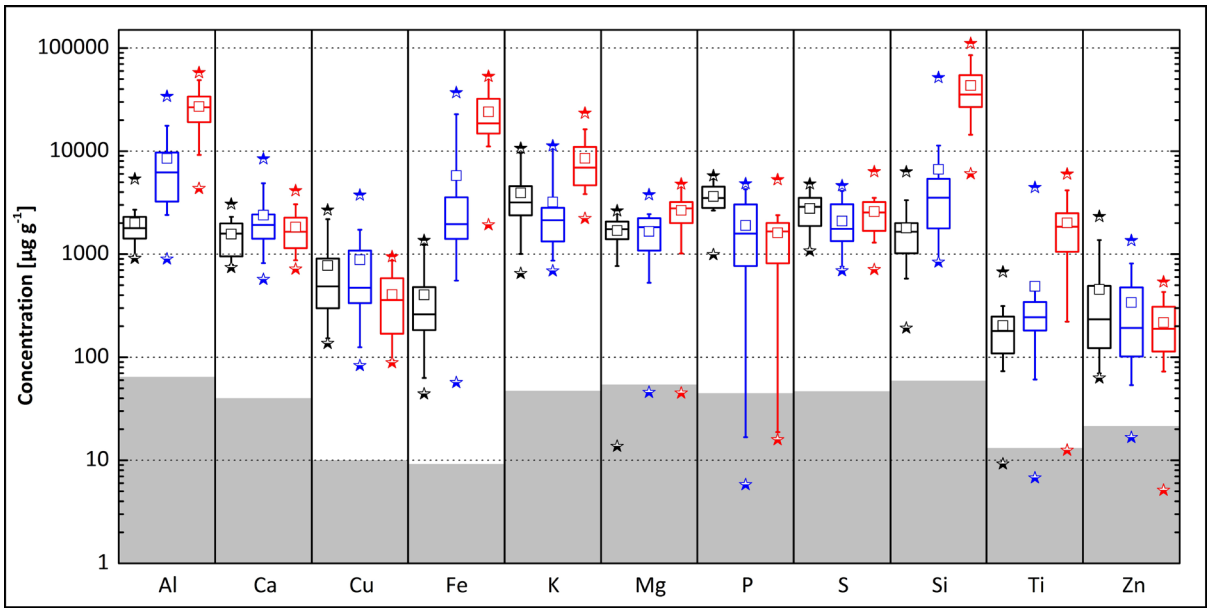

Figure 3–38 Box-Whisker-plots of concentrations of potentially phytotoxic metals and plant nutrients in the three compartments of ectomycorrhizal short roots sampled from the rhizosphere of the testes birch trees. The samples were taken from trees grown in pots and at the field site, ECM species were *M. bicolor*, *C. geophilum*, and *P. tinctorius*. The dimension of the boxes indicate the range which contains the middle 50 % of the dataset (1. to 3. quartile), the lengths of the whiskers represent the data range of 10-25 % (lower whisker) and 75-90 % (upper whisker), the bar in the boxes displays the median, small squares show the mean, and stars represent minima and maxima values. The short root compartments were color coded as following: black - central cylinder, blue - cortex with Hartig net, red - hyphal mantle. The grey areas indicate the data range below the detection limits (LOD). In the case that not more than 25 % of the dataset of a variable (element) were lacking due to concentrations below the LOD, the missing data were replaced with random numbers between 0 and the LOD (therefore some minima are below the LOD).

For some elements the individual samples showed extremely high varying concentrations in at least one short root compartment (relative standard deviation (RSD) higher or equal than 100 %, see **Table A 1** in the appendix). Examples for this group were Al (RSD in cortex 93 %), Cu (RSD in central cylinder 97 % and cortex 103 %), Fe (RSD in central cylinder 97 % and cortex 167 %), K (RSD in cortex

103 %), Si (RSD in cortex 179 %), Ti (RSD in cortex 210 %), and Zn (RSD in central cylinder 131 % and cortex 105 %).

Exemplarily for each of the three identified mycorrhizae quantitative distribution maps of plant nutrients and possibly phytotoxic metals in mycorrhizal root cross sections of *B. pendula* were displayed (**Figure 3–39**: *M. bicolor*, **Figure 3–40**: *C. geophilum*, **Figure 3–41**: *P. tinctorius*; rows 2-5 in each figure). The different compartments of the short roots could be highlighted via the microscopic images (first row in all figures), especially in the case when transmitted blue light and UV excitation were used. Both showed autofluorescence of lignified xylem and phloem fiber cells, Hartig net hyphae, endodermal cell walls, and cortex-wall tannins induced by blue light/UV excitation (Brundrett *et al.*, 1996). Furthermore autofluorescence of the hyphal mantle sheath was visible. This area corresponded to the whitish outermost part of the short root in the reflected light image. The STIM-density maps overlaid by color coded ROIs mark the distinct short roots tissues (fifth row, third map in each **Figure 3–39**, **Figure 3–40**, and **Figure 3–41**). The elemental distribution patterns within the specific tissues were similar for the three ECM species. The total concentrations however differed within the same order of magnitude among *P. tinctorius* and the other two fungal species. Those had significantly higher concentrations in the case of Al and Fe. Compared to the other compartments the highest amounts of the elements Al, Fe, K, Mg, Ti, Si, and Zn occurred in the hyphal mantle. Thereby just small percentage of the elements Al and K were located in the inner compartments. The Al concentrations were higher in the Cortex and Hartig net structures than in the central cylinder. Ca, P and S were concentrated especially within the compartment of the Cortex and Hartig net structures. The Cu distribution was compared to those of the other measured elements unique: the highest amount was detected in the central cylinder and the inner part of the cortex.

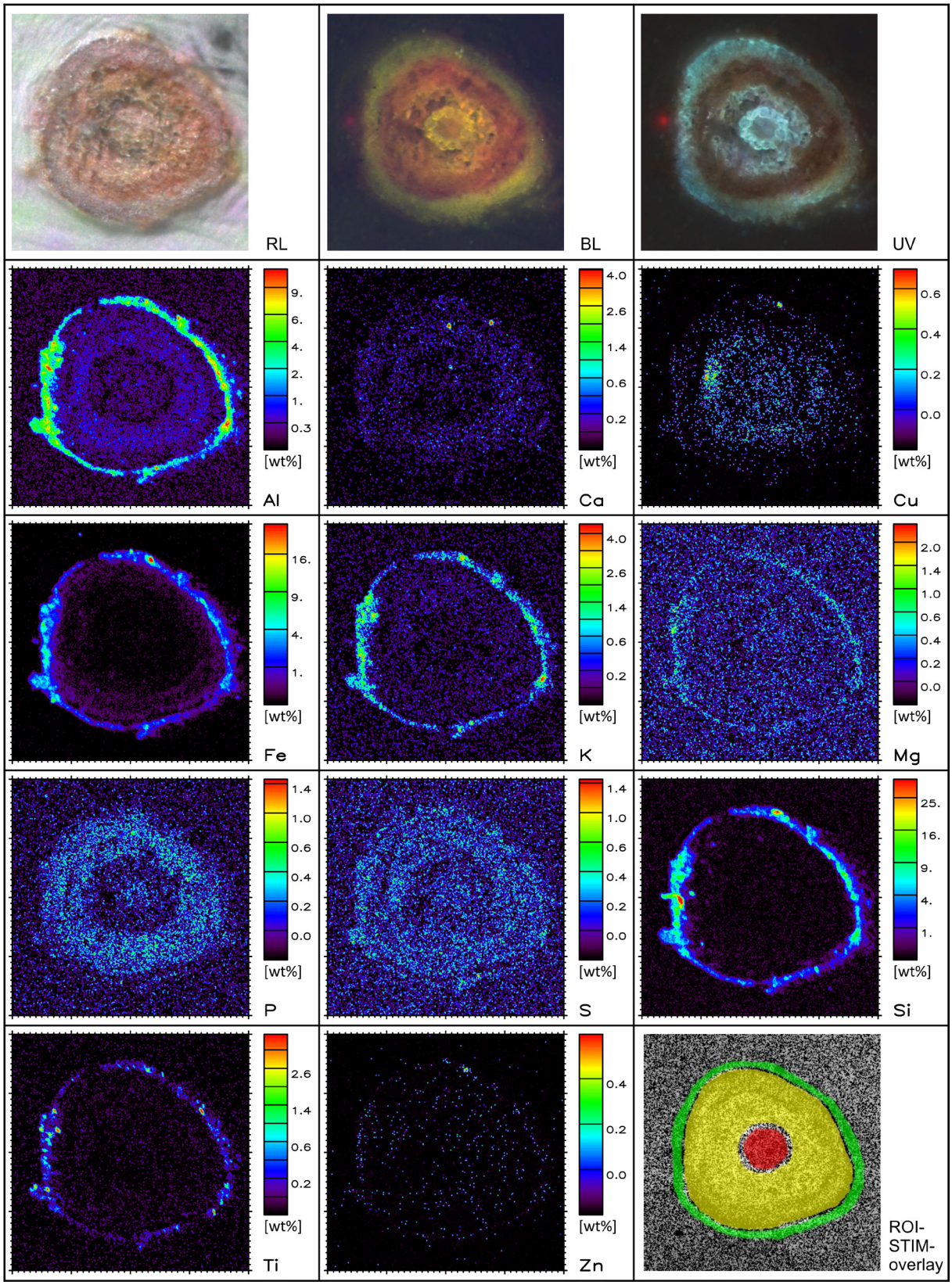

Figure 3–39 A cross-section of an ectomycorrhizal association of birch with the fungus *M. bicolor* (growing site: field). Microscopic images (first row), elemental distribution maps (second to fifth row) and density map (STIM) overlaid by regions of interest (ROI) masking the different short root tissues (fifth row, third map) are shown. The microscopic images were taken with different light sources: RL - reflected light, BL - blue excitation (450-490 nm), UV - ultraviolet excitation (365 nm). The spatially resolved quantitative elemental maps were obtained from the concentration data of the micro-PIXE analysis. The STIM-map shows areas of higher densities with darker hue and the ROIs masking short root tissues: green - hyphal mantle, yellow - cortex with Hartig net, red - central cylinder. The same detail of the sample as in the microscopic images is displayed by the maps; the size of each map is 400x400 µm.

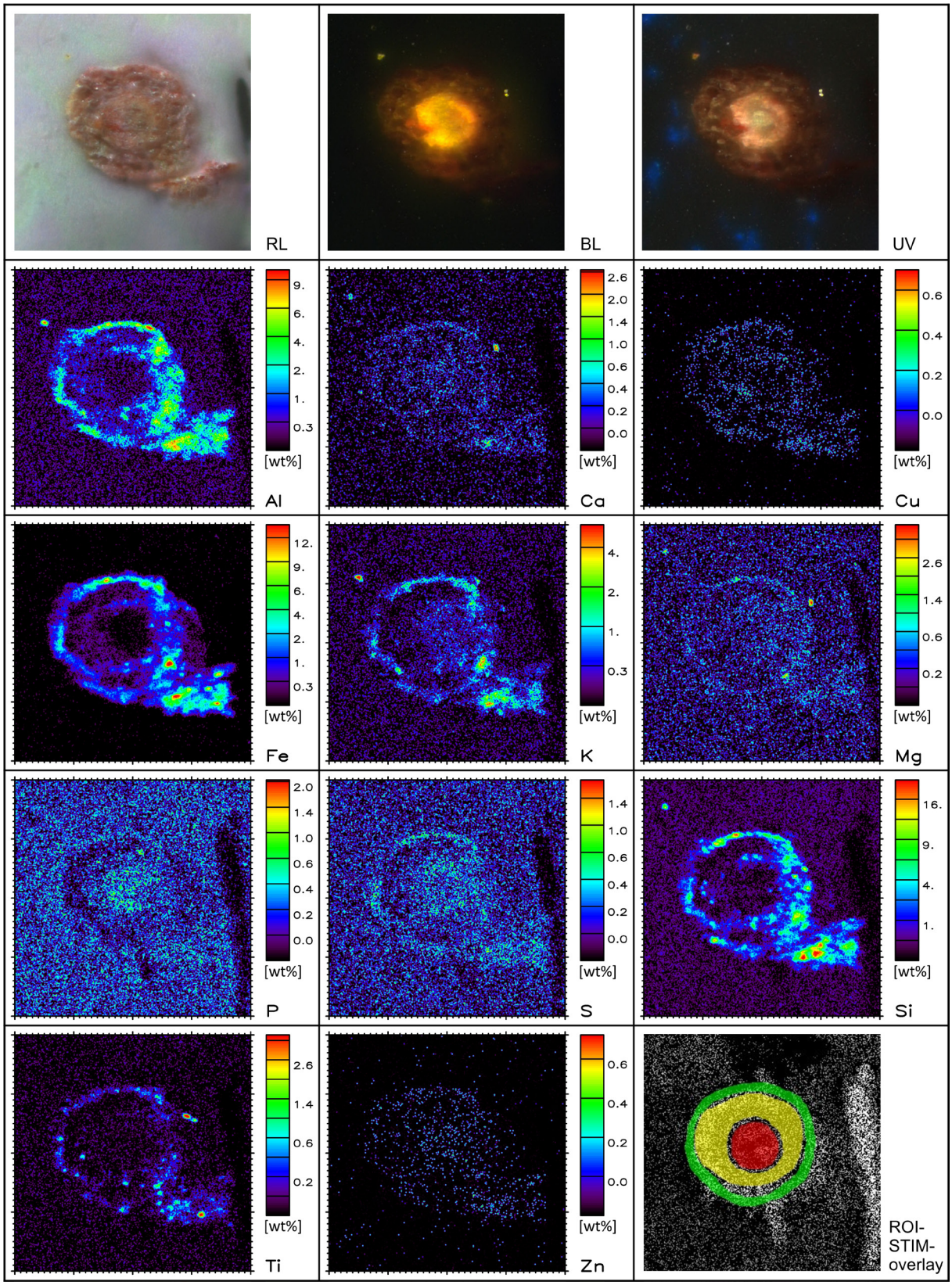

Figure 3–40 A cross-section of an ectomycorrhizal association of birch with the fungus *C. geophilum* (growing site: pot). Microscopic images (first row), elemental distribution maps (second to fifth row) and density map (STIM) overlaid by regions of interest (ROI) masking the different short root tissues (fifth row, third map) are shown. The microscopic images were taken with different light sources: RL - reflected light, BL - blue excitation (450-490 nm), UV - ultraviolet excitation (365 nm). The spatially resolved quantitative elemental maps were obtained from the concentration data of the micro-PIXE analysis. The STIM-map shows areas of higher densities with darker hue and the ROIs masking short root tissues: green - hyphal mantle, yellow - cortex with Hartig net, red - central cylinder. The same detail of the sample as in the microscopic images is displayed by the maps; the size of each map is 400x400 µm.

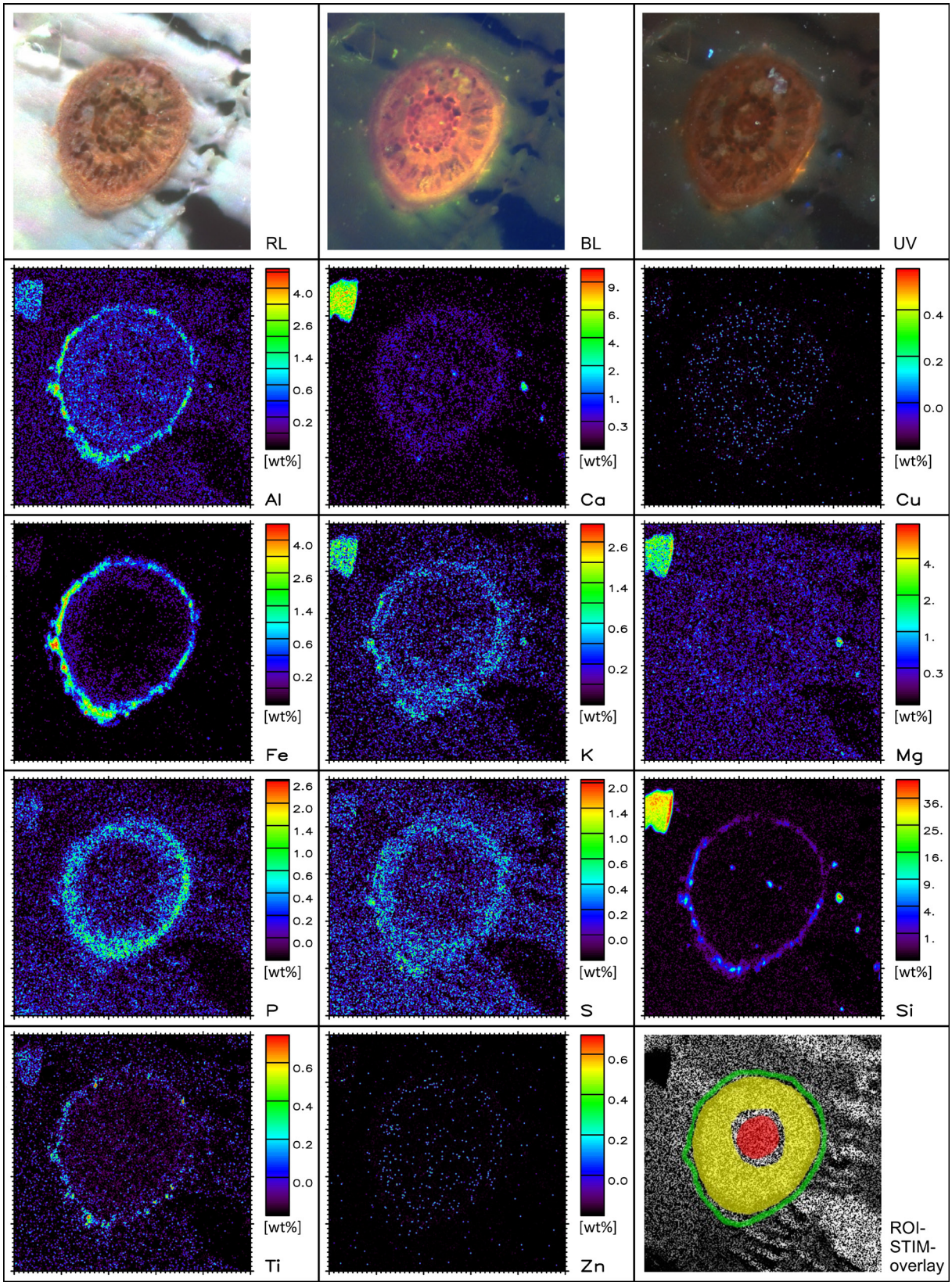

Figure 3–41 A cross-section of an ectomycorrhizal association of birch with the fungus *P. tinctorius* (growing site: field). Microscopic images (first row), elemental distribution maps (second to fifth row) and density map (STIM) overlaid by regions of interest (ROI) masking the different short root tissues (fifth row, third map) are shown. The microscopic images were taken with different light sources: RL - reflected light, BL - blue excitation (450-490 nm), UV - ultraviolet excitation (365 nm). The spatially resolved quantitative elemental maps were obtained from the concentration data of the micro-PIXE analysis. The STIM-map shows areas of higher densities with darker hue and the ROIs masking short root tissues: green - hyphal mantle, yellow - cortex with Hartig net, red - central cylinder. The same detail of the sample as in the microscopic images is displayed by the maps; the size of each map is 500x500 µm.

The cluster analysis of the elements (variables) revealed two main clusters which originated from higher Z-values for the elements of the second cluster Al, Fe, K, Mg, Si, and Ti in the hyphal mantle and reduced Z-values in the other two compartments (**Figure 3–42**, column dendrogram). Higher Z-values indicate increased concentrations compared to the average above all samples per element. Therefore the cluster analysis confirmed the diverse distribution patterns in the different short root tissues. The elements of the first cluster showed a more diverse pattern regarding increased concentrations in particular compartments. For those elements most of the samples showed higher levels in the cortex and central cylinder. A correlation of the individual samples (observations) with the origin of the samples (field or pots) or the fungal species was not possible from the clustering (**Figure 3–42**, row dendrogram). Therefore the results of the discriminant analyses were considered.

The characteristic factors eigenvalue, discrimination (factor loading) and standardized canonical discriminant factor coefficient of the two discriminant analyses described below are listed in **Table A 1** in the appendix. To identify groups and their discriminating attributes within the whole dataset a first discriminant analysis (DA-1) which included all data, regardless of the tissue concentrations, was carried out. Therefore, the data were classified regarding the fungal species and the growing site as following: *M. bicolor*, *C. geophilum*, or *P. tinctorius* each combined with the growing site pots (P) or field (F). Due to the high diversity of the element levels in particular tissues the data dispersal within groups was higher. Nevertheless a separation between different groups was clearly observable. The mycorrhizal roots resemble by their elemental profiles according to growth conditions. Samples of *C. geophilum* grown either in the pots (CG-P) or in the field (CG-F) differed most according to discriminant factor F1 with c. 80 % discrimination (**Figure 3–43**, **(a)**). Variables that contribute most to F1 are the concentrations of Mg, Ca, P, and, S (**Figure 3–43**, **(b)**). Thereby the Mg levels were higher in pots, while Ca, P and, S concentrations were higher under field conditions (compare means by class in **Table A 2** in the appendix). Samples of *M. bicolor* from the pots (MB-P) or the field (MB-F) differed most according to discriminant factor F2 with 13 % discrimination. Variables that contributed most to F2 were the concentrations of K, S, and Zn, which reached higher levels in the samples from the pots. The samples of *P. tinctorius* from the field (PT-F) grouped closely to MB-F. Both discriminant factors together represented about 93 % of the variability between the different samples included in DA-1.

To identify groups and their discriminating attributes on the tissue level a second discriminant analysis (DA-2), which included only the data from the samples grown in pots, was carried out. The data therefore were classified according species and compartment of each short root sample: *M. bicolor* or *C. geophilum* each combined with the tissues hyphal mantle (HM), cortex with Hartig net (CO), or central cylinder (CC). At the tissue level both fungal species behaved similarly. However there was a clear difference in the elemental profiles of the particular tissues. Hyphal mantle and the inner tissues differed according to discriminant factor F1 with c. 17 % discrimination (**Figure 3–44**, **(a)**). The variables which contributed most to F1 were concentrations of Al, Fe, Si, and Ti as well as Mg and K (**Figure 3–44**, **(b)**), which reached their highest levels in HM (compare means by class in **Table A 3** in the appendix). The elemental profiles of cortex and central cylinder varied according to discriminant factor F2 with approx. 73 % discrimination. The variables which contributed most to F2 were concentrations of S and Ca, with S being the most abundant in CC and Ca in CO. Both discriminant factors together explained approx. 90 % of the variability of the DA-2 dataset.

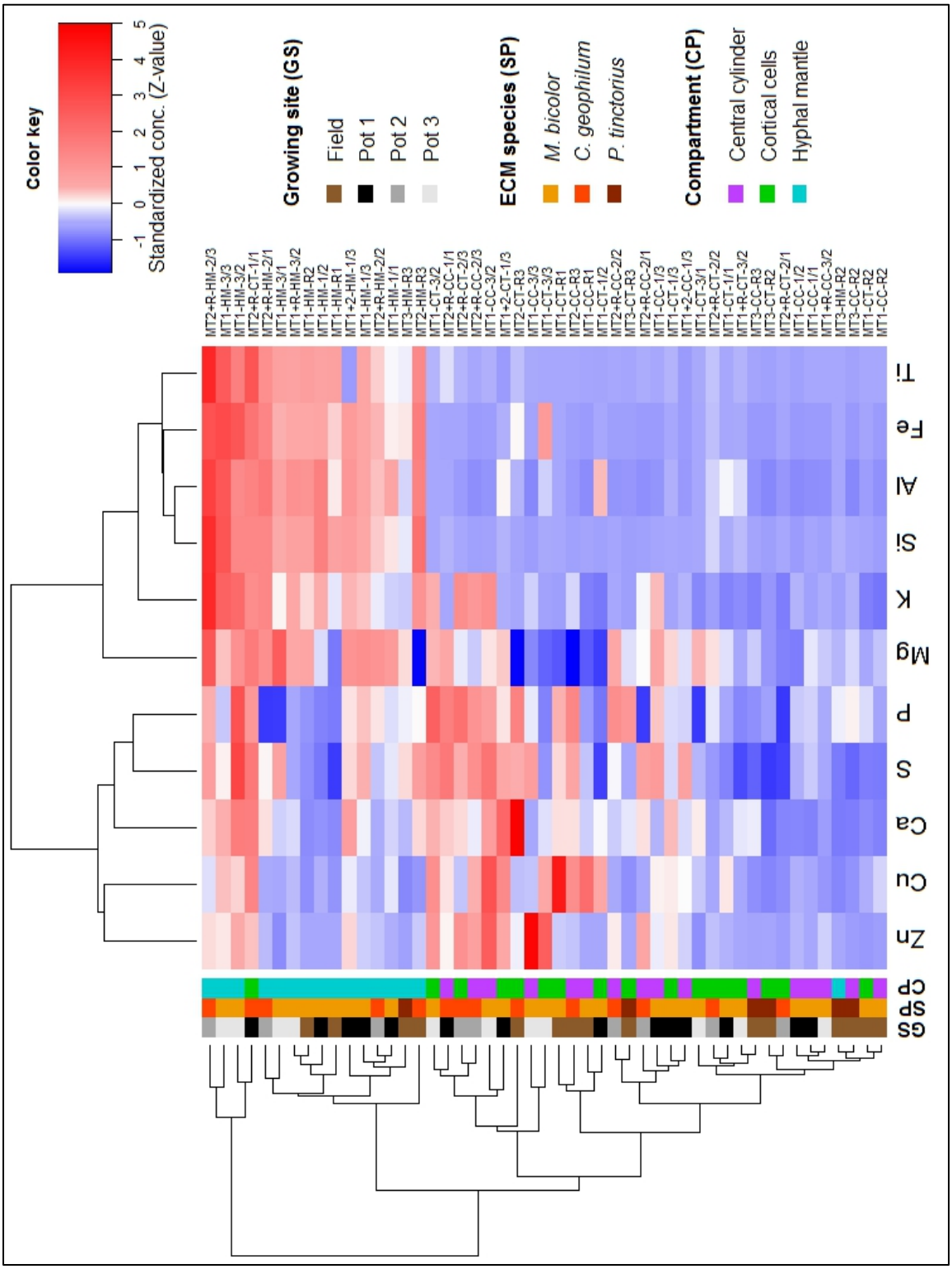

Figure 3–42 Heatmap of Z-standardized (element-wise standardization over all samples) concentrations in the tissues of each sample. Bluish colors represent concentrations below the average of the relative element (averaged per element over all samples), whitish colors represent concentrations around the average and reddish colors stand for values greater than the average. Dendrograms for both variables (elements) and observations (samples) sidewise the heatmap express the result of the cluster analysis (clustering method: Ward, distance measure: squared Euclidean distances). Reordering was performed for both variables and observations regarding their similarity; color coded row side bars (left hand-side) characterize each sample regarding the growing site (GS), ECM species (SP) and short root compartment (CP) and allow to relate each sample to these properties (sample labeling on the right side of the heat map).

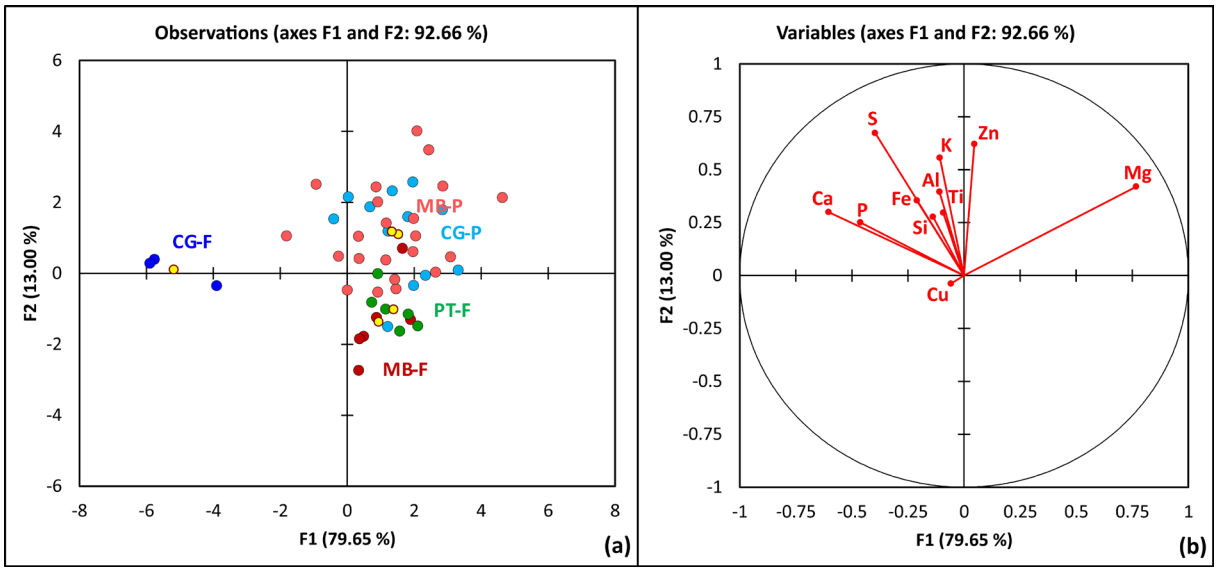

Figure 3–43 a) Discriminant analysis (DA-1) plot of elemental concentrations measured by micro-PIXE in mycorrhizal birch roots colonized by different fungal species (CG – *C. geophilum*, MB – *M. bicolor*, PT - *P tinctorius*) and grown in pots (P) or collected from the field (F). The colored circles (colors assigned group-wise according to the label) represent samples grouped according to species and growing site. The yellow circles represent the mean of each group. **(b)** Plot of correlations between variables (element concentrations) and discriminant factors (F1, F2) of the DA-1 dataset.

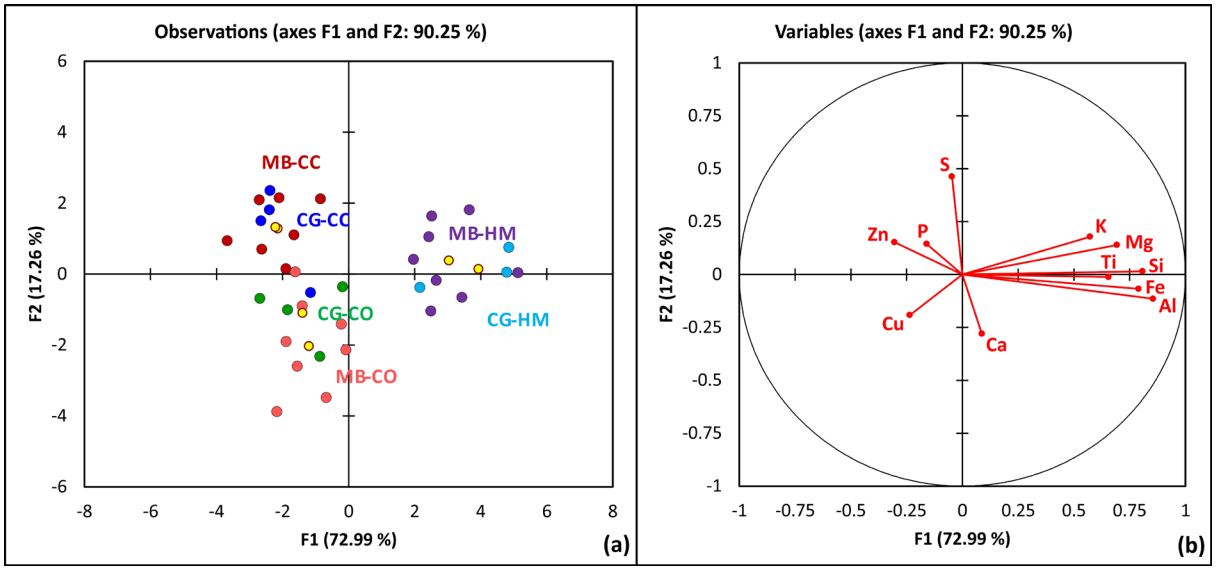

Figure 3–44 (a) Discriminant analysis (DA-2) plot of elemental concentrations measured by micro-PIXE in different tissues (HM - hyphal mantle, CO - cortex with Hartig net, CC - central cylinder) of mycorrhizal birch roots grown in pots and colonized by two fungal species (CG – *C. geophilum*, MB – *M. bicolor*). The colored circles (colors assigned group-wise, according to the label) represent samples grouped according to tissue and species. The yellow circles represent the mean of each group. **(b)** Plot of correlations between variables (element concentrations) and discriminant factors (F1, F2) of the DA-2 dataset.

4 DISCUSSION

4.1 Soil properties, mineralogy, physico-chemistry, and element concentrations of the study site substrate

The geological background of the base rock is mainly siliceous sediments like quartzite and different kinds of shale e.g. siliceous shale, alum shale, and argillaceous shale (Hiekel *et al.*, 2004, Wismut GmbH, 1994). Therefore, the weathered substrate at the study site, which has developed from the local waste rock dumped on the former heap, is carbonate free and consists mainly of SiO_2, as proofed by XRF and XRD analyses. The low substrate pH of 4.17, classified as (very) strong acidic, is within the Al-buffer range (pH 4.3-3.0). This pH range is dominated by strong up to complete cation leaching as well as Al-toxicity due to an excess of Al^{3+}-ions (Eckelmann *et al.*, 2005; Blume *et al.*, 2010). The high acidity most probably originated from acid mine drainage (AMD) that percolated through the heap material into the pristine soil and bedrock. AMD is often produced by oxidation of pyrite (FeS_2) containing waste rock material. On average, the heap material contained 3.3 wt% pyrite. Thereby pyrite reacts with oxygen and water and forms ferrous iron, sulfate, and hydrogen ions that decrease the pH. This process is often facilitated by microorganisms (Akcil & Koldas, 2006). The AMD probably percolated through the former heap into the underlying material and led to its contamination due to acidification and input of metals leached from the waste rock material. The heap was excavated in the context of the remediation to the level of the pristine ground surface which was exposed thereby. The low pH impedes plant growth as well as increases the release of Al-ions from silica, resulting in Al-toxicity (Blume *et al.*, 2010).

The pH lies within the pH range of 3.9-4.5, which is typical for the organic horizons in northern forests (Clarholm & Skyllberg, 2013). As a legacy of the former mining activities, by AMD formation, and geogenically determined the total concentration of the elements Al, Cu, Fe, K, Ni, P, Ti, and U in the substrate that was used for the pot experiments were at least twice and maximum fivefold as high as the reference values of European subsoils (Salminen *et al.*, 2005). Cu and Ni actually exceeded precautionary levels for these metals in the German federal soil protection ordinance (BBodSchV, 1999). This implies that despite the removal of the heap the substrate of the study area 'Kanigsberg' is still moderately enriched with some potentially phytotoxic metals. However, the bioaccessible concentrations of those elements except Al and Cu were low compared to the total contents, although the acidic conditions of the substrate typically increase the mobility of many elements and therefore their availability for the plant uptake.

Al is an important growth limiting factor for plants growing on acidic soils with pH below 5. Under this acidic regime its phytotoxic form is dominant, causing mainly root growth inhibition (thickening and stubby appearance of lateral root, lacking fine branching) as a symptom (Rout *et al.*, 2001). Organic ligands like oxalate and citrate that are released by plant roots and soil microorganisms form strong complexes with Al^{3+} cations and therefore lower the concentration of Al in solution. These complexes are less toxic to plants than free Al^{3+} (Landeweert *et al.*, 2001). At pH above 5.0 free Al^{3+}, typically originating from silicate weathering, is instantly precipitated as the secondary mineral gibbs-

ite ($Al(OH)_3$). Above pH 4.5 the gibbsite formation leads to acidification due to the release of H^+. Below pH 4.5 gibbsite is decomposed under consumption of H^+, Al has therefore a base cation character like Ca and Mg and its buffering effect is facilitated by complexation with organic functional groups. The complexation process mainly takes place in surface horizons with soil organic matter (Clarholm & Skyllberg, 2013). Due to the fact that the total carbon content in the substrate of the study area is low the described neutralization effect by Al at pH below 4.5 is probably not much facilitated. Likewise, Cu has a high affinity for binding to dissolved organic matter in the soil solution. It has been shown that most of the dissolved Cu was bound to organic ligands, for most soils in a range of about 98 %. In general, the amount of free Cu^{2+}-ions decrease with increasing pH. Even though copper is an essential micronutrient for plants (e.g. cofactor in many enzymes, essential for photosynthesis), an excess could lead to phytotoxic symptoms like reduced root elongation and stunting (rhizotoxicity) (Alloway, 2013). Therefore, the higher bioavailability of Al and Cu, compared to other metals that occurred with high total concentrations in the substrate of the study site, could induce phytotoxic effects. These include a reduced root growth and therefore growth limitations of the affected trees. Further obstacles for normal growth of trees might be a deficiency of bioavailable Ca, K, and P in the substrate of the study site. It is probably caused by leaching of these plant macronutrients due to the high acidity and low nutrient storage capability of the weathered base rock material, which is still in the initial stage of soil formation. These assumptions are supported by the low CEC_{eff} of the substrate (c. 4 cmol kg^{-1}), that indicates a poor nutrient binding capability and a low amount of humus of approx. 2 wt% (Eckelmann, 2005).Compared to agricultural soils the substrate is poor in the above-mentioned nutrients, their values are far below usual concentrations. Standard nutrient levels of agricultural 'undisturbed' soils are reviewed in Schilling (2000). Normal Ca concentrations in soils reach from 0.1 to 1.5 %, and K contents are in the range of 0.2-3 %. Typical P total concentrations in soils lie between 0.02 and 0.15 % and depend strongly on the organic substance content. Nutrient deficiency induces additional stress to plants growing on such harsh substrate.

The substrate at the study site could be therefore classified as nutrient poor, acidic, and moderately metal contaminated material with poor soil fertility.

4.2 Temporal developing of physico-chemistry and metal concentrations in the substrate solution

The pH value of an aqueous solution in equilibrium with the soil is an important soil parameter that enables to deduce the behavior of contaminants and nutrients as well as allows conclusions on the soils potential filter-properties for pollutants and its appropriateness for plant growths (Blume *et al.*, 2016). The observed pH decreases in the substrate solution with increasing depth and ongoing duration of the pot experiment, that existed in the planted pots as well as in the control (although to varying extents), could be explained by the concept of soil acidification. The soil acidity increases if within a specific time span more protons are released from soil. Proton excess usually originates from soil-internal processes, introduction by water or occurs if soluble products of proton-consuming reactions were leached from the soil by percolating water (Blume *et al.*, 2010). Acidification starts after the leaching of lithogenic carbonates or, as in the case of the study site substrate, immediately

due to their absence into the parent rock material from which the soil developed. Especially the Silurian siliceous and alum shales as well as the aluminosilicates (Ockerkalk formation), which form i.a. the bedrock of the study area and were mined from the former 'Lichtenberg' open pit mine, were almost carbonate free as a result of weathering processes (Wismut GmbH, 2010). Due to the lacking carbonate, a rapid and effective pH buffer is absent; this is why presumably the buffering through the Al-buffer system is dominant in the substrate of the study area. This leads at pH below 4.5, as monitored for the substrate solution of all pots, to an increasing occupation of the cation exchanger sites of the base cations Ca^{2+}, Mg^{2+}, K^{+}, and Na^{+} by acid Al^{3+}-ions (Blume *et al.*, 2016). In this acidic pH-range depletion of exchangeable bound nutrients and the production of phytotoxic Al^{3+}-ions occurs. On the other hand, Al works as a buffer at a pH below 4.5 when Al^{3+}-ions are released under consumption of protons from gibbsite ($Al(OH)_3$), which is formed as a secondary mineral during silica weathering (Clarholm & Skyllberg, 2013).

The removal of the substrate from the study site, the sieving and homogenization, as well as the layer-wise infilling in the mesocosm pots very probably led to a disaggregation and ventilation of the material. Furthermore, the substrate water saturation of c. 15 vol% in the pots differed to the field conditions, which are influenced by periodically changes of the soil moisture due to drought and heavy rain events. As a result of the ventilation, the higher soil moisture, and the exposition of fresh unweathered mineral surfaces, weathering processes like pyrite oxidation, as described in subchapter **4.1**, might have been strengthened and accelerated in the course of the pot experiment. As a result, a further acidification of the substrate and an increased release of base and acid cations may have taken place. Therefore, the pH decrease with increasing duration of the experiment within all pots could be explained by the increasing saturation of the DI-water with products of the proceeding weathering like base and acid cations as well as protons leading to further acidification. The depth related pH decrease could be explained by a dilution effect due to the watering. While the proceeding weathering lead to further acidification in the deeper layers of the substrate (e.g. pH below 3.7 in the control pot in 38 cm depth, week 55), the substrate solution in the shallower depths was diluted with fresh DI-water with a higher pH (mean pH of DI-water: 5.4). DI-water is water from which mostly all unwanted ions (cations and anions) are removed, usually by ion-exchangers cascaded in a water stream (Mortimer & Müllller, 2007). A cation-exchanger removes cations by liberating the protons and an anion-exchanger removes anions by liberating hydroxides. Often (synthetically) zeolites or synthetically polymeric ion-exchangers are used, that consist of a matrix carrying ionic charges with space for water and exchangeable counterions (*ibid.*). Due to the removal of most of the cations and anions the specific electrical conductivity of DI-water is low; the DI-water used in the pot experiment had on average an EC of 0.9 µS cm^{-1}. Rainwater typically has an EC of 5-30 µS cm^{-1}, groundwater 30-2000 µS cm^{-1}, and the EC threshold for drinking water in Germany is 2500 µS cm^{-1} (Hölting & Coldewey, 2013). By watering the pots with DI-water the undersaturation with ions might have led to an acceleration of the substrate weathering due to its corrosive character by the ambition to reach the solution equilibrium.

The described effects of decreased pH with higher depths in the course of the experiment were mitigated in the planted pots compared to the unplanted control. That can be explained by the buffering of the substrate acidification by the birch roots. The ability of plant roots to change the pH in

their rhizosphere substantially is well known. Various origins of root-mediated pH changes in the rhizosphere were reviewed by Hinsinger *et al.*, 2003. In general, when more anions than cations are taken up in to the cytosol of the root cells hydroxide (OH^-) is released in the apoplast or protons (H^+) are taken up from it. This is crucial for the compensation of the electrical charges in order to regulate the cytosol pH maintained around 7.3. Within the cytosol of the roots cells excessing protons are consumed by decarboxylation of organic acids like citric, oxalic, and malic acid. These acids, which are stored intracellularly in vacuoles, dissociate in the neutral cytosol and can be released therefore as organic anions into the apoplast. If the external pH is lower than the cytosolic pH the organic anions can increase the rhizosphere pH by their pronation or decomposition (e.g. by microorganisms). In acidic soils reduction zones can occur around roots due to root and microbial respiration causing an O_2 concentration decrease as well as due to reductase systems on the root surfaces. In these zones, with the help of electrons produced by oxidation of organic matter, Fe(III) in minerals like goethite can be reduced to Fe(II). This reaction consumes protons which results in an increase of the pH in the rhizosphere reduction zones. While in response to environmental stress like Al-toxicity and shortage of P usually leads to a release of protons in normal plants, Al-resistant plants are able to alkalinize their environment. Moreover, the before mentioned stress factors often enhance the exudation of organic anions, leading again to an increased pH. As reported for other (herbaceous) plants in the review of Hinsinger *et al.*, 2003 also birch trees seem aiming to avoid extreme low pH values by root-induced alkalization of the rhizosphere in order to reduce the effects of increasing acidification like Al-toxicity. Summarized, possible pathways of buffering low pH in the soil solution are the release of hydroxides or uptake of protons, the release of organic anions and their subsequent protonation, and proton consuming reduction processes.

In contrast to these findings of the pot experiment many other investigations reported that afforestation with trees lead to an acidification of the soil**.** In a global meta-analysis study (Berthrong *et al.*, 2009), in which the pH of 153 afforestation sites planted with trees of different genera were compared, it was shown that on average the initial soil pH decreased about 0.3 units in the top soil (first 30 cm) due to the tree plantations. Also Binkley, 1995 reviewed many studies that investigated temporal changes in top soil pH in forest stands. Most of the studies found a lowering of the soil pH which dropped about 0.3-1.3 units, depending on the tree species (often genera *Pinus* and *Eucalyptus*) and the age of the afforestation. In this review only one study was mentioned where the pH in the top soil of over 50 years old stands of sugar maple (*Acer saccharum*), balsam fir (*Abies balsamea*), jack pine (*Pinus banksiana*), and black spruce (*Picea mariana*) had increased by 0.0-0.6 units. Another study (Tamminen & Derome, 2005) investigated the soil pH change within 12-24 years in 53 forest stands of different trees species like Scots pine (*Pinus sylvestris*), Norway spruce (*Picea abies*), Siberian larch (*Larix sibirica*), and silver birch (*B. pendula*) in southern Finland. They found a pH increasing trend of 0.1-0.34 units, depending on the layer of the 30 cm trenches. These studies showed contradictory results to the findings of this work, which shows that those results were not transferrable to all soils and tree species.

The strong increase of the Al soil solution concentrations measured in greater depths of the unplanted pot in the course of the experiment might be related to the intensified release of soluble Al-ions as a result of silica weathering. The Al^{3+} release at pH values below 4.5 (as in the pot experiment)

results in the consumption of protons on a charge basis without hydrolysis. Therefore, Al ions at such acidic pH can be considered to have a base cation character liker Ca, Mg, and K-ions (Clarholm & Skyllberg, 2013). The inorganic Al^{3+} is the principal plant-rhizotoxic form and dominates soil solutions with pH below 5. It buffers the pH of mineral low-organic soils to values around pH 4 and is therein plant-available in its toxic form. By growing under such conditions plant races can develop Al-tolerance to some degree (Kidd & Proctor, 2000). Silver birch is considered as an Al-tolerant plant and was found to tolerate concentrations of up to 81 mg L^{-1} without any growth reduction; however additional stress due to low nutrient supply lowered the tolerance levels to c. 5 mg L^{-1} (Clegg & Gobran, 1995). Another study investigated the Al-tolerance in *B. pendula* races originating from natural soils in Scotland, UK with different pH conditions ranging from acidic to neutral (Kidd & Proctor, 2000). It was shown that the races from the acidic sites, under which a lot of the monomeric Al exists in its most toxic form, were Al-tolerant to different extends. The authors stated that the response of the different *B. pendula* races to toxic Al could be predicted from soil conditions of the site, e.g. the race from the site with the highest concentrations of monomeric Al and a pH of 4.3 had the highest tolerance. These findings indicate that also the *B. pendula* trees used in the pot experiment can probably be considered as Al-tolerant race based on their origin from a field site with acidic conditions and high Al concentrations in solution and their ability not only to survive but to grow under these conditions. The lowered Al substrate solution concentrations in the planted pots can be explained by the root-induced pH increases, which may reduce the dissolution of Al from the substrate. Furthermore, a translocation of Al by hyphae of mycorrhizal fungi like *Pisolithus tinctorius* as well as its incorporation and accumulation in the hyphal mantle of mycorrhizal tree roots (like *P. tinctorius* colonized loblolly pine roots, see Moyer-Henry *et al.*, 2005; Clarholm & Skyllberg, 2013) can contribute to the decrease in the soil solution. Since the roots of the birches growing in the pots were substantially colonized by ectomycorrhizal fungi (see colonization rates in **Figure 3–36**), the tree-fungi-interaction can be considered as a possible sink for Al in the substrate solution. The accumulation of Al in the associated mycorrhizal fungi is discussed in detail in subsection **4.7.**

The metals Cu, Fe, Ni, U, and Zn showed similar depths and time related trends like Al in the substrate solution of the pots. At a soil pH below 7 as it was the case in the pots, the most significant species of Cu in soil solution are hydrolysis products of the cations $CuOH^{+}$ and $Cu_2(OH)_2^{2+}$. The main variables controlling the Cu mobility are (in descending order of importance) SOM, DOM, pH, and the Cu soil content. Cu in solution binds to organic substances and c. 80 % of the soluble organic Cu species in soil solutions exist as soluble organic chelates (summarized in Kabata-Pendias, 2011). The Cu concentrations in the substrate solution of the pots exceeded typical levels given for Cu in soil solutions in uncontaminated soils (0.5-135 µg L^{-1}; Kabata-Pendias & Sadurski, 2004) to one to two orders of magnitude already at the beginning of the experiment and especially in greater depths and later stages of the experiment. Presumably Cu was highly (plant-) available in the substrate solution of the pots due to the increased Cu concentration in the substrate, the acidic and oxidizing conditions under which Cu is (very) mobile (pH range in solution 3.6-4.3; Eh: 750-850 mV), and the low content of SOM. SOM usually dominates the adsorption and retaining of Cu in soils (Oorts, 2013); therefore a low TC content in the substrate used for the pot experiment may have contributed in a higher availability of Cu in solution. Even though it causes toxicity in plants like chlorotic small leaves and stunted

growths when occurring in excess concentrations (c. 20 mg kg^{-1} in biomass, see Momčilović, 2004), Cu is also essential for plants as constituent of several enzymes. Those have vital functions in metabolism and physiological processes like photosynthesis and respiration, carbohydrate and nitrate metabolism, water permeability, reproduction, and disease resistance (Kabata-Pendias, 2004).

Compared to the other metals Al, Cu, Ni, and Zn iron had low concentrations in the substrate solution of the pots probably based on the fact that Fe^{3+} is close to insoluble from Fe-hydroxides in soil at pH around 4 and above. Fe is needed as nutrient in plants for photosynthesis, respiration, and N fixation and it is a commonly limited nutrient in plant nutrition besides N and P. Thus a deficiency of Fe leads to chlorotic damages of the leaves (reviewed in Schümann & Elsenhans, 2004). Due to the fact, that the pH in pots was below 4 in greater depths with ongoing experimental duration, iron was potentially available in the solution, however to a limited extend. Nevertheless deficiency symptoms like yellowing of leaves were observed in the second growing season whereupon this symptom is not attributed merely to Fe deficiency and can also be related to plant metal toxicity and deficiency in other nutrients.

Like for Cu and Fe the Ni mobility strongly depends on the soil pH with an inverse relationship. In general Ni is slightly mobile in soils. Mobile forms of Ni are e.g. easily soluble chelates, the exchangeable Ni fraction, and Ni bound to Fe-Mn-oxides or to organic-matter. If not complexed Ni occurs in (acidic) soil solution as the inorganic cation species Ni^{2+} and $NiOH^{+}$ (reviewed in Kabata-Pendias, 2011). Below pH 6 the most abundant Ni form is $Ni(H_2O)_6^{2+}$(Gonnelli & Renella, 2013), which was probably the dominant species that occurred in solution of the pots. The Ni levels therein were in the order of magnitude of the range given for those of unpolluted soils (3-150 µg L^{-1}, Kabata-Pendias & Sadurski, 2004); only in greater depths the maximum of the range was exceeded. This implies that in the pot-experiment the Ni (plant-) availability did not pose a relevant contaminating factor and is not considered to induce additional phytotoxic stress to the trees.

U is present as the mobile and bioavailable (hydrated) UO_2^{2+} (uranyl) with the valency U (VI) under acidic (pH below 5) and oxidizing conditions (Alloway, 2013; Vandenhove *et al.*, 2007), as they were prevalent in the pots. Its sorption on negatively charged mineral binding sites is generally weak at low pH and the concentrations in the soil solution remain high. Anyway a hypothesized general significant positive relationship between increasing U concentrations in the soil solution with decreasing pH was not proven in the lower pH range < 6. A significant relation exists indeed between the K_d (dissociation constant of U concentrations) and the contents of organic matter and soil amorphous Fe (Vandenhove *et al.*, 2007). Mitchell *et al.*, 2013 stated that organic matter and clay minerals provide exchange sites for U (in solution), therefore increase its sorption and thus influence its mobility. The U concentrations in the substrate solution of the pots were comparable to that of a natural slightly acidic Cambisol (pH: 5.2, U soil conc. after HNO_3 digest: 15.2 µg g^{-1}, U in solution: c. 5 µg L^{-1}, see Tyler & Olsson, 2001) and below the concentration of a U mining heap soil (NH_4OAc (pH 5) extract; soil pH: 4.5, U total soil conc. 59.7 ± 25.9 mg dm^{-3}, U in extract: 20.7 ± 6.5 µg L^{-1}, see Thiry *et al.*,2005). It can be concluded, that U in the substrate solution of the pots was probably highly mobile due the acidic pH regime and the low TC content. However the levels of soluble U were in the range of a comparable but mining unaffected natural soil. Therefore U can be considered as relict of the former mining activities but not as contaminant in the substrate's aqueous phase.

The Zn levels in the substrate solution showed similar trends to the aforementioned elements. Zn is generally very mobile in soils and the adsorption, e.g. onto clay lattice, is low at low pH around 4. Several ionic species of Zn are readily soluble and can therefore be easily mobilized. For Zn in solution of uncontaminated soils a broad range of 1-750 µg L^{-1} is reported (Kabata-Pendias, 2011). In Zn contaminated soil Zn^{2+}, the mobile form in solution, increases with decreasing soil pH and decreases with rising content of organic carbon and clay minerals (Rutkowska *et al.*, 2015). Per unit pH decrease the Zn concentrations in soil solution increase fivefold (Mertens & Smolders, 2013). The Zn soil solution concentration in the pot experiment exceeded the reference values for uncontaminated soil, especially in greater depths at the end of the first growing season. It can be concluded that even though the Zn total concentrations in the initial substrate were slightly below precaution values for Germany and far below typical concentrations of mining contaminated soils, due to the low substrate pH Zn was highly mobile and available in the pot experiment. It could have had therefore possibly the character of a contaminant because the concentrations in the solution exceeded Zn levels for optimal plant growth of c. 15 µg L^{-1} (Peganova & Eder, 2004) to about two orders of magnitude. This may have contributed to the generation of additional stress to the birch trees.

The reduced concentrations of the metals Cu, Fe, Ni, U, and Zn in the substrate solution of the planted pots compared to the unplanted control are considered to be related to the root-induced pH increase described above for Al. Due to the inverse pH dependency of these metals, their solubility and therefore their availability in the solution is reduced. Furthermore it can be assumed that due to the essentiality of Cu, Fe, and Zn as plant (micro-) nutrients (as mentioned in the previous sections) the trees aim to take up and accumulate those metals into the biomass, which may have contributed to their reduction in the solution. Nevertheless the pH buffering by the roots is considered as the key factor for the reduced metal concentrations in the substrate solution.

The trends of in the S solution levels were contrarily to those of the metals mentioned before. With increasing duration of the experiment the S concentrations in the control decreased whereas in the planted pots the concentrations increased with greater depths and experiment duration. In the second growing season, the S concentration curves of the planted pots diverged, whereas one curve (Pot 1) converged to that of the control. It can be assumed that the S levels reflect the accelerated weathering in the planted pots. As a result of the higher water use by transpiration the residence time of the undersaturated water is shorter, which might have resulted in increased dissolution of ions from silicate and accelerated pyrite oxidation. Whereas Fe^{2+} as the product of pyrite oxidation is rapidly oxidized at pH around 4 and then precipitated as iron hydroxide, S remains in solution as sulfuric acid and is therefore increased in the planted pots. The weathering rate and pyrite oxidation in the control might have been slower due to the lower water use, hence consequently less S is released in the solution. Antagonistic to the increased weathering rates in the planted pots was the postulated pH-buffering by the tree roots. This could explain that the S concentration curve of Pot 1 converged to that of the control in the second growing season since the trees growing in Pot 1 had apparently the highest pH-buffering capability of all planted pots. The resulting higher pH may have reduced the pyrite oxidation and thus the release of S in the solution.

The divergence of the pH curves as well as the metal concentration curves between the three planted pots in the second growing season was attributed to the diversity in tree growth and biomass production and finally to the differences in the trees' physiological and metabolic activity. That seemed to have influenced the pH-buffering capability of the roots resulting in the diverged pH-curves especially in second growing season. Since the pH was considered as the main factor for the mobility of the metals discussed herein, their concentrations curves were inversely correlated to those of the pH. In consequence Pot 1 showed the strongest pH-buffering effect and the lowest metal concentration in solution of all planted pot and was accounted to have the physiological and metabolically most active ('healthiest') trees. This was confirmed by the apparent best 'health'-status of the trees growing in Pot 1, as observed from foliage color and leave fall.

Another, more critical explanatory approach to interpret the observed effects of reduced metal concentrations in the solution of the planted pots is that their reduction was not related to the pH buffering effect or metal accumulation by the birch roots but arose from the longer residence time of the DI-water in the control pot. As described in the section above the DI-water is undersaturated in ions and therefore takes up those from the soil. As long as the solid-liquid phase saturation equilibrium is not reached soluble (metal-) ions are taken up from the substrate. Until achieving saturation a longer residence time of the water in contact with the substrate leads to higher concentrations of metals-ions. As a result of the lacking transpiration by the vegetation the water use was lower in the control pot than in the planted pots. For this reason the concentrations in the solution of the unplanted pot may have been higher and the pH lower due to longer water residence time and lower dilution by 'fresh' DI-water. This effect cannot be distinguished from the postulated birch root mediated effect of lowered metal concentrations by pH-buffering and biomass accumulation.

4.3 Tree growth, biomass production, and metal concentrations in tree tissues

An intraspecific variability of the birches in growth and in biomass production within the duration of the pot experiment occurred even though the trees were chosen in the field regarding similar morphological properties like height, diameter, and obvious health status. The age was not estimable at the beginning of the experiment. It can be assumed that the transplantation from the natural stand in the field into the pots and the adaption to the new environment of the birch saplings strongly contributed in the diversity in growths. In many pot experiments with woody species a transplantation lead to increased mortality rates (reviewed in Kawaletz *et al.*, 2014), hence this step at the beginning of each pot experiment seems to be a key factor for the further development of the plants. In this experiment the birch saplings were transplanted to the pots in spring with already developed foliage. This might have caused additional stress to the plants, due to partially cutting off long ranging roots during the removal from the natural stand, which affects the supply of the shoots with water and nutrients. Although none of the birch saplings in the pot-experiment died off completely, one tree was seriously affected and produced a new main shoot. Mostly all trees lost some leaves after the transplantation in the pots. The heterogeneity of naturally regenerated seedlings as used in the pot experiment can mask abiotic experimental factors and can influence tree physiology even in the

following growing season (*ibid.*). A clear positive or negative correlation between initial age of the trees and their growth or biomass production was not distinguishable; therefore the differences in age were not considered as a determining factor for the diversity between the individuals in this pot experiment.

The metal concentration distribution patterns in the different compartments of the analyzed birches were similar in the case of the metals Al, Cu, Fe, and U. These metals had the highest concentrations in the roots and very low concentrations in the wood and the foliage. A similar pattern was found for Al in silver birches grown on soil in the vicinity of a former industrial site where Al-fluoride was produced (Frankowski, 2016). An important adaption of woody plants to acidic soil with a high level of rhizotoxic Al-ions is the immobilization of the rhizotoxic Al^{3+} at negative binding sites in the root apoplast. These binding sites in the roots cell walls are presumably pectins, whereas the amount of Al^{3+} that can be bound strongly seems to depend strongly on the pectin content and the degree of pectin methylation. The Al biomass-concentrations in fine roots of temperate and boreal trees like *Abies alba*, *Fagus sylvatica*, *Picea abies*, and *Pinus montana* often range between 1-10 mg g^{-1} and are exceeding the threshold for Al hyperaccumulators of 1 mg g^{-1} (reviewed in Brunner & Sperisen, 2013). Taking into account this threshold value the roots of the *B. pendula* trees from the pot experiment have to be defined as Al-hyperaccumulating tissues. Also Cu (as well as for Cd and Zn) in different clones of willow (*Salix viminalis*) treated with the metals in hydroponics was reported to be concentrated most in the roots (Greger & Landewert, 1999). Likewise such pattern was found for U in the root system of Scots pine (*P. sylvestris*) growing on a revegetated U mining heap with the roots acting as the main storage site (Thiry *et al.*, 2005). Several other studies documented a limited transport of Al within plants, mainly herbaceous and crop plants. The same applies to Cu and U that are typically accumulated in the roots and therefore reach the highest concentrations therein (Cu: Oorts, 2013; U: Mitchell *et al.*, 2013). The described pattern of the above mentioned metals were also reflected by the translocation factors which had the lowest values amongst all metals and express therefore the restricted metal translocation from the roots to the above-ground biomass. For instance in the Cu plant uptake a strong translocation-barrier between the accumulating roots and the shoots, unaffected by Cu excess, has been proven (Oorts, 2013). The distribution pattern discussed here indicates two possible tolerance strategies of birch (*B. pendula*) to grow on sites affected by increased concentrations of one or multiple of the metals Al, Cu, Fe, and U (according to Prasad, 2004): (1) Avoidance of metal induced stress by reducing the translocation of the metals to the shoots in order to protect the photosynthesis. (2) Immobilize the metals in the roots, as found for plants growing on tailings and near metal smelters. Compared to the other metals the highest root tissue concentrations were reached for Al and Fe. The measured levels exceeded reference values for plant tissues to 1-2 orders of magnitude (compare 'normal composition of trace elements in plants' by Markert 1994 as cited in Prasad, 2004; Al: 80 µg g^{-1} and Fe: 150 µg g^{-1}). Also the Cu root tissue concentrations were approximately one order of magnitude higher than the given 'normal' value (same reference as previous; Cu: 10 µg g^{-1}) and lie within a range that is reported to be critical for roots (100-400 mg kg) due to the occurrence of rhizotoxic effects (Oorts, 2013). Anyway Cu rhizotoxicity symptoms like reduced elongation, thickened and stunted roots, or dark coloration were not

observed at the birch roots after the pot experiment. The root tissue U levels of the analyzed birches were in the range of the values published for roots of *P. sylvestris* trees grown on a U mining influenced site (Thiry *et al.*, 2005; U: 1-15 µg g^{-1}).

The elemental distribution patterns of Ni and Zn were contrary to those of the aforementioned elements. While the highest Zn concentrations were reached in the above-ground biomass, particularly in the leaves, and the lowest in the roots, Ni was concentrated nearly to the same level in the leaves and the roots (slightly lower in the roots). Even though it is reported to be essential for plants, Ni is needed only in small amounts for the normal plant metabolism (Gonnelli & Renella, 2013). Within plants it is generally mobile, is metabolically-controlled transported and stored (in leaves and seeds) or, as in the most plants, accumulated in the roots (Kabata-Pendias, 2011). The results of this work indicate that *B. pendula* growing on substrate with low Ni-availability uses the foliage as main Ni-storage, nevertheless a similar high amount is retained in the root system (as implied by the low translocation factor). Ni concentrations in plants generally ranging from 0.05 to 10 mg kg^{-1}, which are similar to those found in stems and branches of the pot-experiment birches (Gonnelli & Renella, 2013). Plants are considered as Ni hyperaccumulators when exceeding leaf concentrations of at least 1 mg g^{-1} in dry matter (Prasad, 2004) but many hyperaccumulating plants are able concentrate 1-3 % Ni in dry matter (Gonnelli & Renella, 2013). The Ni concentrations in leaves and roots of the birches are fare below those values and correspond to literature values for twigs of spruce (*Picea* sp.) grown on metal processing industry site (6-14 mg kg^{-1}; Kabata-Pendias, 2011). An investigation of white birch (*Betula papyrifera*) seedlings grown on soil treated with high dosages of Ni (1600 mg kg^{-1} in dry soil) showed that tolerant genotypes strongly restricted the Ni translocation from roots to shoots and did not suffer from chlorosis/necrosis damages. The susceptible genotypes had higher leaf concentrations and showed strong damages (Theriault & Nkongolo, 2016). Referred to the mentioned study it can be assumed that the bioaccessible Ni concentration in the substrate was that low (0.5 µg g^{-1} in the initial substrate) that no restriction to the roots was apparent in *B. pendula* trees from the pot-experiment. Zn was concentrated mainly in the leaves and branches of the investigated birches, which seems the main tissues for accumulation in this species. This could be mainly due to its essentiality in plants metabolism as important component of a variety of enzymes like dehydrogenases, proteinases, peptidases, and phosphohydrolases (Kabata-Pendias, 2011) and is therefore concentrated at the place where the production of photosynthetic and metabolic products takes place. A similar distribution pattern was described for *B. pendula* grown at diverse sampling sites in Europe on substrate with high Zn levels due to long-term metal processing (Unterbrunner *et al.*, 2007). In this study the highest concentrations were reached in the leaves and the roots (c. 50 % of the foliage level). Also another study mentioned high Zn transfers in in above-ground plant parts of silver birch growing on both Zn-contaminated and uncontaminated sites (c. 125-225 mg kg^{-1} in twigs and leaves; Rosselli *et al.*, 2003). Therefore the authors suggest a potential applicability of this tree species for phytoextraction purposes, even though *Betula* sp. is not considered as Zn accumulator plant. The high Zn tissue concentrations in foliage and branches of the birches grown in the pot experiment reflect therefore typical natural intra-plant distribution patterns for this tree species. This is supported by the highest translocation factor amongst all metals discussed herein.

The reduced metal concentrations in all tissues of the trees from the field site compared to the birches in the pots (both had the same age ± 1-2 yrs.) can be explained by the controlled environmental conditions and soil moisture in the pot experiment. The growth conditions of the trees were optimized in the pot-experiment as they were grown under greenhouse conditions with an optimal water supply. In contrast, the field conditions were affected by reduced water availability due to temporary drought in summer. The increased water availability might have facilitated the following effects which, separately or in combination, resulted in increased plant tissue metal concentrations in the pot experiment: First, the growth of the birches from the pots could have been higher compared to the trees naturally grown under field conditions. The higher growths rates and biomass production may have resulted in higher concentrations due to an increased uptake of ions via the transpiration stream. Second, the moist conditions of the substrate in the pots (c. 15 vol% water saturation) could have accelerated the weathering rates in the substrate resulting in an increased release of metal ions into the soil solution. A higher availability of metals in the soil (solution) often leads to increased plant tissue concentrations, which has been shown for many plants for Cu, Fe, U, and Zn (see Kabata-Pendias, 2011). It could therefore be assumed that the improved growths conditions in the pot experiment and the better availability and increased release of the metals in the pots had been main drivers for the observed enlarged plant tissue concentrations compared to those in plants of the field site.

The transfer factors (TFs) > 1 for all metals considered here from the bioavailable fraction in substrate to the roots of the birch trees indicate that this *B. pendula* race accumulates these elements in its root system, especially Fe, Ni, and Zn (TFs > 10). The TFs of the bioavailable substrate fraction to the above-ground biomass < 1 illustrate that all metals with the exception of Fe and Zn are not accumulated in the aerial parts of the birch trees. In the literature transfer factors are given usually in as the ratio of the amount of metals in the biomass and the total amount in the soil. Indeed using the bioavailable metal concentrations in soil instead (determined from the cumulated metal concentrations of the first two fractions of the sequential extraction method) for the calculation of the TFs, a better estimation of the ecotoxicological risks arising from (heavy) metal contaminations can be achieved (Kothe *et al.*, 2005).

4.4 Soil physico-chemistry and metal concentrations in post-experiment substrate

The observed reduction of the post-experiment substrate pH of c. 0.1 pH units compared to that of the initial occurred in all pots in greater depth, and was slightly mitigated in the planted pots. This trend can be explained by increased soil acidity in the deeper layers of the pots. It is assumed that mineral weathering was increased there due to the slightly higher soil moisture conditions. This might have caused higher oxidative weathering rates of iron sulfides like pyrite which resulted in a higher release of sulfuric acid in the deeper layers of the pots. The acid neutralization capacity therefore decreased since during weathering chemical reactions in which protons were consumed are depleted (Blume *et al.*, 2016). The slightly higher substrate pH in deeper layers of the planted pots

can be considered to be related to pH-buffering effect of the birch roots described in the previous subchapter.

The EC in post-experiment substrate of planted pots was decreased in upper layers and increased in greater depths compared to the initial substrate. Since the substrate EC reflects the total content of ions in a water extract it reflects basically the observed EC monitored in the substrate solution (as shown in **Figure A 7** in the appendix). The data indicate that ions like Al^{3+} and Ca^{2+}, which were probably the main cations influencing the EC in the substrate solution, were transported with the gravitation driven percolating water downwards and thus were depleted in the upper layers and enriched in the lower. This trend was stronger in the planted pots due to the higher water volumes applied in order to supply the water demand needed for the trees' transpiration.

The CEC_{eff} in the post-experiment substrate did not differ significantly from that of the initial substrate since the deviations are within the standard errors. At a soil pH around 4 as in the substrate of the pots, the CEC_{eff} reaches its minimum. The cation exchanger surfaces are occupied to c. 80 % with the acid cations Al^{3+} and H^{+}, and only small amounts of the base cations Ca^{2+}, Mg^{2+}, K^{+}, and Na^{+} remain. Since those base cations are essential for plants, nutrient deficiency can occur. At the same time the Al concentration in solution increases and may induce Al-toxicity stress (reviewed in Blume *et al.*, 2016).

No significant depth or birch root related trends can be deduced from the metal concentrations in the post-experiment substrate, neither in the differentially bound fractions extracted by sequential extraction nor in the total concentrations. Appearing trends lie in mostly all cases within the range of the error whiskers. The error whiskers of the initial substrate that were used as guideline to estimate whether concentration increases or decreases were significant represent the inhomogeneity of the initial substrate as well as the errors of the analytical methods sequential extraction or total digestion. Only for three elements significant trends in single fraction were observed from the data: The post-experiment concentrations of Al and Cu occluded in crystalline Fe-oxides (fraction VI) were reduced in all pots compared to the initial concentrations in this fraction. Furthermore the easily deliverable (fraction II) and organically bound (fraction III) U concentrations were increased in the post-experiment substrate. The Al and Cu mass balance revealed that that there was a slightly but significant (twice the error) reduction of the Al and Cu mass in this fraction after the experiment referred on the whole pot. Nevertheless these amounts seem to 'disappear' since they were not shifted to other fractions or removed from the closed systems by output through water or biomass. The same applies the increase of the U masses in the easily deliverable fraction as well as the organically bound fraction. Since there was no decrease in one of the other fractions, these effects cannot be explained by the data.

It can be assumed that the observed trends were not significant, even though they were higher than the error whiskers (maximum 3 times the error). Probably the error of the method, especially in fraction six is higher than the actual differences between the substrate samples. In conclusion, no substantial changes of the metal concentrations and total masses were found in the post-experiment substrate. The birch trees were not able to remove measurable amounts of the metals considered in this work within the (short) duration of the pot experiment.

4.5 Abundance and species variability of ECM fungi in the pots and at the field site

The mycorrhizal colonization rate of birch rhizospheres differ strongly between field and pots. This could be explained by some major differences in the soil properties between both growing sites. The biggest discrepancy to the field was that within the duration of the pot experiment the soil humidity was held in the range of 50 % FC_{eff}. In contrast in the field the soil humidity varied strongly, especially in the summer the substrate was often affected by drought. Furthermore the initial heap substrate was sieved before it was filled into the pots. Therefore bigger clasts, naturally forming the coarse-grained part of soil, were absent. Finally the space that could be claimed by the roots was limited to a relatively small volume of the pots (approx. 0.13 m^3). All these factors could influence the abundance and percentage of the ECM fungi colonizing the birch roots and therefore might have caused differences between field and pots in the mycorrhizal infection.

The most abundant ECM fungus in both the field and the pots *Meliniomyces bicolor* belongs to the class of Leotiomycetes within the phylum of Ascomycota and is part of the so called *Hymenoscyphus ericae* aggregate. Besides *M. bicolor* this species complex contains at least four other clades of mycorrhizal fungi including *M. variabilis*, *M. vraolstadiae*, *Rhizoscyphus ericae* as well as *Cadophora finlandica* (Hambleton & Sigler, 2005). *M. bicolor* and the closely related *C. finlandica* are clades typically forming the characteristic ECM short root morphotype *Piceirhiza bicolorata* with host trees like spruce, pine, and birch (Agerer, 2012) Even though the morphotype was firstly described as mycobiont of Norway spruce (*Picea abies*) it could be also found on a variety of other conifers and hardwoods (Vralstad *et al.*, 2000). The investigations of the ECM community diversity on birch roots on a U mining heap close to the study area revealed that one of the most abundant morphotypes could be classified as member of the genus C*adophora*, formerly named *Phialophora* (Staudenrausch *et al.*, 2005). *C. finlandia* is one species of this genus and as mentioned above closely related to *M. bicolor*, that was the predominant morphotype in this work in the pots as well as in the field. Gherghel *et al.* (2009) also identified a representative of the genus *Hymenoscyphus* as part of the mycorrhizal community isolated from the rhizosphere of pedunculated oaks (*Quercus robur*) growing on the former heap site close to the study area. Thus, the findings of the two last-mentioned investigations combined with the results of this work allow the assumption that ECM fungi of the *H. ericae* aggregate are typical mycobionts of birches growing under the harsh conditions like on former U mining heaps.

As reviewed in Cairney & Chambers (1997) *P. tinctorius* is an ECM fungus of the Gasteromycete group within the phylum of Basidiomycota and has a worldwide widespread dissemination. It is able to colonize diverse habitats like forests, urban and orchard sites as well as devastated and mining influenced soils. Usually fruiting bodies of *P. tinctorius* are found on relatively dry locations with little humus or along roadsides. The fungus is assumed to be an early colonizer and noncompetitive with other ECM fungi. Considering these characteristics of *P. tinctorius* the study area 'Kanigsberg' as a mining influenced site, which is affected by changing soil moisture, drought, and low soil TC content seems to be typical habitat for that fungus. However, the substrate of the pots had constantly high soil moisture, which could explain that the fungus was not present there. Moreover *P. tinctorius* belongs to the so called long-distance exploration types since it forms far-reaching rhizomorphs in order to explore the substrate for nutrients and water far from the rhizosphere (Agerer, 2001). This

delivers a reason why this ECM species was found only in the field but not in the pots. Whereas in the field the ability of *P. tinctorius* to form rhizomorphs is an advantage, it is not ecologically reasonable in the case of the pots due to the limited substrate volume. Only at the field site typical earthball like shaped fruiting bodies of *P. tinctorius* were found in high abundance. Likewise in a study of Staudenrausch *et al.* (2005) fruiting bodies of the fungus were found during field work on a bare U mining heap close to the study area. However, colonization of birch roots by *P. tinctorius* could not be verified by molecular techniques for that habitat. Gherghel (2009) also found fruiting bodies of this species on the 'Kanigsberg' study area without proof by isolation or direct sequencing of the ITS-region.

The third ECM fungus that was found colonizing the birch roots in the pots was *C. geophilum*. Like *M. bicolor* it belongs to the phylum of Ascomycota. It is ubiquitous and one of the most dominant and frequent ECM types (Jany *et al.*, 2002). Due to the structure and the properties of the hyphal mantle and the emanating hyphae *C. geophilum* belongs to the so called short-distance exploration types. This implies that the substrate in the closer distance of the roots is explored by the emanating hyphae of the short roots in order to take up nutrients and water (Agerer, 2001). That could explain why *C. geophilum* was predominantly found in the pots where due to the limited substrate volume an exploration close to the mycorrhizal mantle is ecologically worthwhile. Also the investigations of Staudenrausch *et al.* (2005) showed that *C. geophilum* was part of the ECM community on a former U mining heap close to the study area. However this ECM species occurred with a marginal abundance, similar to the findings in this work. Contrarily to those findings Gherghel (2009) found out that *C. geophilum* was the most abundant ECM species on another part of the 'Kanigsberg' study area, however as a mycobiont of *Q. robur*. In undisturbed environments like in Fennoscandian forests or beech forests in northeastern France *C. geophilum* is one prominent or even the most abundant fungi within each ECM community (summarized in Jany *et al.*, 2002). A reason for the low abundance of *C. geophilum* on disturbed sites like the area investigated in this study could be the lacking specialization of this ubiquitous and generalist fungus.

4.6 Micro-PIXE as technique for the spatially resolved elemental analysis of biological specimens

The microanalysis of ECM short roots using a nuclear microprobe like PIXE has been carried out only in two studies up to now. In a first study Turnau *et al.* (2001) used the micro-PIXE technique to investigate the metal distribution in short roots of Scots pine (*Pinus sylvestris*) infected with *Suillus luteus* ECM. In that work for the first time true elemental maps of ectomycorrhizal short roots were obtained. Thereby a nuclear microprobe with a 3 MeV proton beam focused to 3x3 µm for raster scanning of areas of interest was used. In comparison to that work the nuclear microprobe at JSI (Ljubljana) which was used in this study provides higher proton beam brightness (14 A m^{-2} rad^{-2} eV^{-1}) and a smaller beam size (1 µm) on the sample surface. Therefore it allows the acquisition of high resolution true elemental maps of any kind of biological tissues in both freeze-dried and frozen-hydrated states (Vavpetic *et al.*, 2015). In a second study PIXE-technique was used for the analysis of the nutrient uptake and deposition (K, Ca, P) from minerals like apatite or biotite by ECM rhizo-

morphs of *Rhizopogon* sp. colonizing bishop pine (*Pinus muricata*) (Wallander *et al.*, 2002). Besides the above mentioned plant nutrients also element distribution maps of metals like Cu, Fe, Mn, Ni, Sr, Ti, and Zn were generated and subsequently used for the calculation of mean concentrations. Thereby the nuclear microprobe had a sub-micron setup (beam focusing to minima 0.3 µm). However, relative amounts and no true elemental maps were obtained. Several studies applied PIXE to investigate the distribution of both plant nutrients and phytotoxic metals in plant roots colonized with arbuscular mycorrhiza (e.g. Weiersbye *et al.*, 1999; Orlowska *et al.*, 2008; Mesjasz-Przybylowicz & Przybylowicz, 2011; and Bothe *et al.*, 2013). The mentioned studies contributed from the high resolution (1-3 µm) and the sufficient low detection limits (lower ppm-range) of the PIXE-method that allowed to allocate the accumulation of macro- and micronutrients and even trace elements either to the different host plant tissues or to fungal structures, even on the cellular level.

4.7 Concentration and spatial distribution of elements in ECM short root tissues

The different percentages of the elements in each of the three short root tissues can be partially explained by their relevance for the tree nutrition or their potential phytotoxicity. Following the average spatial element distributions within ECM short roots, as revealed by statistical analysis (calculation of mean concentrations, heat-mapping with cluster-analysis, discriminant analysis) of the micro-PIXE true elemental maps are discussed.

All three ECM fungi identified in the pots and the field showed the same spatial distribution pattern of the metals Al, Ti, and Fe within the short roots. Those were mainly concentrated in the hyphal mantle, thereby Al and Fe showed outstanding high average concentrations in the range of c. 3 wt%. Al is one of the four most common elements in soils and determines like Si the crystalline structure of soil minerals (Frankowski, 2015). Under acidic conditions (soil-pH < 5-5.5) where the phytotoxic form Al^{3+} is predominant, Al toxicity is an important plant growth-limiting factor. The major toxicity symptom that was observed in many studies was the inhibition of the root growth (reviewed in Rout *et al.*, 2001). A typical effect is the stubby appearance of the roots because Al intoxication inhibits lateral root formation and a swelling to the axes (Gregory, 2007). The affected roots are therefore inefficient in absorbing nutrients and water. Mechanisms of the Al toxicity are e.g. the interference with the cell division in root tips and lateral roots as well as an increase of the rigidity of cell walls and the DNA double helix. The latter causes a reduction of the DNA replication (Foy, 1992). ECM colonized plants could have an enhanced Al tolerance compared to non-mycorrhizal plants. *P. sylvestris* seedlings that were inoculated with *Laccaria bicolor* did not show decreased growth after the addition of 0.74 mM Al whereas the non-mycorrhizal control did. While the P uptake was reduced by Al in the control the mycorrhizal pine seedlings showed a normal uptake. Moreover the inoculation led to an increase of the soil-solution pH by 0.5 units. It was concluded that ECM fungal mycelium may decrease the leaching of Al and base cations from the soil (Ahonen-Jonnarth *et al.*, 2003). It is assumed that a transport of Al from mineral to organic horizon in acidic forest soils is actively controlled by fungi to keep the pH in an acceptable level. The import of Al prevents an increased input of H^+ that would replace otherwise free binding sites of leached Ca^{2+} and NH_4^+. This assumption is supported by studies revealing the ability of the ECM fungi *Paxillus involutus* and *P. tinctorius* with *P. sylvestris* as

host to incorporate large amounts of Al in their hyphae. Moreover the transport and uptake of Al might be a reason for its accumulation in mycorrhizal roots, where the mantle forming hyphae concentrate the Al from the soil (reviewed in Clarholm & Skyllberg, 2013). Also Fe is needed by the fungi e.g. in a reaction step of lignin degradation. Thereby Fe^{3+} is reduced to Fe^{2+} and superoxide, which generates hydroxyl radicals that convert lignin into a further cleavable form (Rabinovich *et al.*, 2004). It was assumed that both Al and Fe are collected from mineral soil by the extramatrical mycelium of the fungi and lifted up and turned over in the organic layer by hyphal death (Clarholm & Skyllberg, 2013). The microanalytical analysis of mycorrhizal roots of pine colonized by *S. luteus* demonstrated the accumulation of Al and Fe within the fungal mantle where maximum concentrations of 8400 ppm for Al and 13600 ppm for Fe were detected (Turnau *et al.*, 2001). However the average concentrations within the fungal sheath analyzed by micro-PIXE in this work were nearly four times higher for Al and twice as high for Fe. This might be explained by the elevated background concentrations of Al and Fe in the substrate (3-4 times as high as the average of European subsoils), which are derived on the one hand from the geogenically situation and on the other hand from residual contaminations of the past U mining.

It can be concluded that the ECM fungi *M. bicolor*, *P. tinctorius,* and *C. geophilum* identified as the dominating fungal species in this study show a similar 'biofiltering' effect of the metals Al, Ti and Fe as described for the Scots pine mycorrhizas *Rhizopogon roseolus* concerning Al and Cd (Turnau *et al.*, 1996) and *S. luteus* concerning Al, Fe, Pb, and Zn (Turnau *et al.*, 2001). The described metal filtering of the hyphal mantle may result from fungal metal tolerance mechanisms like extracellular binding on the hyphal mantle by excreted chelating ligands, cell wall binding, intracellular chelation by metallothionein or glutathione and the separation in or on internal compartments as the vacuole (Bellion *et al.*, 2006).

The metals Cu and Zn showed an outstandingly different distribution compared to the other elements: from the outer to the inner compartments the concentrations were increasing, both elements were accumulated mostly in the central cylinder. A similar but not equal spatial distribution was described for Cu in Turnau *et al.* (2001) that was slightly enriched in the cortex and Hartig net of the investigated mycorrhizal root with concentrations not exceeding 100 ppm. Nevertheless some mycorrhizal fungi are able to protect their host trees from Cu toxicity originating from oxidative stress by high Cu tissue levels. Van Tichelen *et al.* (2001) tested the ECM fungi *S. bovinus* and *Thelephora terrestris*, occurring commonly on metal contaminated sites, for their potential to reduce Cu sensitivity of *P. sylvestris*. They reported that both mycobionts were able to protect root growth as well as to reduce the Cu transfer to their host. The Cu sensitivity of *P. sylvestris* was directly influenced while this effect was not attributed to a dilution effect via increased plant biomass. Thereby two different tolerance mechanisms were revealed for the two mycobionts: whereas *Suillus bovinus* accumulated high amounts of Cu into its extramatrical mycelium, the Cu absorption of *T. terrestris* was distinctly low. The study furthermore pointed out that Zn was in contrast to the findings of the current work accumulated in the fungal mantle with concentrations of 2000-4000 ppm. A 6-month-lasting field experiment with Japanese pine (*Pinus densiflora*) and Chinese cork oak (*Quercus variabilis*) that were planted into a former Cu mining tailing showed that an inoculation with ECM fungi could increase seedling survival, growth, and nutrient uptake in the case of *P. densiflora* (Zong *et al.*, 2015). For this

trees species the Cu and Zn concentrations in shoots were significantly reduced compared to the non-mycorrhizal trees, whereby an inoculation with *P. tinctorius* was more effective than the other used mycobionts *C. geophilum* or *L. laccata*. Simultaneously the Cu and Zn concentrations in roots were increased for two mycobionts (*P. tinctorius* and *C. geophilum*) of Japanese pine. The authors presumed as possible reasons therefore the higher volume of extramatrical mycelium or the higher metal binding capacities of those two ECM species. The mycorrhizal infection decreased from initially c. 90 % to c. 3-16 % after 6 months, depending on the relative ECM species. Turnau *et al.* (2002) analyzed the spatial distribution of several metals in Scots pine mycorrhizal roots from Polish industrial waste sites. Metals like Fe, Zn, and Pb were accumulated in the hyphal mantles of most of the different ECM genera like *Hebeloma*, *Rhizopogon*, and *Suillus*. In that study the highest amounts compared to the other mycorrhizas were found for Zn and Pb in the fungal mantle of suilloid mycorrhizas: Zn had concentrations of over 2 % and the Pb level exceeded even 4 % dry weight.

It can be assumed that Cu and Zn were taken up and translocated by the different ECM fungi analyzed in this study fundamentally different than the other phytotoxic metals. Presumably the bioavailable concentrations of these two elements in the soil did not in reach the plant toxicity thresholds. As essential micronutrients Cu and Zn are needed for plant metabolism. Therefore they were taken up and translocated in the central cylinder and subsequent into the aboveground biomass.

In this study the highest P contents were reached on average for all ECM species in the central cylinder and the cortex with the Hartig net structures. Nevertheless, the concentrations did not differ significantly from those of the mantle. In contrast to that Carrec & Gay (1978, cited in Smith & Read, 2008) showed that P was mainly accumulated in the hyphal mantle and Hartig net region of Aleppo pine (*Pinus halepensis*) mycorrhizas and to a lower extent in the plant tissue, whereas it was unclear whether the nutrient is stored in the mycorrhizal roots permanently or temporarily. Bücking & Heyser (2000 a) showed that the P nutrition of *P. sylvestris* was increased in the case of an infection with the ECM fungus *S. bovinus*. Thereby the absorption across the mycorrhizal interface and the translocation to the plant was dependent on the external P supply and the mycobiont species. Whereas during an infection of the roots with *S. bovinus* the supply did not have an effect on P translocation, a supply-dependent effect was observed in the case of a *P. tinctorius* mycorrhiza. Jones *et al.* (1998) demonstrated that the rate of P inflow into Tasmanian snow gum (*Eucalyptus coccifera*) colonized by ECM mycobionts was increased on average by 3.8 times compared to the non-mycorrhizal condition. Other Investigations of *P. involutus* ECM with Norway spruce as a host reveal a contribution of 52 % to the total P plant uptake by fungal hyphae (Jentschke *et al.,* 2001).

Sulfur was accumulated more or less evenly in all three compartments of the mycorrhizal roots and showed a similar distribution pattern like P. In the literature the role of mycorrhiza in sulfur nutrition of plants is discussed controversially and understood marginally. In contrast to arbuscular mycorrhiza ECM seems to have no promoting effect on the sulfate uptake from soil (Mansouri-Bauly *et al.*, 2006). However, *L. laccata* ECM of pedunculated oak increased the amount of sulfate that was loaded into the xylem after root uptake (Seegmüller *et al.*, 1996). The interaction of both mycorrhizal partners seems to influence the sulfate xylem loading. Nevertheless this interaction cannot be directly induced by the mycobiont because the hyphae in ectomycorrhizal roots do not reach past the endodermis (Rennenberg, 1999). More recent investigations of the sulfate uptake into the isolated

mycobiont *L. bicolor* (Mansouri-Bauly *et al.*, 2006) support the hypotheses of the authors that the S uptake in the form of sulfate is increased by ECM fungi.

In this work in all analyzed ECM short roots K was predominantly accumulated in the outer hyphal mantle and only to a small amount (approx. 3 times lower concentrations) in the two inner compartments. Harley (1978) emphasized that the fungal sheath works as absorber and accumulator organ and is therefore an important storage compartment for soil derived nutrients like K which can be re-mobilized later. Thereby the K uptake by the short roots occurs against a concentration gradient. Investigations with excised ECM from European beech (*Fagus sylvatica*) roots showed, that c. 67 % of K^+ absorbed from a solution is retained in the fungal sheath of the short root (Edmonds & Harley unpublished, cited in Smith & Read, 2008). The K^+ uptake of several ECM plants could be enhanced by the fungal hyphae by 5 % (Jentschke *et al.*, 2001). Thereby the capability to enhance K^+ uptake in ECM plants differs depending on the species of the ECM fungi. A study by Plassard *et al.* (2002) showed for two different ECM fungi contrary capabilities to enhance the K^+ uptake into maritime pine (*Pinus pinaster*): While the fungal species *R. roseolus* was able to increase the uptake, nothing of the kind was observed in the case of the mycobiont *Hebeloma cylindrosporum*. Contrarily to those findings Bücking & Heyser (2000 b) stressed that mycorrhizal short roots of the host *P. sylvestris* infected with *S. bovinus* or *P. involutus* showed the highest K contents in the inner part. Furthermore in ECM infected trees no effect regarding the K concentration in any compartment compared to the non-mycorrhizal trees was detected.

Similar to K the highest concentrations of Mg were found in the fungal sheath. That could circumstantiate the barrier like function of the hyphal mantle for some nutrients. Investigations of the nutrient uptake of *P. sylvestris* roots inoculated with the ECM fungi *P. tinctorius* and *S. bovinus* (Bücking *et al.*, 2002) revealed that the uptake of Mg into the cortical apoplast was hold up but not completely inhibited by the hyphal mantle of the two different fungal species. Nevertheless after a longer exposure time to nutrient solutions no differences regarding the spatial distribution of Mg were found within the mycorrhizal roots. Pot experiments with Greggs pine (*Pinus greggii*) inoculated with the ECM fungus *Hebeloma mesophaeum* revealed that the Mg levels in shoots of the mycorrhizal trees are approximately 7 times higher than those in the control (Martinez-Reyes *et al.*, 2012). They concluded that an inoculation with *H. mesophaeum* as mycobiont has beneficial effects for the nutrition in the case of N, P, K, Ca, and Mg and therefore provokes an increase of the shoot biomass.

Like K and Mg also Si had the highest concentrations in the outer hyphal mantle whereas the Si levels in the cortex/Hartig net and the central cylinder were on average at least one order of magnitude lower. The same distribution pattern was found by Turnau *et al.* (2001) in mycorrhizal roots of Scots pine with *S. luteus* as mycobiont. The reported concentrations in the fungal mantle were in the range of 2 %, whereas in this work twice as high Si levels were calculated for this short root compartment. The authors of the aforementioned study suggest using the Si elemental maps to distinguish between the different tissues of the mycorrhiza, especially between endodermis and vascular tissue. A study with spruce seedlings inoculated with *P. involutus* could not find increased tissue Si concentrations in contrast to the non-mycorrhizal control but a higher accumulation resulting from improved growth of the mycorrhizal seedlings. The same was significant for the elements Fe and Al (van Hees *et al.*, 2004).

Due to its high background resulting from the interference of the weak Na-peak with the Bremsstrahlung peak and a potentially overlap with the Zn L-line, Na was excluded from the data evaluation. Other investigations where the Na levels of ectomycorrhizal roots could be analyzed showed a nearly equal distribution within the different short root compartments (Bücking & Heyser, 2000 b). Thereby the Na concentrations of roots and shoots determined in *P. sylvestris* infected with *S. bovinus* were independent of the external levels. This was explained by the reduced radial apoplastic movement of nutrients in the fungal sheath. In the case of a mycorrhizal interaction with *P. involutus* the Na was slightly increased in the cortex and Hartig net structures.

The Ca levels were lower compared to the other nutrients in all three ECM short root compartments. In the fungal sheath no Ca accumulation like in the case of K was observable. A study of Bücking *et al.* (2002) stressed that the fungal sheaths of the ECM fungi species *P. tinctorius* and *S. bovinus* colonizing *P. sylvestris* roots slowed down the uptake of the elements Ca and Mg into the cortex of the mycorrhizal roots through the apoplast. After 24 h incubation in labeled nutrient solutions the *S. bovinus* infected roots showed higher Ca and Mg levels in the cortical apoplast than those infected with *P. tinctorius* and the non-mycorrhizal plants. A study by Turnau *et al.* (2001) where a nuclear microprobe was used to analyze the spatial distribution of various elements in ECM short roots of *P. sylvestris* with the mycobiont *S. luteus* came to contrarious results. The elemental maps revealed that Ca was mainly concentrated in the hyphal mantle with levels of c. 20,000-30,000 ppm. In the cortex and the vascular tissue the concentrations were one order of magnitude lower. The high Ca-concentrations arose probably from the calcareous soil type of the investigated area that is contrary to the study site investigated in this work, where Ca was lacking.

The cluster analysis of the standardized mean concentrations showed different element accumulation patterns in the analyzed mycorrhizal roots. The clustering of the observations (samples) tissue-wise originated from the huge diversity in elemental accumulation capability within the different short compartments, as shown by the dedicated heatmap. Differences in the elemental profiles between the fungal species and growths conditions were revealed by two separate discriminant analyses (DA), wherefore the observations were grouped regardless the compartment tissue concentrations. The mycorrhizal root samples resembled by differential elemental profiles and were separated in a first DA (DA-1) according to their growth either in the field or in the pots. The growing conditions are considered as an important parameter that influences the mycorrhizal root ionome. Under field conditions the fungal species significantly predisposed the ionome of the relative mycorrhizal root, while in the pots these differences were blurred. This was displayed by the DA-plots of the observations: *M. bicolor* and *C. geophilum* samples grown in the field were clearly separated, whereas samples of the two ectomycorrhizal fungi grown in pots grouped very closely. *P. tinctorius* only occurred in the field and resembled *M. bicolor* regarding the ionome. The differences in the water supply, namely temporarily drought in the field and the permanent optimal substrate humidity in the pots are considered as main drivers of the observed discrepancies. This factor seems to affect strongly the uptake and incorporation of the plant and fungal macro- and micro-nutrients Ca, K, Mg, P, S, and Zn, which were the main separating variables in DA-1. On the tissue level both *M. bicolor* and *C. geophilum* behave similar. Clear differences appear for both between the tissue specific elemental profiles, which were shown by the second DA for the samples from the pots (DA-2). Variables that

separated the hyphal mantle from the inner tissues most were Al, Fe, Si, Ti as well as Mg and K. Those had also the highest concentrations in the outmost part of the short roots. That refers to the above mentioned function of the hyphal mantle as a 'biofilter' concerning those elements. Ca, Cu, and S were variables that separated the inner tissues most from each other. This might be attributed to the highest abundance of Cu in the central cylinder compared to Ca and S, which accumulated most in the cortex/Hartig net tissue. Besides its essentiality for plants as in proteins, Cu-excess may provoke toxicity e.g. by producing radicals in the Fenton reaction resulting in cell injury (Merian *et al.*, 2004). In a study by Bojarczuk & Kieliszewska-Rokicka (2010) the growth and metal content of mycorrhizal silver birch seedlings on Cu and Pb contaminated soil were tested. Trees with higher rates of mycorrhizal colonisation had increased Cu and Pb concentrations in roots and lower levels in the foliage. It was postulated that the allocation of the metals to leaves was restricted due to the accumulation by ectomycorrhiza. This outcome is contrarily to the findings in this work where the highest amounts of Cu were found in the short roots' central cylinder. From there a transport with the sap flow upwards would mean an allocation to the aboveground biomass of the birch trees. Summing up the findings of the multivariate statistics conducted in the course of the work: Presumably the distinct elemental patterns of the mycorrhizal birch root compartments originate from the elements' metabolic function, either as essential plant nutrient or its concentration-dependent character as possible phytotoxin.

5 SUMMARY AND CONCLUSIONS

In this work the influence of silver birch vegetation (*Betula pendula*), growing on a site affected by former U mining, on the metal availability and concentrations in soil, soil solution, and biomass was investigated. The effect of associated mycorrhizal fungi on the trees' metal tolerance was studied by PIXE-microanalysis.

To eliminate distracting fluctuations of environmental conditions in the field like temperature, rainfall, and erosion, a pot experiment with controlled conditions (water supply and temperature) was carried out. The specifically designed mesoscale-sized pots allowed a highly time and depth resolved monitoring of the physico-chemistry and the metal concentrations in substrate solution in a closed system. All inputs and outputs, as well all spatial and temporal changes were completely quantifiable. Four pots were filled comparably with homogenized substrate originating from a study site affected by past U mining. Three of them were planted with birch saplings. The young trees with an initial age of mainly 1-2 years originated from a natural stand at the study area and were therefore already adapted to the substrate conditions. The pots were equipped with probes and suction cups for regular physico-chemical characterization of the substrate solution as well as for permanent in-situ logging of the redox potential. The experiment duration covered two growing seasons and the intermediate dormancy and lasted for approximately 70 weeks.

The substrate used in the pot experiment was characterized as strong acidic, moderately metal contaminated, nutrient poor due to deficiency in Ca, K, and P, and had poor soil fertility. Due to their high mobility and bioavailability Al and Cu were addressed as the main metal contaminants which could potentially induce phytotoxicity. The contaminations were probably the result of AMD that percolated through the formerly overlaid heap material and polluted the pristine ground surface. In addition recent pyrite oxidation processes of the material, which was exposed to weathering after the removal of the heap, may contribute in further acidification.

The monitoring of the substrate solution physico-chemistry and metal concentrations over the duration of 67 weeks within the period of the pot experiment revealed depth and time related trends occurring in all pots as well as differences that were related exclusively to the trees' transpiration and metabolic activity. Generally the trends indicate that weathering processes like pyrite oxidation might have been strengthened in the course of the experiment, resulting in further acidification and raised release of metal cations in the solution with increasing duration of the experiment. The exposition of fresh mineral surfaces and the ventilation resulting from homogenizing and sieving of the substrate at the beginning of the experiment as well as the high soil moisture were presumably key factors for the accelerated weathering.

A decrease in the soil solution pH with increasing depth in the course of the experiment occurring in all pots, whether planted or not, was attributed to a dilution effect by watering with deionized water having a higher pH than the solution. This might have resulted in a positive shift of the pH in the shallow zones of the soil columns. The described trends of higher acidity with increasing depth and duration of the experiment were mitigated in the planted pots, wherein the pH was temporarily

and in some depths up to 0.4 units higher compared to the control. That was explained by a buffering of the substrate acidification by the birch roots. It is assumed that the trees aiming to avoid extreme low pH values by root-induced alkalization of the rhizosphere by the release of hydroxide or uptake of protons, the release of dissociated organic acids (like citric, malic, and oxalic acid) into the root apoplast and their subsequent protonation, and proton consuming reduction processes in order to attenuate the harmful effects of increased acidification like Al-rhizotoxicity.

In greater depths the Al concentrations in the solution were extremely high which was assumed to follow from the intensified release of Al^{3+}-ions from silica weathering in pH environments below 4.5. *B. pendula* trees transplanted from the study area into the pots were considered as Al-tolerant race due to their ability to grow despite the high levels of available Al. The observed trends of lowered Al substrate solution concentrations in the planted pots compared to the control were explained by the root-induced pH buffering which probably had reduced the Al-dissolution from the substrate. Furthermore the interaction with mycorrhizal fungi as observed from the colonization rates of the birch roots was postulated to be a further sink for Al in the substrate solution. This presumption was investigated and discussed by a microanalytical study of ectomycorrhizal short roots conducted subsequent to the pot experiment.

The trends of reduced concentrations in the planted pots compared to the control pot in the course of the experiment as observed and described for Al applied also to the metals Cu, Fe, Ni, U, and Zn. Due to the inverse dependency of the solubility of those metals from the pH, the postulated acidity buffering capability of the birch roots was believed to be the main driver responsible for the metals' lowered concentrations in the solution of the planted pots. Due to their essentiality as micronutrients involved in the trees' metabolism, the uptake and accumulation of Cu, Fe, and Zn into the biomass may have contributed to a certain amount to their reduction in solution. Besides their essentiality as micronutrients, in excess Cu and Zn may cause phytotoxicity in plants. Based on their high concentrations in solution the metals Al and Cu were considered as relevant contaminants of the substrate, which probably induced stress to the birch trees by heavily exceeding concentrations facilitating optimal growth. U in the substrate's aqueous phase was presumed as relict of the former mining activities but not as contaminant, so as Ni which did not pose a relevant contamination. Fe was available in solution only to a limited extend and thus was regarded as a possibly growth limiting micro-nutrient in the substrate.

The higher S concentrations in the planted pots were referred to increased weathering coupled to higher pyrite oxidation rates in the planted pots due to higher water use and shorter residence time of the water. The divergence of the trends in pH and the metal concentrations between the three planted pots, occurring in the second growing season, was attributed to the diverging trees' physiological and metabolic activity. Critically discussed was the higher residence time of the water and the lower dilution by DI-water in the control pot as a result of the lower water use compared to the planted pots. This may lead to a higher saturation of the DI-water with cations and therefore higher concentrations measured in the solution of the control pot. This effect cannot be distinguished from the postulated effect of lowered metal concentrations attributed to the birch root mediated pH-buffering and biomass accumulation.

The diverging growth and biomass production of the birch individuals was explained by the stress induced by transplantation of the naturally grown saplings from field condition into the new environment of the pots. Similar distribution patterns in the different tissues of the trees were detected for the metals Al, Cu, Fe, and U which were predominantly concentrated in the roots. The translocation of these metals to the above-ground biomass was reduced and their accumulation seems to be restricted to the roots. Due to exceeding threshold values the birch roots from the pot experiment can be considered as Al-hyperaccumulating tissues. It was assumed that the observed distribution represents a possible tolerance strategy of silver birch against excess concentrations of the mentioned metals. In contrast Ni and Zn were transported to the foliage and reflect natural intra-plant distribution patterns. The higher total tissue concentrations in the plants grown in pots compared to comparable plants from a natural stand at the study area were explained by the higher availability of the metals and the improved growth conditions in the pots. Transfer factors greater than one (based on bioavailable concentrations in the substrate) indicated that all metals were accumulated in the roots, especially Fe, Ni, and Zn (TFs > 10). Moreover Ni and Zn were accumulated (TFs > 1) in the aboveground biomass, mainly in the foliage

Based on the analyses of post-experiment substrate concentrations it was shown that the birch trees were not able to remove measurable amounts of the metals considered in this work within the (short) duration of the pot experiment.

The investigation of the community of the symbiotic fungi associated to the trees (ectomycorrhiza - ECM) in the pots and the field showed that only three different species of mycobionts colonized the birch roots (*Meliniomyces bicolor*, *Pisolithus tinctorius*, and *Cenococcum geophilum*). The structure of the ectomycorrhizal fungi community was different in the field and in the pots, where *P. tinctorius* was absent. This might be explained by its ecological strategy as long-distant exploration type which is beneficial only in the field but not in the limited substrate volume in the pots. It was suggested that the most dominant ECM fungus in both field and pots *M. bicolor* might be a typical mycorrhiza for trees growing on U mining influenced habitats as confirmed by other studies conducted in the vicinity of the study area.

For the first time quantitative elemental maps of mycorrhizal roots of birch were obtained. Therefore micro-PIXE analysis was applied that allows due to its high resolution of 1 µm and its sufficient low detection limits of 10-60 ppm for most elements the allocation of nutrients and even trace elements on a cellular level in plant tissues or fungal structures. The quantitative elemental maps of ECM short roots of silver birch using micro-PIXE analysis revealed an accumulation of the potentially phytotoxic metal Al and some macro- and micronutrients (Fe, K, Si). The tissue concentrations of those elements reached multiples of the bioaccessible soil concentrations. Therefrom, a filter-like function of the fungal sheath concerning these elements in order to protect the host trees from phytotoxic effects was assumed. In contrast Cu and Zn were mainly accumulated in the inner, more tree related compartments of the mycorrhizal roots. This was related to their importance as micronutrients in the plant metabolism and the underrunning of threshold values for phytotoxicity.

Under field conditions the ionome, meaning the elemental composition of the tissues, of mycorrhizal birch roots was significantly affected by species of the relative mycobiont. The ability to take

up nutrients under the harsh environmental conditions in the field differed strongly differed between the miscellaneous fungal species.

Based on the questions this work aimed to elucidate, the following conclusions can be drawn from the obtained results and findings:

1) Roots of silver birch (*Betula pendula*) can buffer the pH in acidic substrate, presumably by releasing dissociated organic acids that are protonated in the apoplast in order to decrease the availability of phytotoxic metals.
2) The metals Al and Cu, but also Fe, Ni, and Zn were strongly reduced in the substrate solution of the rhizosphere. It was hypothesized that the pH buffering capability of the birch roots was the main driver for their lowered availability. As further sinks the accumulation of Al in the biomass of root associated fungi was postulated as well as the uptake of Cu, Fe, and Zn into birch tissues due to their essentiality as micronutrients.
3) A significant contribution of the birch vegetation in a decrease of total metal concentrations in the substrate within the (short) experiment duration was not proven.
4) Deduced from the plant tissue concentrations birch roots can be considered as Al-hyperaccumulating tissues. Al, Cu, Fe, Ni and U are accumulated in the roots whereas Zn is mainly accumulated in the leaves. For phytoremediation applications birch might be suitable, due to the ability to grow under metal excess at acidic soil conditions. An approach aiming the stabilization of the metals Al and Cu, preferentially accumulated in high amounts in the rhizosphere of silver birch, might be promising.
5) The diversity of the fungal community in the pots and the field was small as only three different species formed an ectomycorrhiza with the birch roots. One species, *Meliniomyces bicolor*, is postulated to be a typical mycobiont of trees growing on U mining influenced habitats.
6) A filter-like function of the mycobionts concerning Al was proven for short roots of mycorrhizal birch trees as the hyphal mantle accumulated multiples of the bioaccessible concentrations. In contrast Cu was not accumulated in the fungal tissues. The mycobionts are believed to contribute substantially in the trees Al-tolerance.
7) Under field conditions the elemental composition of the tissues of the mycorrhizal roots was significantly dependent on the species of the relative mycobiont.

REFERENCES

Agerer R. 2001. Exploration types of ectomycorrhizae - A proposal to classify ectomycorrhizal mycelial systems according to their patterns of differentiation and putative ecological importance. *Mycorrhiza* **11**(2): 107-114.

Agerer R. 2006. Fungal relationships and structural identity of their ectomycorrhizae. *Mycological Progress* **5**(2): 67-107.

Agerer R. 2012. *Colour Atlas of Ectomycorrhizae*. Schwäbisch Gmünd: Einhorn-Verlag.

Ahonen-Jonnarth U, Goransson A, Finlay RD. 2003. Growth and nutrient uptake of ectomycorrhizal *Pinus sylvestris* seedlings in a natural substrate treated with elevated Al concentrations. *Tree Physiology* **23**(3): 157-167.

Akcil A, Koldas S. 2006. Acid Mine Drainage (AMD): causes, treatment and case studies. *Journal of Cleaner Production* **14**(12-13): 1139-1145.

Alloway BJ. 2013. *Heavy Metals in Soils. Trace Metals and Metalloids in Soils and their Bioavailability*. Dordrecht, Heidelberg, New York, London: Springer.

Alloway BJ 2013. Uranium. In: Alloway BJ ed. *Heavy Metals in Soils: Trace Metals and Metalloids in Soils and their Bioavailability*. Dordrecht: Springer Netherlands, 565-577.

Altschul SF, Madden TL, Schaffer AA, Zhang JH, Zhang Z, Miller W, Lipman DJ. 1997. Gapped BLAST and PSI-BLAST: a new generation of protein database search programs. *Nucleic Acids Research* **25**(17): 3389-3402.

BBodSchV 1999. Bundes-Bodenschutz- und Altlastenverordnung vom 12. Juli 1999 (BGBl. I S. 1554): Bundesministeriums der Justiz und für Verbraucherschutz in Zusammenarbeit mit der juris GmbH. [WWW document] URL https://www.gesetze-im-internet.de/bundesrecht/bbodschv/gesamt.pdf. [accessed 2 February 2017].

Bellion M, Courbot M, Jacob C, Blaudez D, Chalot M. 2006. Extracellular and cellular mechanisms sustaining metal tolerance in ectomycorrhizal fungi. *Fems Microbiology Letters* **254**(2): 173-181.

Bergemann SE, Garbelotto M. 2006. High diversity of fungi recovered from the roots of mature tanoak (*Lithocarpus densiflorus*) in northern California. *Canadian Journal of Botany* **84**(9): 1380-1394.

Berthrong ST, Jobbagy EG, Jackson RB. 2009. A global meta-analysis of soil exchangeable cations, pH, carbon, and nitrogen with afforestation. *Ecological Applications* **19**(8): 2228-2241.

Binkley D 1995. The influence of tree species on forest soils: processes and patterns. In: Mead D, Comfort I eds. *Proceedings Trees and Soil Workshop 1994, Agronomy Society of New Zealand*. Canterbury: Lincoln University Press, 1-33.

BIOS - Büro für Umweltgutachten 2010. Exkursionsführer zur botanisch-zoologischen und ökologisch-naturschutzfachlichen Exkursion an ausgewählte Standorte des ehemaligen Uranerzbergbaus im Landkreis Greiz: BIOS - Büro für Umweltgutachten. [WWW document] URL http://www.bios-bfu.de. [accessed 2 May 2010].

Blume HP, Brümmer GW, Horn R, Kandeler E, Kögel-Knabner I, Kretzschmar R, Stahr K, Wilke BM. 2010. *Scheffer/Schachtschabel: Lehrbuch der Bodenkunde*. Heidelberg: Spektrum Akademischer Verlag.

Blume H-P, Brümmer GW, Fleige H, Horn R, Kandeler E, Kögel-Knabner I, Kretzschmar R, Stahr K, Wilke B-M. 2016. *Scheffer/Schachtschabel: Soil Science*. Berlin, Heidelberg: Springer-Verlag.

Bojarczuk K, Kieliszewska-Rokicka B. 2010. Effect of ectomycorrhiza on Cu and Pb accumulation in leaves and roots of silver birch (*Betula pendula* Roth.) seedlings grown in metal-contaminated soil. *Water Air and Soil Pollution* **207**(1-4): 227-240.

Bothe H, Katarina VM, Paula P, Matevz L, Neva S, Primoz P, Primoz V, Luka J, Marjana R. 2013. Metallophyte status of violets of the section *Melanium*. *Chemosphere* **93**(9): 1844-1855.

Brundrett M, Bougher N, Dell B, Grove T, Malajczuk N. 1996. *Working with Mycorrhizas in Forestry and Agriculture*. Canberra: Australian Centre for International Agricultural Research (ACIAR).

Brunner I, Sperisen C. 2013. Aluminum exclusion and aluminum tolerance in woody plants. *Frontiers in Plant Science* **4**: 12.

Bücking H, Heyser W. 2000. Subcellular compartmentation of elements in non-mycorrhizal and mycorrhizal roots of *Pinus sylvestris*: an X-ray microanalytical study. I. The distribution of phosphate. *New Phytologist* **145**(2): 311-320.

Bücking H, Heyser W. 2000. Subcellular compartmentation of elements in non-mycorrhizal and mycorrhizal roots of *Pinus sylvestris*: an X-ray microanalytical study. II. The distribution of calcium, potassium and sodium. *New Phytologist* **145**(2): 321-331.

Bücking H, Kuhn AJ, Schroder WH, Heyser W. 2002. The fungal sheath of ectomycorrhizal pine roots: an apoplastic barrier for the entry of calcium, magnesium, and potassium into the root cortex? *Journal of Experimental Botany* **53**(374): 1659-1669.

Cairney JWG, Chambers SM. 1997. Interactions between *Pisolithus tinctorius* and its hosts: a review of current knowledge. *Mycorrhiza* **7**(3): 117-131.

Clarholm M, Skyllberg U. 2013. Translocation of metals by trees and fungi regulates pH, soil organic matter turnover and nitrogen availability in acidic forest soils. *Soil Biology & Biochemistry* **63**: 142-153.

Clegg S, Gobran GR. 1995. Effects of aluminum on growth and root reactions of phosphorus stressed *Betula-pendula* seedlings. *Plant and Soil* **168**: 173-178.

Cunningham SD, Berti WR. 1993. Remediation of contaminated soils with green plants - An overview. *In Vitro Cellular & Developmental Biology-Plant* **29P**(4): 207-212.

DIN - Deutsches Institut für Normung 1997. DIN ISO 10390-05: Bodenbeschaffenheit - Bestimmung des pH-Wertes: Beuth Verlag.

DIN - Deutsches Institut für Normung 1997. DIN ISO 11265-06: Bodenbeschaffenheit - Bestimmung der spezifischen elektrischen Leitfähigkeit: Beuth Verlag.

DIN - Deutsches Institut für Normung 2011. DIN EN ISO 11260: Bodenbeschaffenheit - Bestimmung der effektiven Kationenaustauschkapazität und der Basensättigung unter Verwendung von Bariumchloridlösung. Berlin: Beuth Verlag.

Dmuchowski W, Gozdowski D, Bragoszewska P, Baczewska AH, Suwara I. 2014. Phytoremediation of zinc contaminated soils using silver birch (Betula pendula Roth). *Ecological Engineering* **71**: 32-35

Eckelmann W, Ad-hoc Arbeitsgruppe Boden. 2005. *Bodenkundliche Kartieranleitung. 5. verbesserte und erweiterte Auflage (KA 5)*. Stuttgart: Schweizerbart Science Publishers.

ecoTech 2017. Product page of lab lysimeters and redox measuring equipment. Bon: ecoTech. [WWW document] URL https://www.ecotech-bonn.de/de/produkte/bodenkunde/laborlysimeter/ecotech_laborlysimeter/. [accessed 6 June 2017].

Federal Ministry of Economics and Technology, Becker J, Ruhrmann G, Wismut GmbH 2011. 20 Years Wismut GmbH - Remediation for the future: Federal Ministry of Economics and Technology (BMWi). [WWW document] URL http://www.bmwi.de/English/Redaktion/Pdf/20-years-wismut-gmbh,property=pdf, bereich=bmwi2012,sprache= en, rwb=true.pdf. [accessed 8 October 2014].

Foy CD 1992. Soil chemical factors limiting plant root growth. In: Hatfield JL, Stewart BA eds. *Limitations to Plant Root Growth*. New York, NY: Springer New York, 97-149.

Frankowski M. 2016. Aluminum uptake and migration from the soil compartment into *Betula pendula* for two different environments: a polluted and environmentally protected area of Poland. *Environmental Science and Pollution Research* **23**(2): 1398-1407.

Gadd GM, Rhee YJ, Stephenson K, Wei Z. 2012. Geomycology: metals, actinides and biominerals. *Environmental Microbiology Reports* **4**(3): 270-296.

Gherghel F. 2009. *Identification and characterization of Quercus robur ectomycorrhiza in relation to heavy metal contamination.* Dr. rer. nat. Dissertation, Friedrich Schiller University Jena.

Gonnelli C, Renella G. 2013. Chromium and Nickel. In: Alloway BJ ed. *Heavy Metals in Soils: Trace Metals and Metalloids in Soils and their Bioavailability*. Dordrecht: Springer Netherlands, 313-333.

Grawunder A, Merten D, Büchel G. 2014. Origin of middle rare earth element enrichment in acid mine drainage-impacted areas. *Environmental Science and Pollution Research* **21**(11): 6812-6823.

Greger M, Landberg T. 1999. Use of willow in phytoextraction. *International Journal of Phytoremediation* **1**(2): 115-123.

Gregory PJ 2007. Roots and the physico-chemical environment. *Plant Roots: Growth, Activity and Interaction with Soils*. Oxford, Ames, Carlton: Blackwell Publishing Ltd, 131-173.

Hall JL. 2002. Cellular mechanisms for heavy metal detoxification and tolerance. *Journal of Experimental Botany* **53**(366): 1-11.

Hambleton S, Sigler L. 2005. Meliniomyces, anew anamorph genus for root-associated fungi with phylogenetic affinities to Rhizoscyphus ericae (Hymenoscyphus ericae), Leotiomycetes. *Studies in Mycology* **53**: 1-27.

Harley JL. 1978. Ectomycorrhizas as nutrient absorbing organs. *Proceedings of the Royal Society Series B* **203**(1150): 1-21.

Hiekel W, Fritzlar F, Nöllert A, Westhus W. 2004. *Die Naturräume Thüringens - Naturschutzreport Heft 21*. Jena: Thüringer Landesanstalt für Umwelt und Geologie (TLUG).

Hinsinger P, Plassard C, Tang CX, Jaillard B. 2003. Origins of root-mediated pH changes in the rhizosphere and their responses to environmental constraints: A review. *Plant and Soil* **248**(1-2): 43-59.

Hölting B, Coldewey WG. 2013. *Hydrogeologie, Einführung in die Allgemeine und Angewandte Hydrogeologie*. Berlin Heidelberg: Springer-Verlag.

Jany JL, Garbaye J, Martin F. 2002. *Cenococcum geophilum* populations show a high degree of genetic diversity in beech forests. *New Phytologist* **154**(3): 651-659.

Jenk U, Zimmermann U, Uhlig U, Schopke R, Paul M. 2014. In situ mine water treatment: field experiment at the flooded Konigstein uranium mine (Germany). *Mine Water and the Environment* **33**(1): 39-47.

Jentschke G, Brandes B, Kuhn AJ, Schroder WH, Godbold DL. 2001. Interdependence of phosphorus, nitrogen, potassium and magnesium translocation by the ectomycorrhizal fungus *Paxillus involutus*. *New Phytologist* **149**(2): 327-337.

Jones MD, Durall DM, Tinker PB. 1998. Comparison of arbuscular and ectomycorrhizal *Eucalyptus coccifera*: growth response, phosphorus uptake efficiency and external hyphal production. *New Phytologist* **140**(1): 125-134.

Kabata-Pendias A. 2011. *Trace Elements in Soils and Plants*. Boca Raton (FL), USA: CRC Press.

Kabata-Pendias A, Sadurski W 2008. Trace elements and compounds in soil. *Elements and Their Compounds in the Environment*: Wiley-VCH Verlag GmbH, 79-99.

Kawaletz H, Molder I, Annighofer P, Terwei A, Zerbe S, Ammer C. 2014. Pot experiments with woody species - a review. *Forestry* **87**(4): 482-491.

Kidd PS, Proctor J. 2000. Effects of aluminium on the growth and mineral composition of *Betula pendula* Roth. *Journal of Experimental Botany* **51**(347): 1057-1066.

Kothe E, Bergmann H, Büchel G. 2005. Molecular mechanisms in bio-geo-interactions: From a case study to general mechanisms. *Chemie der Erde - Geochemistry* **65**: 7-27.

Kushwaha A, Rani R, Kumar S, Gautam A. 2016. Heavy metal detoxification and tolerance mechanisms in plants: Implications for phytoremediation. *Environmental Reviews* **24**(1): 39-51.

Landeweert R, Hoffland E, Finlay RD, Kuyper TW, van Breemen N. 2001. Linking plants to rocks: ectomycorrhizal fungi mobilize nutrients from minerals. *Trends in Ecology & Evolution* **16**(5): 248-254.

Malaviya P, Singh A. 2012. phytoremediation strategies for remediation of uranium-contaminated environments: A review. *Critical reviews in environmental science and technology* **42**(24): 2575-2647.

Männel A-T. 2016. *Einfluss von Rendzina-Beimengungen auf bergbaubeeinflussten Oberboden, Kanigsberg/Thüringen.*Bachelor's thesis, Friedrich Schiller University Jena, Germany.

Mansfeldt T. 2003. In situ long-term redox potential measurements in a dyked marsh soil. *Journal of Plant Nutrition and Soil Science-Zeitschrift Fur Pflanzenernahrung Und Bodenkunde* **166**(2): 210-219.

Mansouri-Bauly H, Kruse J, Sykorova Z, Scheerer U, Kopriva S. 2006. Sulfur uptake in the ectomycorrhizal fungus *Laccaria bicolor* S238N. *Mycorrhiza* **16**(6): 421-427.

Martinez-Reyes M, Perez-Moreno J, Villarreal-Ruiz L, Ferrero-Cerrato R, Xoconostle-Cazares B, Vargas-Hernandez JJ, Honrubia-Garcia M. 2012. Growth and nutrient contents of *Pinus greggii* Engelm. inoculated with the edible ectomycorrhizal mushroom *Hebeloma mesophaeum* (Pers.) Quel. *Revista Chapingo Serie Ciencias Forestales Y Del Ambiente* **18**(2): 183-192.

Merian E, Anke M, Ihnat M, Stoeppler M. 2004. *Elements and their Compounds in the Environment. 2nd Edition, Volume 2: Metals and Their Compouds*. Weinheim: WILEY-VCH Verlag GmbH&Co. KGaA.

Merkel BJ, Hasche-Berger A. 2006. *Uranium in the Environment: Mining Impact and Consequence*. Berlin Heidelberg: Springer-Verlag.

Merkel BJ, Hasche-Berger A. 2008. *Uranium, Mining and Hydrogeology*. Berlin Heidelberg: Springer-Verlag.

Mertens J, Smolders E 2013. Zinc. In: Alloway BJ ed. *Heavy Metals in Soils: Trace Metals and Metalloids in Soils and their Bioavailability*. Dordrecht: Springer Netherlands, 465-493.

Mesjasz-Przybylowicz J, Przybylowicz WJ. 2011. PIXE and metal hyperaccumulation: from soil to plants and insects. *X-Ray Spectrometry* **40**(3): 181-185.

Mitchell N, Perez-Sanchez D, Thorne MC. 2013. A review of the behaviour of U-238 series radionuclides in soils and plants. *Journal of Radiological Protection* **33**(2): R17-R48.

MO BIO Laboratories I 2016. PowerSoil DNA Isolation Kit instruction manual. [WWW document] URL https://mobio.com /media/wysiwyg/pdfs/protocols/12888.pdf. [accessed 17 February 2017].

Momčilović B 2004. Copper. *Elements and Their Compounds in the Environment*: Wiley-VCH Verlag GmbH, 731-750.

Mortimer CE, Müller U. 2007. *Chemie: Das Basiswissen der Chemie*. Stuttgart: Georg Thieme Verlag.

Moyer-Henry K, Silva I, Macfall J, Johannes E, Allen N, Goldfarb B, Rufty T. 2005. Accumulation and localization of aluminium in root tips of loblolly pine seedlings and the associated ectomycorrhiza *Pisolithus tinctorius*. *Plant Cell and Environment* **28**(2): 111-120.

Naumann G. 2014. *Untersuchung des Kanigsberges in Hinblick auf Gehalte und Konzentrationen ausgewählter Elemente in Boden- und Wasserproben.*Master's thesis, Friedrich Schiller University Jena, Germany.

Olsson PA, Hammer EC, Pallon J, Van Aarle IM, Wallander H. 2011. Elemental composition in vesicles of an arbuscular mycorrhizal fungus, as revealed by PIXE analysis. *Fungal Biology* **115**(7): 643-648.

Oorts K 2013. Copper. In: Alloway BJ ed. *Heavy Metals in Soils: Trace Metals and Metalloids in Soils and their Bioavailability*. Dordrecht: Springer Netherlands, 367-394.

Orlowska E, Mesjasz-Przybylowicz J, Przybylowicz W, Turnau K. 2008. Nuclear microprobe studies of elemental distribution in mycorrhizal and non-mycorrhizal roots of Ni-hyperaccumulator *Berkheya coddii*. *X-Ray Spectrometry* **37**(2): 129-132.

Pallon J, Ryan CG, Marrero NA, Elfman M, Kristiansson P, Nilsson EJC, Nilsson C. 2009. STIM evaluation in GeoPIXE to complement the quantitative dynamic analysis. *Nuclear Instruments & Methods in Physics Research Section B-Beam Interactions with Materials and Atoms* **267**(12-13): 2080-2084.

Peganova S, Eder K 2004. Zinc. *Elements and Their Compounds in the Environment*: Wiley-VCH Verlag GmbH, 1203-1239.

Plassard C, Guerin-Laguette A, Very AA, Casarin V, Thibaud JB. 2002. Local measurements of nitrate and potassium fluxes along roots of maritime pine. Effects of ectomycorrhizal symbiosis. *Plant Cell and Environment* **25**(1): 75-84.

Prasad MNV. 2004. *Heavy Metal Stress in Plants: From Biomolecules to Ecosystems*. Berlin, Heidelberg: Springer-Verlag.

Pulford ID, Watson C. 2003. Phytoremediation of heavy metal-contaminated land by trees - a review. *Environment International* **29**(4): 529-540.

Rabinovich ML, Bolobova AV, Vasil'chenko LG. 2004. Fungal decomposition of natural aromatic structures and xenobiotics: A review. *Applied Biochemistry and Microbiology* **40**(1): 1-17.

Rennenberg H. 1999. The significance of ectomycorrhizal fungi for sulfur nutrition of trees. *Plant and Soil* **215**(2): 115-122.

Rosselli W, Keller C, Boschi K. 2003. Phytoextraction capacity of trees growing on a metal contaminated soil. *Plant Soil* **256**(2): 265-272.

Rout GR, Samantaray S, Das P. 2001. Aluminium toxicity in plants: a review. *Agronomie* **21**(1): 3-21.

Rutkowska B, Szulc W, Bomze K, Gozdowski D, Spychaj-Fabisiak E. 2015. Soil factors affecting solubility and mobility of zinc in contaminated soils. *International Journal of Environmental Science and Technology* **12**(5): 1687-1694.

Salminen R, Batista MJ, Bidovec M, Demetriades A, De Vivo B, De Vos W, Duris M, Gilucis A, Gregorauskiene V, Halamic J, et al. 2005. *Geochemical Atlas of Europe. Part 1: Background Information, Methodology and Maps*. Espoo: Geological Survey of Finland.

Salt DE, Smith RD, Raskin I. 1998. Phytoremediation. *Annual Review of Plant Physiology and Plant Molecular Biology* **49**: 643-668.

Schilling G. 2000. *Pflanzenernährung und Düngung*. Stuttgart: Verlag Eugen Ulmer.

Schümann K, Elsenhans B. 2004. Iron. *Elements and Their Compounds in the Environment*: Wiley-VCH Verlag GmbH, 811-824.

Seegmüller S, Schulte M, Herschbach C, Rennenberg H. 1996. Interactive effects of mycorrhization and elevated atmospheric CO2 on sulphur nutrition of young pedunculate oak (*Quercus robur* L) trees. *Plant Cell and Environment* **19**(4): 418-426.

Sheoran V, Sheoran AS, Poonia P. 2010. Soil reclamation of abandoned mine land by revegetation: A review. *International Journal of Soil, Sediment and Water* **3**(2): 1-20.

Smith SE, Read D. 2008. *Mycorrhizal Symbiosis (Third Edition)*. London: Academic Press.

Staudenrausch S, Kaldorf M, Renker C, Luis P, Buscot F. 2005. Diversity of the ectomycorrhiza community at a uranium mining heap. *Biology and Fertility of Soils* **41**(6): 439-446.

Tamminen P, Derome J. 2005. Temporal trends in chemical parameters of upland forest soils in southern Finland. *Silva Fennica* **39**(3): 313-330.

Theriault G, Nkongolo K. 2016. Nickel and copper toxicity and plant response mechanisms in white birch (*Betula papyrifera*). *Bull Environ Contam Toxicol* **97**(2): 171-176.

Thiry Y, Schmidt P, Van Hees M, Wannijn J, Van Bree P, Rufyikiri G, Vandenhove H. 2005. Uranium distribution and cycling in Scots pine (*Pinus sylvestris* L.) growing on a revegetated U-mining heap. *Journal of Environmental Radioactivity* **81**(2-3): 201-219.

Turnau K, Kottke I, Dexheimer J. 1996. Toxic element filtering in *Rhizopogon roseolus Pinus sylvestris* mycorrhizas collected from calamine dumps. *Mycological Research* **100**: 16-22.

Turnau K, Mleczko P, Blaudez D, Chalot M, Botton B. 2002. Heavy metal binding properties of *Pinus sylvestris* mycorrhizas from industrial wastes. *Acta Societatis Botanicorum Poloniae* **71**(3): 253-261.

Turnau K, Przybyłowicz WJ, Mesjasz-Przybyłowicz J. 2001. Heavy metal distribution in *Suillus luteus* mycorrhizas – as revealed by micro-PIXE analysis. *Nuclear Instruments and Methods in Physics Research Section B: Beam Interactions with Materials and Atoms* **181**(1–4): 649-658.

Tyler G, Olsson T. 2001. Concentrations of 60 elements in the soil solution as related to the soil acidity. *European Journal of Soil Science* **52**(1): 151-165.

Unterbrunner R, Puschenreiter M, Sommer P, Wieshammer G, Tlustos P, Zupan M, Wenzel WW. 2007. Heavy metal accumulation in trees growing on contaminated sites in Central Europe. *Environ. Pollut. (Amsterdam, Neth.)* **148**(1): 107-114.

van Hees PAW, Jones DL, Jentschke G, Godbold DL. 2004. Mobilization of aluminium, iron and silicon by *Picea abies* and ectomycorrhizas in a forest soil. *European Journal of Soil Science* **55**(1): 101-111.

van Laaten N. 2015. *Chemometrische Auswertung des Metall-Transports zwischen Boden und Pflanze in Topfversuchen mit Energiepflanzen.*Master's thesis, Friedrich Schiller University Jena, Germany.

Van Tichelen KK, Colpaert JV, Vangronsveld J. 2001. Ectomycorrhizal protection of *Pinus sylvestris* against copper toxicity. *New Phytologist* **150**(1): 203-213.

Vandenhove H, Van Hees M, Wouters K, Wannijn J. 2007. Can we predict uranium bioavailability based on soil parameters? Part 1: Effect of soil parameters on soil solution uranium concentration. *Environmental Pollution* **145**(2): 587-595.

Vavpetic P, Pelicon P, Vogel-Mikus K, Grlj N, Pongrac P, Jeromel L, Ogrinc N, Regvar M. 2013. Micro-PIXE on thin plant tissue samples in frozen hydrated state: A novel addition to JSI nuclear microprobe. *Nuclear Instruments & Methods in Physics Research Section B: Beam Interactions with Materials and Atoms* **306**: 140-143.

Vavpetič P, Vogel-Mikuš K, Jeromel L, Ogrinc Potočnik N, Pongrac P, Drobne D, Pipan Tkalec Ž, Novak S, Kos M, Koren Š, et al. 2015. Elemental distribution and sample integrity comparison of freeze-dried and frozen-hydrated biological tissue samples with nuclear microprobe. *Nuclear Instruments and Methods in Physics Research Section B: Beam Interactions with Materials and Atoms* **348**: 147-151.

VDLUFA. 1991. *Handbuch der Landwirtschaftlichen Versuchs- und Untersuchungsmethodik (VDLUFA-Methodenbuch) - Band I: Die Untersuchung von Böden* Speyer: VDLUFA-Verlag.

Venkateswarlu K, Nirola R, Kuppusamy S, Thavamani P, Naidu R, Megharaj M. 2016. Abandoned metalliferous mines: ecological impacts and potential approaches for reclamation. *Reviews in Environmental Science and Bio-Technology* **15**(2): 327-354.

Vogel-Mikus K, Pelicon P, Vavpetic P, Krett I, Regvar M. 2009. Elemental analysis of edible grains by micro-PIXE: Common buckwheat case study. *Nuclear Instruments & Methods in Physics Research Section B-Beam Interactions with Materials and Atoms* **267**(17): 2884-2889.

Vralstad T, Fossheim T, Schumacher T. 2000. *Piceirhiza bicolorata* - the ectomycorrhizal expression of the *Hymenoscyphus ericae* aggregate? *New Phytologist* **145**(3): 549-563.

Wallander H, Johansson L, Pallon J. 2002. PIXE analysis to estimate the elemental composition of ectomycorrhizal rhizomorphs grown in contact with different minerals in forest soil. *Fems Microbiology Ecology* **39**(2): 147-156.

Weiersbye IM, Straker CJ, Przybylowicz WJ. 1999. Micro-PIXE mapping of elemental distribution in arbuscular mycorrhizal roots of the grass, *Cynodon dactylon*, from gold and uranium mine tailings. *Nuclear Instruments & Methods in Physics Research Section B: Beam Interactions with Materials and Atoms* **158**(1-4): 335-343.

Wismut GmbH. 1994. Sanierungskonzept Standort Ronneburg. Chemnitz: Wismut GmbH.

Wismut GmbH. 2010. *Chronik der Wismut*. Chemnitz: Wismut GmbH.

Zeien H, Brümmer GW. 1989. Chemische Extraktionen zur Bestimmung von Schwermetallbindungsformen in Böden. *Mitteilung der Deutschen Bodenkundlichen Gesellschaft* **59**(1): 505-510.

Zong K, Huang J, Nara K, Chen YH, Shen ZG, Lian CL. 2015. Inoculation of ectomycorrhizal fungi contributes to the survival of tree seedlings in a copper mine tailing. *Journal of Forest Research* **20**(6): 493-500.

APPENDIX

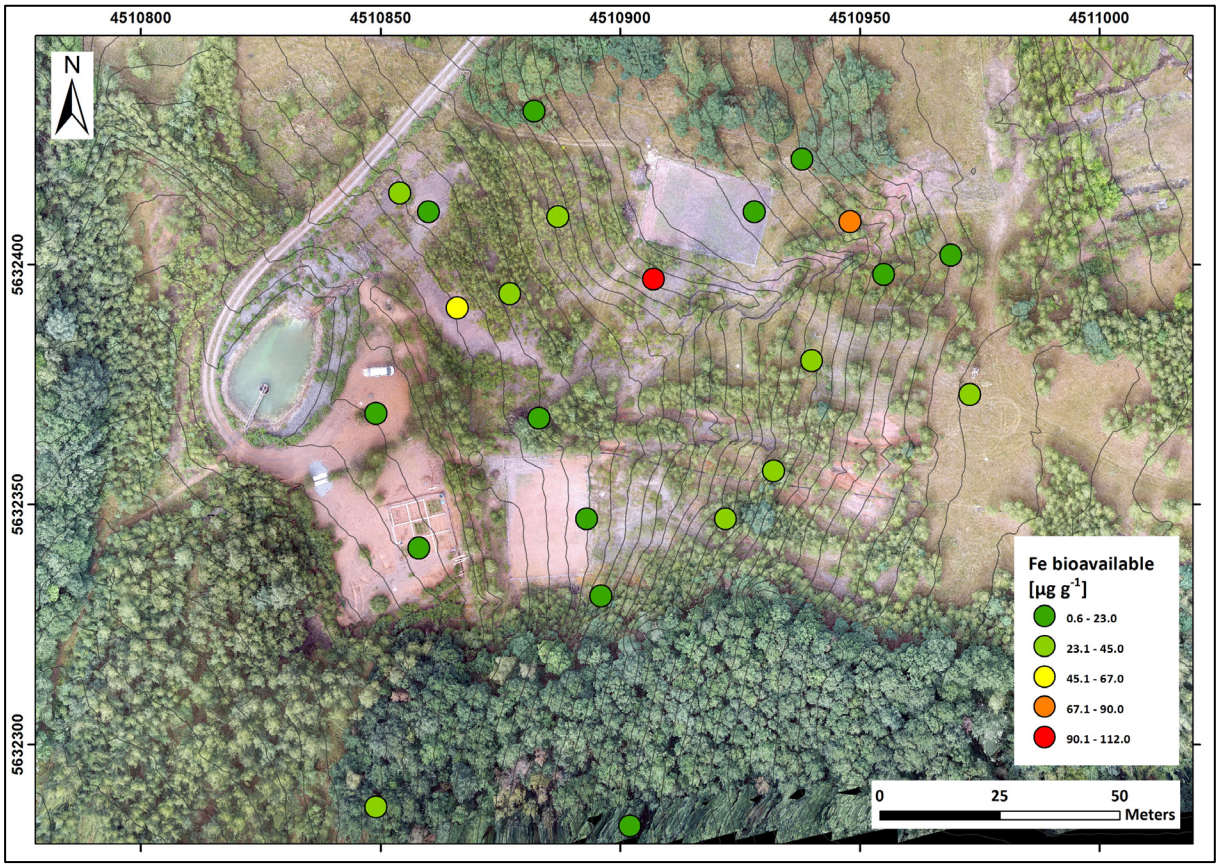

Figure A 1 Results of the screening for the bioavailable Fe concentration of the substrate at the study area by core sampling. The cumulated concentrations of the first two fractions of the sequential extraction method are considered as the bioavailable fraction. The concentration data used as database for the figure were adapted from Naumann (2013)

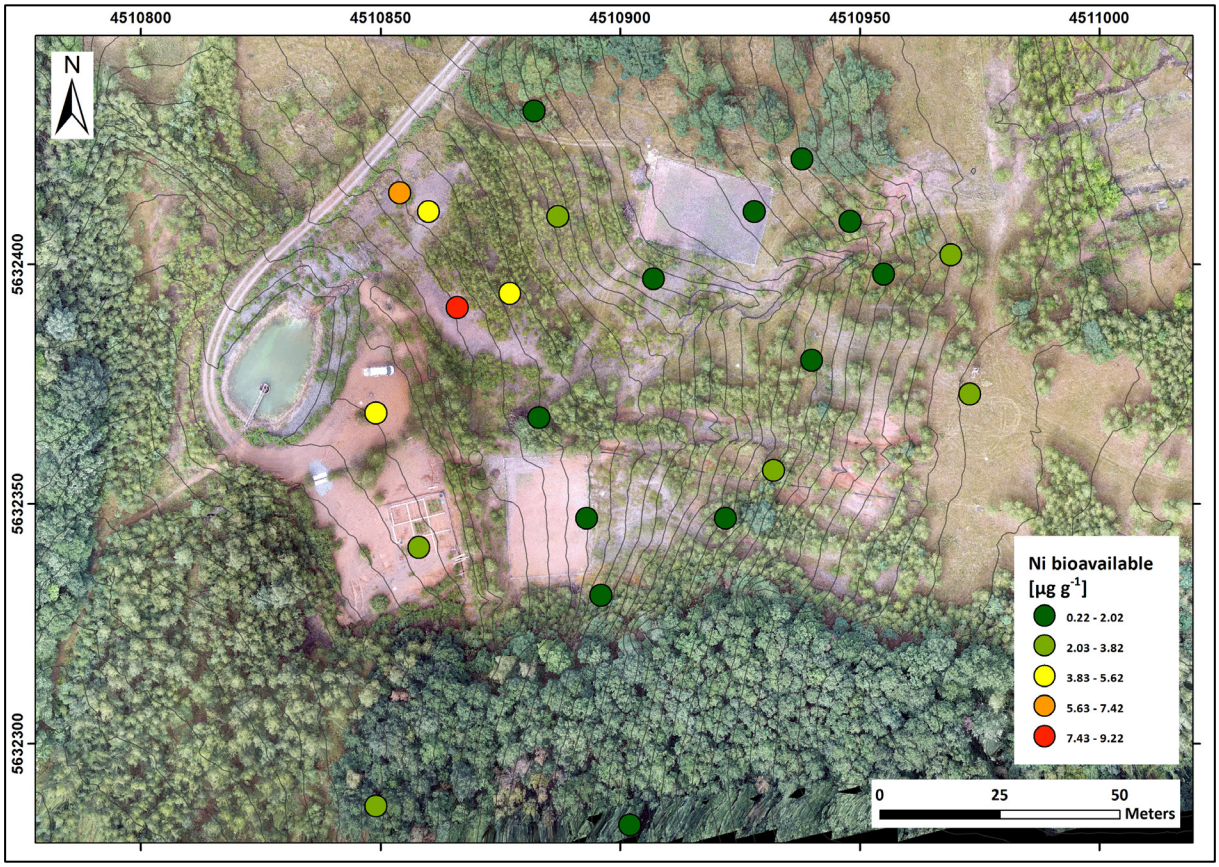

Figure A 2 Results of the screening for the bioavailable Ni concentration of the substrate at the study area by core sampling. The cumulated concentrations of the first two fractions of the sequential extraction method are considered as the bioavailable fraction. The concentration data used as database for the figure were adapted from Naumann (2013).

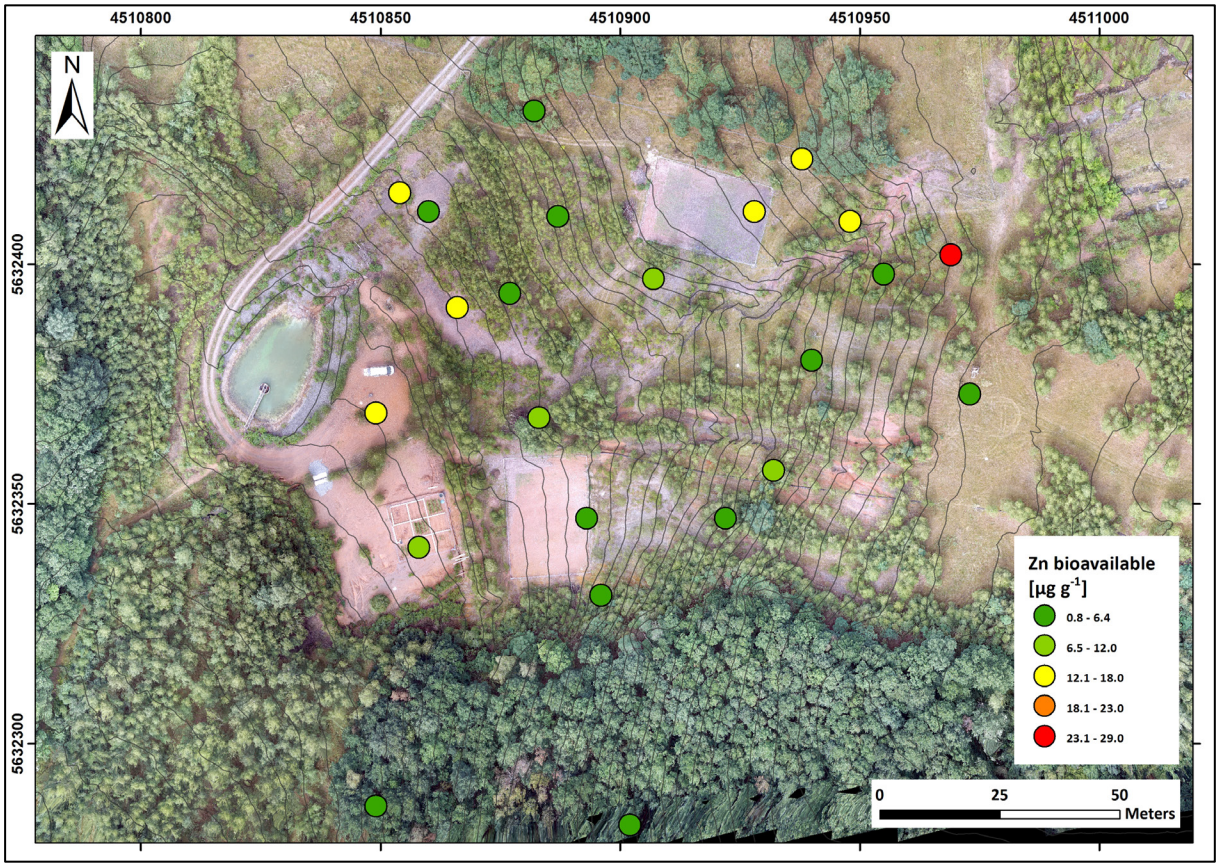

Figure A 3 Results of the screening for the bioavailable Zn concentration of the substrate at the study area by core sampling. The cumulated concentrations of the first two fractions of the sequential extraction method are considered as the bioavailable fraction. The concentration data used as database for the figure were adapted from Naumann (2013).

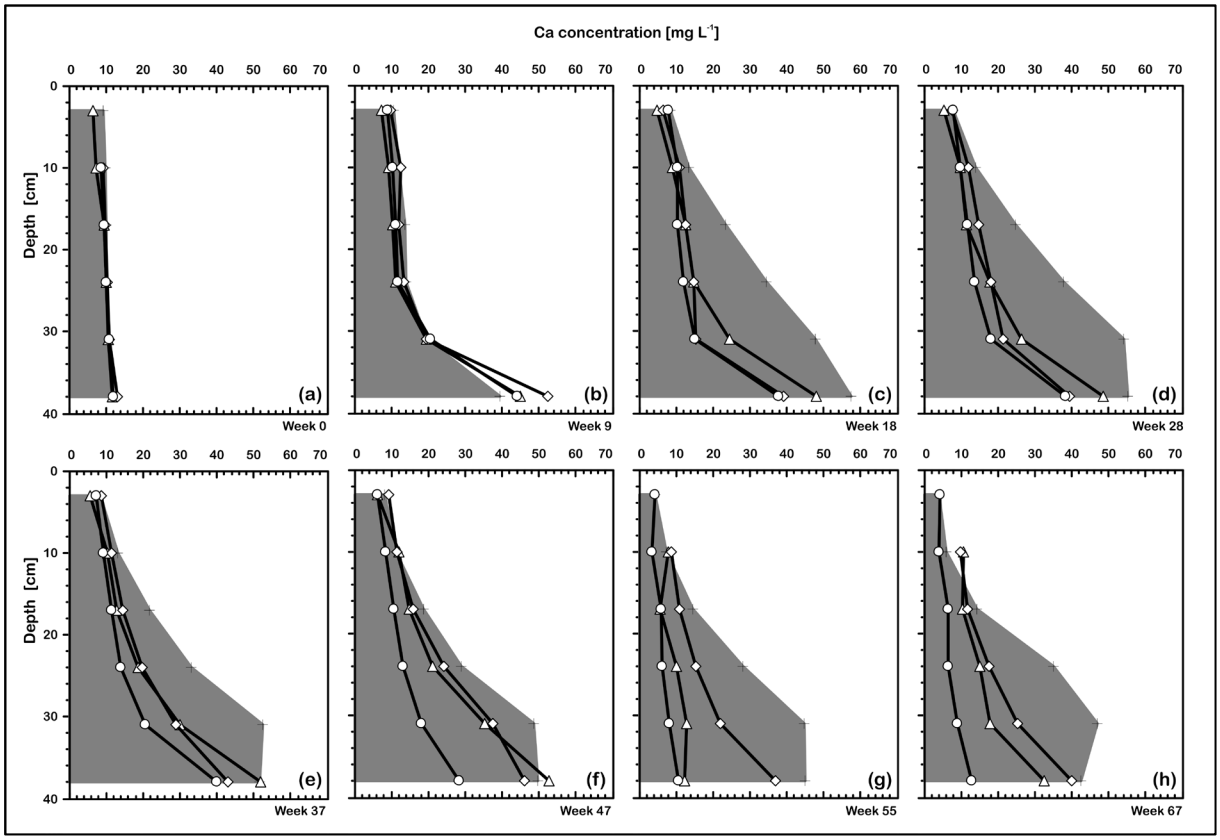

Figure A 4 Temporal development of the substrate solution Ca concentrations of pots planted with birch and the unplanted control pot in different depths (3, 10, 17, 24, 31, and 38 cm b.s.s.). Symbols connected by lines indicate the data points of the planted pots: Circles - Pot 1, diamonds - Pot 2, triangles - Pot 3. The crosses margining the grey colored area indicate the data points of the unplanted control (Pot 4). The diagrams **(a)**-**(h)** represent time slices of the substrate solution monitoring during the pot experiment (week 0 to week 67) including two growing seasons and one dormancy. The first growing season lasted from week 0 to 24 (diagrams **(a)**-**(c)**), the dormancy from week 25 to 44 (diagrams **(d)**-**(e)**), and the second growing season from week 45 to week 67 (diagrams **(f)**-**(h)**). Lacking data points are due to too less substrate solution volume gained on the particular sampling day.

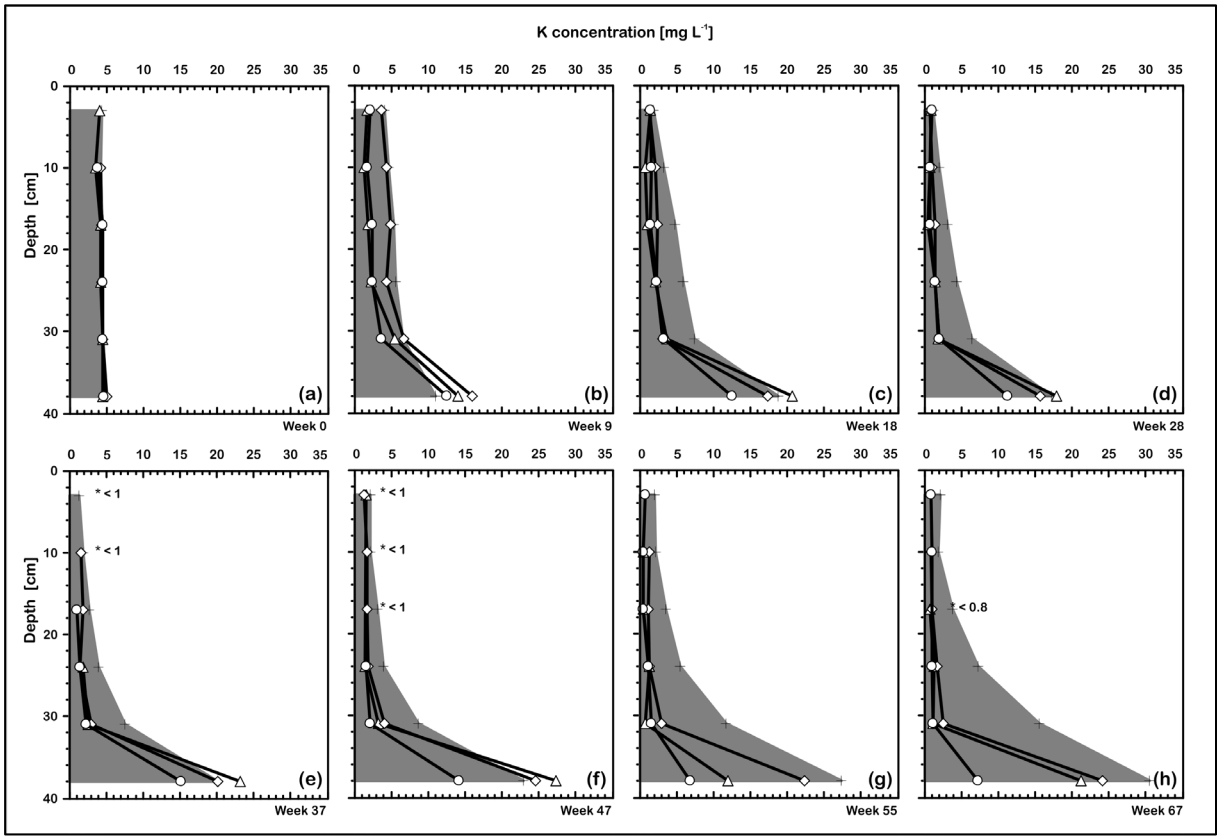

Figure A 5 Temporal development of the substrate solution K concentrations of pots planted with birch and the unplanted control pot in different depths (3, 10, 17, 24, 31, and 38 cm b.s.s.). Symbols connected by lines indicate the data points of the planted pots: Circles - Pot 1, diamonds - Pot 2, triangles - Pot 3. The crosses margining the grey colored area indicate the data points of the unplanted control (Pot 4). The diagrams **(a)**-**(h)** represent time slices of the substrate solution monitoring during the pot experiment (week 0 to week 67) including two growing seasons and one dormancy. The first growing season lasted from week 0 to 24 (diagrams **(a)**-**(c)**), the dormancy from week 25 to 44 (diagrams **(d)**-**(e)**), and the second growing season from week 45 to week 67 (diagrams **(f)**-**(h)**). Lacking data points are due to too less substrate solution volume gained on the particular sampling day. The asterisks indicate data that were below the detection limit which is given next to the symbol.

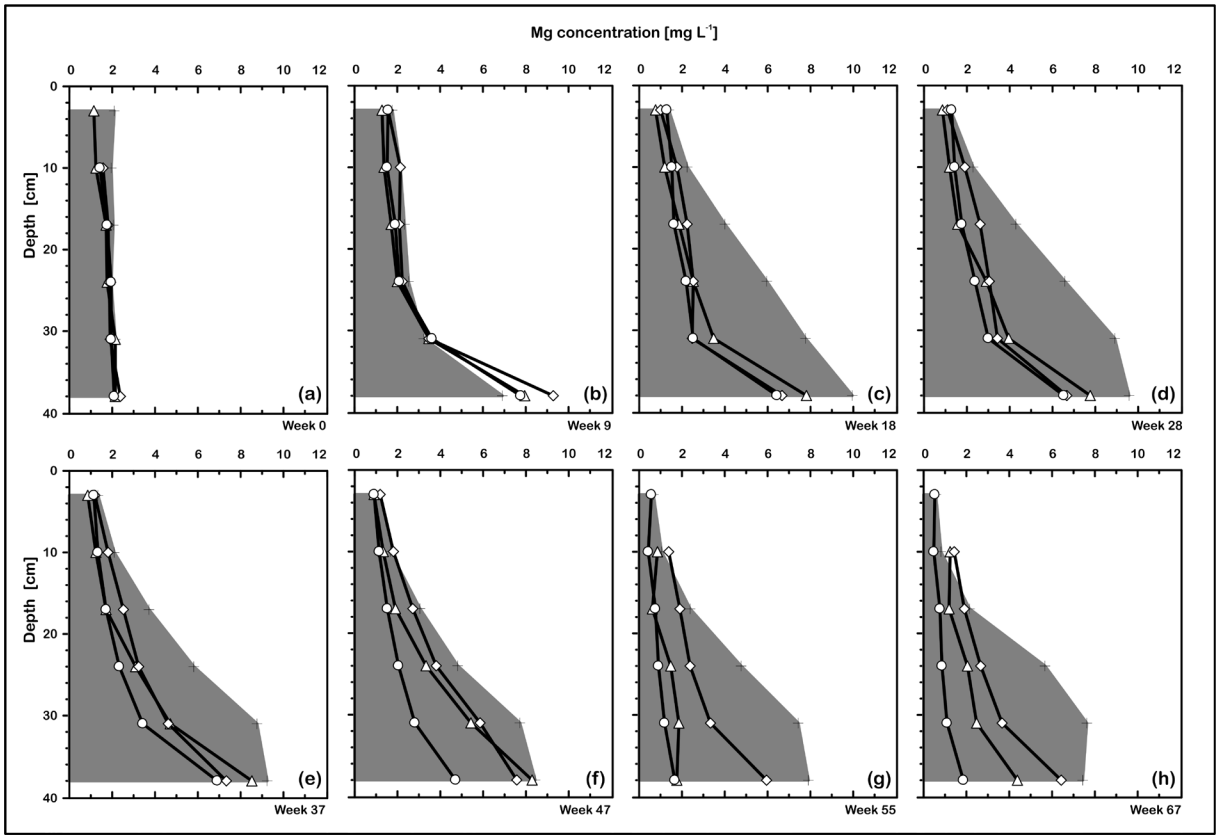

Figure A 6 Temporal development of the substrate solution Mg concentrations of pots planted with birch and the unplanted control pot in different depths (3, 10, 17, 24, 31, and 38 cm b.s.s.). Symbols connected by lines indicate the data points of the planted pots: Circles - Pot 1, diamonds - Pot 2, triangles - Pot 3. The crosses margining the grey colored area indicate the data points of the unplanted control (Pot 4). The diagrams **(a)**-**(h)** represent time slices of the substrate solution monitoring during the pot experiment (week 0 to week 67) including two growing seasons and one dormancy. The first growing season lasted from week 0 to 24 (diagrams **(a)**-**(c)**), the dormancy from week 25 to 44 (diagrams **(d)**-**(e)**), and the second growing season from week 45 to week 67 (diagrams **(f)**-**(h)**). Lacking data points are due to too less substrate solution volume gained on the particular sampling day.

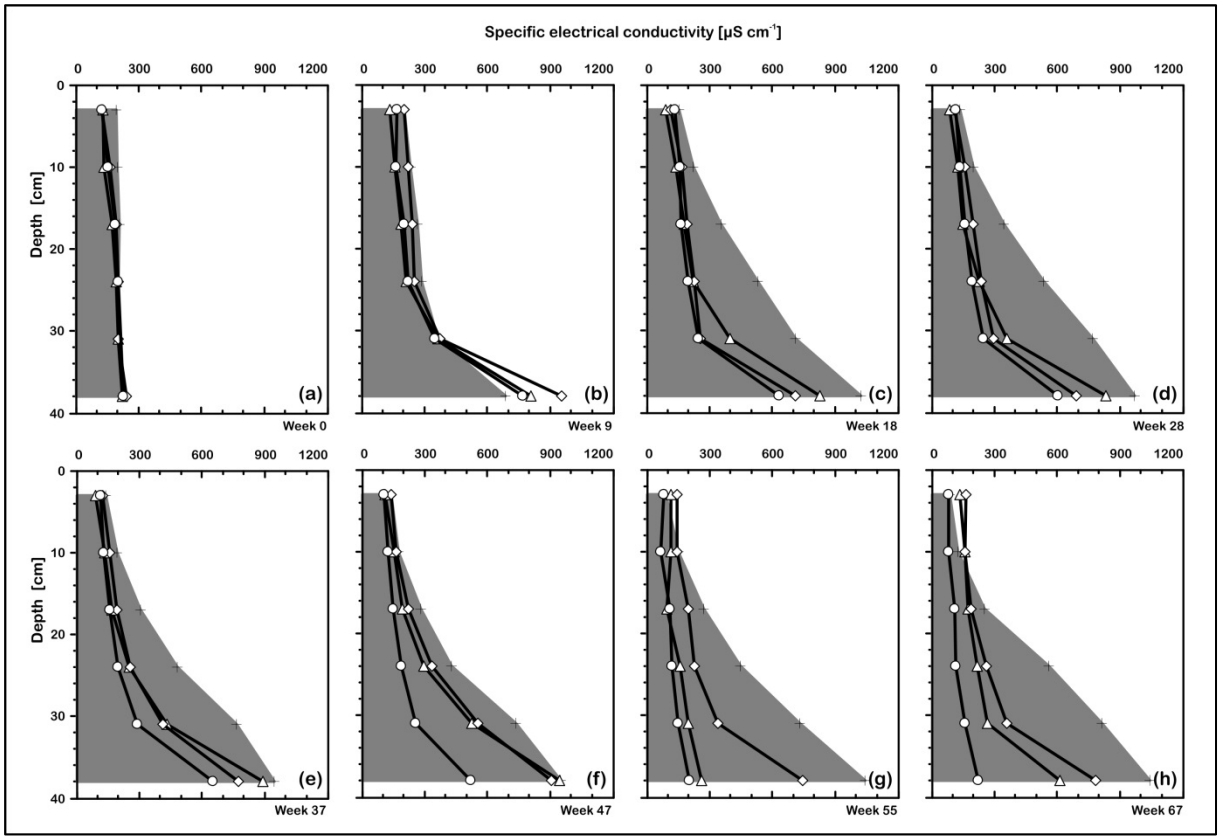

Figure A 7 Temporal development of the substrate solution specific electrical conductivity (EC) in the pots planted with birch and the unplanted control pot in different depths (3, 10, 17, 24, 31, and 38 cm b.s.s.). Symbols connected by lines indicate the data points of the planted pots: Circles - Pot 1, diamonds - Pot 2, triangles - Pot 3. The crosses margining the grey colored area indicate the data points of the unplanted control (Pot 4). The diagrams **(a)**-**(h)** represent time slices of the substrate solution monitoring during the pot experiment (week 0 to week 67) including two growing seasons and one dormancy. The first growing season lasted from week 0 to 24 (diagrams **(a)**-**(c)**), the dormancy from week 25 to 44 (diagrams **(d)**-**(e)**), and the second growing season from week 45 to week 67 (diagrams **(f)**-**(h)**). Lacking data points are due to too less substrate solution volume gained on the particular sampling day.

Table A 1 Dataset and statistics displayed by the Box-Whisker-Plots in Fig. 2. In the case that not more than 25 % of the data per element were lacking due to concentrations below the detection limit, missing data were replaced by a random number between 0 and the detection limit.

Element - Short root tissue	*n*	Mean [µg g^{-1}]	SD [µg g^{-1}]	rel. SD [%]	Minimum [µg g^{-1}]	1. Quartile [µg g^{-1}]	Median [µg g^{-1}]	3. Quartile [µg g^{-1}]	Maximum [µg g^{-1}]
Al - CC	16	2008 .		52	910	1420	1790	2299	5360
Al - CT/HN	17	8485	7902	93	895	3239	6229	9694	33986
Al - HM	16	27029	13710	51	4338	19092	26676	33788	57707
Ca - CC	16	1564	654	42	743	953	1582	1985	3060
Ca - CT/HN	17	2396	1898	79	569	1413	1921	2433	8423
Ca - HM	16	1835	899	49	718	1144	1652	2259	4137
Cu - CC	16	776	750	97	136	299	488	906	2676
Cu - CT/HN	17	882	911	103	83	335	472	1083	3749
Cu - HM	16	405	261	64	88	169	359	584	947
Fe - CC	16	402	388	97	44	183	260	480	1361
Fe - CT/HN	17	5790	9666	167	57	1407	1959	3557	36906
Fe - HM	16	24025	15141	63	1928	14787	18611	32239	53052
K - CC	16	3933	2881	73	649	2380	3184	4571	10645
K - CT/HN	17	3209	3310	103	689	1329	2135	2816	11217
K - HM	16	8523	5620	66	2219	4661	6911	10969	23334
Mg - CC	16	1697	696	41	14	1396	1745	2075	2631
Mg - CT/HN	17	1664	895	54	46	1084	1826	2234	3777
Mg - HM	16	2657	1200	45	45	2004	2786	3206	4795
P - CC	16	1947	1102	57	30	1139	1602	2996	3797
P - CT/HN	17	1901	1443	76	6	768	1584	3036	4825
P - HM	16	1611	1222	76	16	815	1660	2006	5286
S - CC	16	2777	1197	43	1076	1879	2878	3518	4807
S - CT/HN	17	2098	1189	57	691	1342	1763	3050	4634
S - HM	16	2587	1298	50	710	1685	2542	3203	6322
Si - CC	16	1792	1421	79	191	1021	1648	2005	6279
Si - CT/HN	17	6644	11900	179	838	1783	3529	5379	51621
Si - HM	16	43299	26887	62	6028	26734	35402	54488	110641
Ti - CC	16	203	151	74	9	109	180	248	672
Ti - CT/HN	17	487	1024	210	7	182	244	344	4431
Ti - HM	16	2011	1473	73	13	1054	1846	2495	5977
Zn - CC	16	454	595	131	63	123	234	492	2320
Zn - CT/HN	17	339	357	105	17	102	193	476	1355
Zn - HM	16	217	149	69	5	114	189	309	537

Table A 2 Means by classes for each variable of the first discriminant analysis (DA-1), given in µg g^{-1}. Data incorporated were elemental concentrations measured by micro-PIXE in mycorrhizal birch roots colonized by different fungal species (CG - *Cenococcum geophilum*, MB - *Meliniomyces bicolor*, PT - *Pisolithus tinctorius*) and grown in pots (P) or collected from the field (F).

Class \ Variable	Al	Ca	Cu	Fe	K	Mg	P	S	Si	Ti	Zn
CG-F	14077	4264	724	14822	5732	35	3031	3282	22966	1084	240
CG-P	16030	1955	573	12944	7383	2656	2113	2914	24063	1439	373
MB-F	8637	1199	1187	5897	2586	1377	1259	1619	12991	739	115
MB-P	13756	2029	774	10896	5383	2153	1679	2648	16884	789	459
PT-F	3298	1174	114	2395	2354	1724	1717	1452	4561	231	89

Table A 3 Means by classes for each variable of the second discriminant analysis (DA-2), given in µg g^{-1}. Data incorporated were elemental concentrations measured by micro-PIXE in different tissues (HM - hyphal mantle, CO - cortex with Hartig net, CC - central cylinder) of mycorrhizal birch roots grown in pots and colonized by two fungal species (CG - *Cenococcum geophilum*, MB - *Meliniomyces bicolor*).

Class \ Variable	Al	Ca	Cu	Fe	K	Mg	P	S	Si	Ti	Zn
CG-CC	2694	1968	609	598	4927	2219	2593	3609	2684	344	496
CG-CO	12139	2045	645	11125	6285	2229	2244	2518	17536	1352	386
CG-HM	37358	1925	420	32439	13263	3723	1470	2708	62484	3207	267
MB-CC	1786	1438	773	408	4742	1763	1772	3011	1336	170	680
MB-CO	9764	2342	957	4969	2445	1762	1452	2001	4290	231	429
MB-HM	29122	2183	570	26028	8704	2981	1815	2938	43524	1899	256

Table A 4 Characteristic factors and standardized canonical discriminant function coefficients for the two most discriminating factors F1 and F2 of both discriminant analyses (DA-1 and DA-2).

	DA-1		DA-2	
Factor	**F1**	**F2**	**F1**	**F2**
Eigenvalue	7.529	1.229	7.606	1.798
Discrimination [%]	79.654	13.002	72.995	17.257
Cumulative [%]	79.654	92.656	72.995	90.252
Standardized canonical discriminant function coefficients				
Al	-1.856	2.620	2.701	-0.432
Ca	-0.367	0.075	-0.889	-1.459
Cu	0.627	-0.462	-0.303	-0.088
Fe	0.997	-0.800	1.332	-0.249
K	0.129	0.572	0.519	-0.209
Mg	1.600	0.106	1.083	-0.205
P	-0.332	-0.312	0.078	-0.520
S	-0.955	0.811	-0.024	2.443
Si	0.540	-1.732	-1.394	1.964
Ti	-0.546	-0.666	-2.533	-1.298
Zn	0.458	0.428	0.090	-0.165

ACKNOWLEDGEMENTS AND DECLARATION OF CONTRIBUTIONS

First of all I want to thank the supervisors of my PhD-project Prof. Georg Büchel, Prof. Erika Kothe, and Dr. Dirk Merten (all from Friedrich Schiller University Jena) for providing the theme as well as for giving any support and help I needed, but for also for granting enough free space for developing my own ideas and point of view.

Greatest gratitude goes to the Jena School for Microbial Communication (JSMC) for the funding of the whole PhD project, as well as for financing the acquisition of the pots and enabling the trip abroad to conduct the micro-PIXE investigations.

The setup of the pots used in the experiment was planned in cooperation with Dr. Franziska Mosebach, I want to thank her for sharing valuable experiences and providing help in setting the soil columns and installing the measuring equipment.

Likewise many thanks to Markus Riefenstahl and Dietrich Berger (both FSU Jena) for their permanent support during the pot experiment, the help during planting and harvesting of the trees as well as for the fruitful discussion about occurring problems. Most importantly, I thank you for your friendship and unlimited readiness to help in many situations.

Moreover I appreciated the cooperation with the Thuringian State Institute for Agriculture (TLL) in Jena for the possibility to use their facilities for the pot-experiment, especially Hubert Schröter and Günter Nussbaum for taking care about the trees several times over the weekend.

I also thank Gerald Naumann, Anna-Theresia Männel, and Neele van Laaten who contributed to the work by providing data for the soil characterization which were collected in the course of their Bachelor's/Master's theses.

The enormous analytical effort was just possible due to the valuable work of the staff of the Laboratory for Hydrogeochemistry (Institute of Geosciences, FSU Jena) Ines Kamp, Ulrike Buhler, and Gerit Weinzierl as well as the head of the laboratory Dr. Dirk Merten. They performed the chemical analyses of the substrate solution and the biomass, measured the soil physico-chemistry, and conducted the sequential extractions, total digestions, and the analytical evaluation of the results. Many thanks go to all of them for their contribution to this work.

Furthermore I want to thank the workgroup of Plant Physiology (Biotechnical Faculty, University of Ljubljana) for their hospitality and the support during the sample preparation. Anja Kavčič and Tanja Murn provided lots of help and guidance during the sample preparation. In particular I owe Katarina Vogel-Mikuš the chance to perform micro-PIXE investigations. My greatest gratitude goes to her for her limitless will to help and share her awesome scientific knowledge. Thank you therefore!

Lots of thank to all my colleagues of the work group Applied Geology at the Institute of Geosciences (FSU Jena) and to the work group Microbial Communication (Institute of Microbiology, FSU Jena) who gave me always a great working atmosphere and helped a lot in stressful time (e.g. morally and with food and cake). Particularly I want to thank Luise Eichhorn and Markus Riefenstahl for proofreading the work.

Finally, I am grateful that my family always supported and encouraged me to decide freely and move on my way. I thank you with all my heart.

The micro-PIXE experiment and the writing of an unpublished manuscript integrated in this thesis was accomplished in cooperation with Assistant Prof. Katarina Vogel-Mikuš (workgroup Plant Physiology, Biotechnical Faculty, University of Ljubljana), Mitja Kelemen, Dr. Primož Vavpetič, and Dr. Primož Pelicon (all from Jožef Stefan Institute (JSI), Ljubljana), Dr. Steffi Formann (formerly Institute of Microbiology, FSU Jena), and Dr. Dirk Merten (Institute of Geosciences, FSU Jena). I myself performed the sample preparation for the micro-PIXE measurements, analyzed the data and wrote the manuscript. Dirk Merten supervised the pot experiment, discussed results, and proof-read the manuscript. Steffi Formann supervised and conducted the identification of ectomycorrhiza fungal species. Mitja Kelemen, Primož Vavpetič, and Primož Pelicon performed the micro-PIXE measurements, analyzed the PIXE-spectra, and generated the elemental distribution maps. Katarina Vogel-Mikuš planned the micro-PIXE experiment, performed and supervised the sample preparation, proofread the manuscript and provided guidance for the discriminant analyses.

SELBSTÄNDIGKEITSERKLÄRUNG

Ich erkläre hiermit, dass ich die vorliegende Arbeit selbständig und unter Verwendung der angegebenen Hilfsmittel, persönlichen Mitteilungen und Quellen angefertigt habe.

Die Beiträge der verschiedenen Personen und Institutionen bei der Anfertigung der vorliegenden Arbeit sind unter dem Punkt „ACKNOWLEDGEMENTS AND DECLARATION OF CONTRIBUTIONS" angegeben.

.....	.....
(Ort, Datum)	(Unterschrift)